Master’s degree in civil engineering

SHEAR BEHAVIOR OF POST-INSTALLED ANCHOR CONNECTIONS STRENGTHENED WITH CFRP LAMINATES

Kevin Andrés Tami Torres

Bogotá, D.C., July 18th, 2024

SHEAR BEHAVIOR OF POST-INSTALLED ANCHOR CONNECTIONS STRENGTHENED WITH CFRP LAMINATES

Thesis to Attain a Master's Degree in Civil Engineering with Emphasis in Structural Engineering

Gustavo Tumialán, PhD.

Advisor

Nancy Torres Castellanos, PhD.

Co-advisor

Bogotá, D.C., July 18th, 2024

The thesis titled “Shear behavior of post-installed anchor connections strengthened with CFRP laminates”, presented by Kevin Andrés Tami Torres, complies with the requirements established to opt for the title of Magister in Civil Engineering with emphasis in Structural Engineering.

Advisor

Gustavo Tumialán, Ph.D.

Co-advisor

Nancy Torres Castellanos, Ph.D.

Jury member 1

William J. Gold, MSc.

Jury member 2

Matías Urrejola Corre, MSc.

Bogotá, D.C., July 30th, 2024

To my family,

my friends,

and every genuine connection

that life has awarded me with.

Acknowledgments

First and foremost, I am grateful to my advisors, Dr. Gustavo Tumialán and Dr. Nancy Torres, for their constant input and patience during the development of this investigation. Their guidance and feedback were essential for the completion of this work and their teaching always encouraged me to trust in myself.

I am also thankful to the personnel of the laboratory of structures at Universidad Escuela Colombiana de Ingeniería for their company, their support, and for always encouraging me to achieve my goals.

Finally, I would also like to express my gratitude to my colleagues, family, friends and students that accompanied me in this process. Your patience has showed me how fortunate I am for having you in my life.

Abstract

Concrete breakout is a common failure mode that limits the maximum achievable capacity of shear-loaded anchoring systems installed close to a free edge. Cast-in anchor reinforcement has proved to improve the behavior of this type of anchors. However, this alternative is most effective if the fastening system is also cast-in place. As a result, an experimental program was carried out to assess the shear response of bonded single anchors strengthened with post-installed CFRP laminates and compare their results with those of unreinforced specimens and anchors strengthened with a cast-in alternative (steel hairpin). Four CFRP reinforcement configurations were evaluated for each edge distance considered (50 mm, 100 mm). Strut-and-tie models were elaborated for the design of each reinforcement alternative, while also varying the area of CFRP reinforcement. Ultimate load, absorbed energy, strain unit behavior and failure mode were analyzed. The results showed that CFRP-reinforced specimens achieved ultimate loads that ranged from 2.7 to 5.4 and from 1.8 to 2.1 times that of unreinforced 50 mm and 100 mm specimens, respectively. Also, the failure mode in various specimens changed to anchor rupture, which is the limit state associated with the maximum shear capacity.

Keywords: Anchoring system, anchor reinforcement, FRP laminates, shear load, strengthening.

TABLE OF CONTENTS

LIST OF FIGURES

LIST OF TABLES

1. INTRODUCTION

The accelerated rate in which the population has increased in the last century, has led to a similar rise in the construction industry. Certainly, it is essential that these structures comply with a series of capacity, serviceability, durability and sustainability requirements. As a result, guides, codes and norms have been established throughout history, to standardize good practice in the analysis, design and construction areas involved in civil works projects. However, although modern codes are elaborated with state-of-the-art knowledge, they are relatively recent in history terms. For instance, the Uniform Building Code (now International Building Code) was published for its first time in 1927. It was not until 1976 that it incorporated criteria related to seismic loads, highlighting that in some regions, these actions are critical in structural design.

Consequently, there is a large number of structures built before the adoption of current codes. For example, in the countries that conform the European Union, more than 40% of their residential buildings were constructed before 1960; also, 80% of the total were built before the decade of 1990 (BPIE, 2011; Gkournelos et al., 2021). Thus, a significant joint effort has taken action in improving the structural behavior of these buildings, aiming to make them compliant with current standards, and guaranteeing the safety of their occupants.

In parallel, given this need, the field of assessment, repair, retrofitting and rehabilitation of structures has developed substantially in the last decades. As a result, current structural codes have met the need of updating frequently, striving for incorporating the most recent and relevant advances. In this regard, various international manuals, codes and guides are highly acknowledged, such as ASCE 41, ACI 562, FEMA 154, FEMA 155, FEMA P-2018, Eurocode 8 part 3, among others. These documents incorporate requirements to ensure the quality of the repairs or modifications, providing guidance in activities related to evaluation, design and construction.

To effectuate a structural rehabilitation, it is indispensable to carry out an evaluation of the structure, the diagnosis of the problem, and the determination and implementation of the intervention activities, finalizing with the elaboration of a maintenance guide. Similarly, ASCE proposes the methodology illustrated in Figure 1 for seismic evaluation and retrofitting.

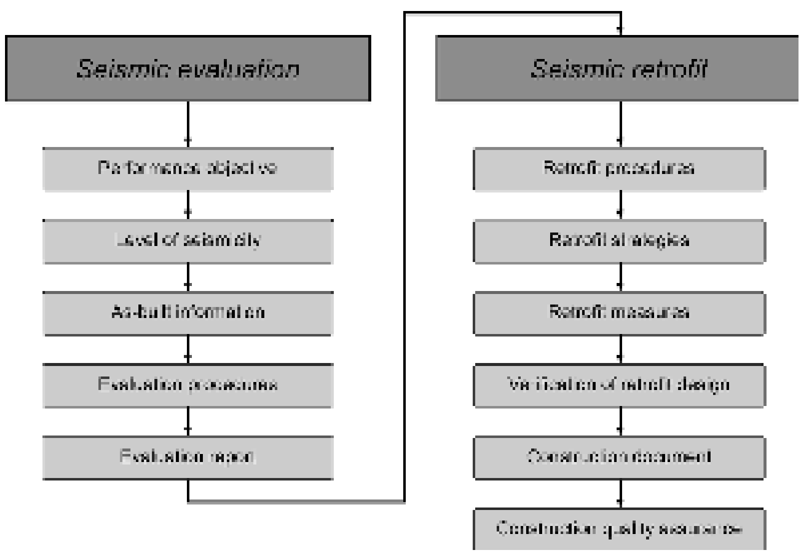

Figure 1 *Seismic evaluation and retrofitting process. Source: Adapted from* (American Society of Civil Engineers & Structural Engineering Institute, 2017)

Retrofitting alternatives may be grouped according to their scope. Some of them act on individual members, while others may apply for modifying the global structural response (Gkournelos et al., 2021, p. 1). On the other hand, the selection of a retrofitting alternative is dictated by the limit state with the highest occurrence probability. In reinforced concrete structures, the most known local and global retrofitting measures are shown in Figure 1. Their incidence over relevant structural parameters is also included.

Table 1 *Local and global retrofitting measures, and their incidence over structural parameters. Source: Adapted from* (Gkournelos et al., 2021, p. 3)

		Strength	Stiffness	Ductility	Irregularity	Force demand	Deformation demand
Local measures	*RC/mortar jacketing*	✓	✓	✓		✗	✓
	Steel jacketing	✓		✓			
	FRP/TRM jacketing	✓		✓			
	Prestressing	✓		✓			
	Strength reduction	✗					
Global measures	*New frames, shear walls, bracing systems*	✓	✓		✓	■	✓
	Mass reduction				✓	✓	✗
	Partial demolition				✓	✓	
	Seismic isolation				✓	✓	✓
	Energy dissipation systems		✓			■	✓
	Isolation joints				✓		
	Connecting independent sections				✓		

It is evident that among local measures, jacketing is an alternative with positive effects on the strength and ductility of the reinforced members. For instance, external reinforcements that incorporate fiber-reinforced polymers (FRP), improve the flexural, shear and axial response of reinforced members. One of the main advantages of FRP is its faculty of adapting to the existing member geometry, providing an effective confinement. For example, it is common to encounter columns reinforced with FRP, which increases their compressive and flexural strength. An illustration of this reinforcement system is presented in Figures 2 and 3:

Figure 2 *FRP jacketing of a column. Source:* (Rendón, 2016, p. 18)

Figure 3 *Strengthening of a beam-column connection with FRP laminates. Source:* (Rendón, 2016, p. 121)

Additionally, there are instances in which the selected retrofitting alternative involves connecting new elements to the existing ones. Over the last decades there has been a substantial increase in the use of post-installed anchors. However, these fastening systems are not limited to retrofitting strategies; they are also employed in new construction and in non-structural applications. For example, Figure 4 shows the connection between a steel staircase and a concrete beam. In that instance, the anchors are subjected to shear.

Figure 4 *Steel staircase connected and supported by a concrete beam. Source: Own.*

As mentioned before, anchors are also used in non-structural applications, such as in railings and façades, where they may be subjected to shear, bending, or a combination of both (Figure 5).

Figure 5 *Metallic railing anchored to a concrete slab. Source:* (Haukohl et al., 2019)

Nevertheless, anchoring systems have a finite strength. When their strength is exceeded, they display a specific mode of failure. One of the most common failure mechanisms in tension or shear-loaded anchors is characterized by the detachment of the concrete in which the anchor is embedded; this is known as concrete breakout. This mode of failure is common in anchors placed near the edge of the concrete member. Figure 6 displays this failure mechanism, as well as the degradation of the surrounding concrete, in a connection between a steel brace and a concrete frame, which corresponds to a common global rehabilitation alternative, as mentioned before.

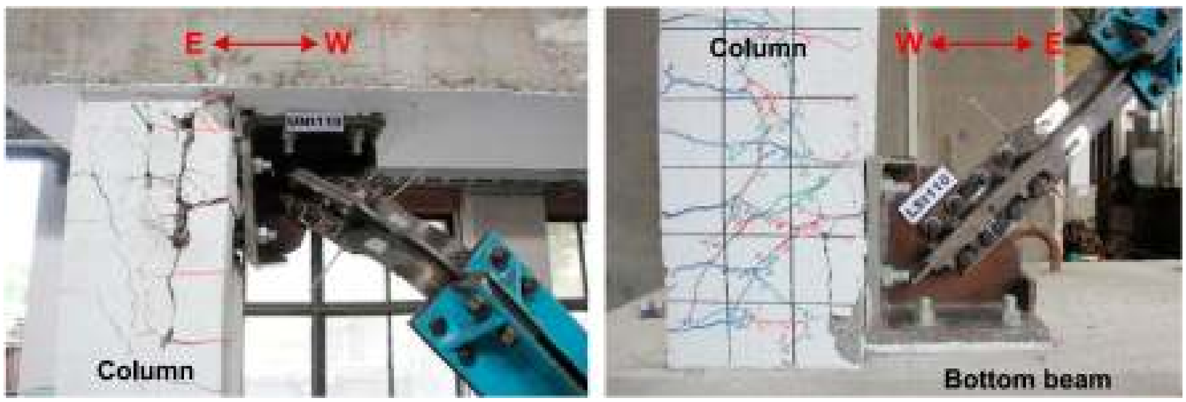

Figure 6 *Failure of the connection of a bracing system anchored to a concrete frame.*
Source: (Mahrenholtz et al., 2015)

A concrete breakout failure is characterized by the detachment of a concrete piece, which results in a sudden loss of load-bearing capacity of the anchor, which cannot transfer the load to a stable substrate. Given the importance and the wide range of applications of cast-in and post-installed fastening systems, the need for appropriately strengthening them has arisen. An effective retrofit alternative would improve the behavior of deficient connections, preventing sudden failures that could compromise the safety of any occupants.

Considering the context previously provided, this document aims to evaluate, in an analytic and experimental manner, the incidence of post-installed CFRP laminates as an alternative for increasing the shear capacity of post-installed bonded anchors placed close to the edge of a concrete member. The above, through the execution of an experimental program that varies different parameters associated with the mechanical response of the anchored connection.

2. THEORETICAL FRAMEWORK

To comprehend the fundamental basis related to the behavior of shear-loaded post-installed anchors, it is important to review some concepts, which is the purpose of this theoretical framework.

2.1. Anchors

The main purpose of a fastening system is to join two different elements. The load-transfer that occurs in this connection is essentially determined by three mechanisms: mechanical interlock, friction, or bond (Mallée et al., 2012) (Figure 7). The latter are the ones encompassed within the scope of this work. In this regard, the strength of these anchors is determined by the interaction of adhesion and micro interlock.

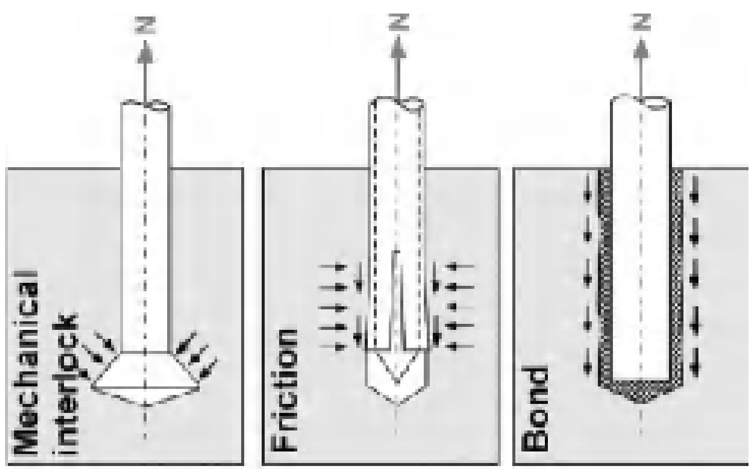

Figure 7 *Load-transfer mechanisms in anchors. Source:* (Mallée et al., 2012, p. 13)

Overall, anchors may be categorized according to their load-transfer mechanism and installation typology, as follows (Figure 8):

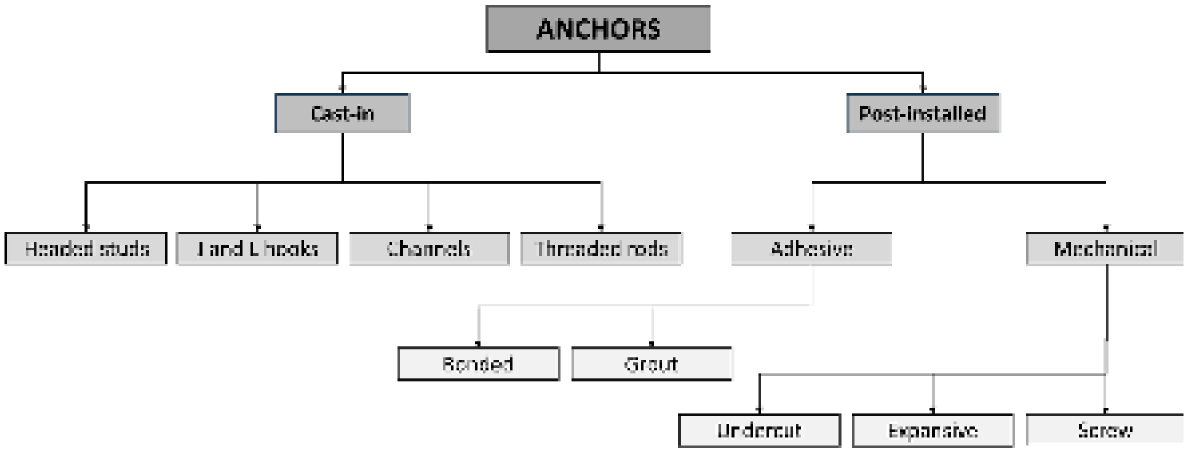

Figure 8 *Anchors classification. Source: Own.*

Cast-in-place anchors are those contemplated since design. As their name suggests, they are installed before the concrete is poured. On the contrary, post-installed anchors are positioned once concrete has already hardened.

Furthermore, the performance of fastening systems is influenced by a wide variety of factors. Firstly, their response depends of the type of stress developed on the anchor, as it could be subjected to normal or tangential stresses. Normal stresses develop from axial loads or bending moments, whereas tangential stresses are the consequence of shear loads or torsional moments.

As this research focuses on post-installed adhesive anchors subjected to shear loads, there will be a greater emphasis in detailing this type of response.

2.1.1. Normal stresses

It is evident that anchors subjected to axial forces will develop normal stresses. Also, for the fastening system to develop an adequate resistance to external bending moments, at least two rows of anchors are required. Consequently, to maintain the static equilibrium, each row of anchors is subjected to an axial force (tension or compression) that contributes to the resistant couple. According to ACI 318-19 (section 17.6) the theoretical resistance to axial loads of a single anchor or group of anchors depends on the failure mode evaluated. Thus, the capacity of the system would correspond to the most critical calculated value (ACI Committee 318, 2019). The modes of failure of bonded anchors that are contemplated in ACI 318-19 are steel failure, pullout, concrete breakout, side-face blowout, and bond failure (Figure 9):

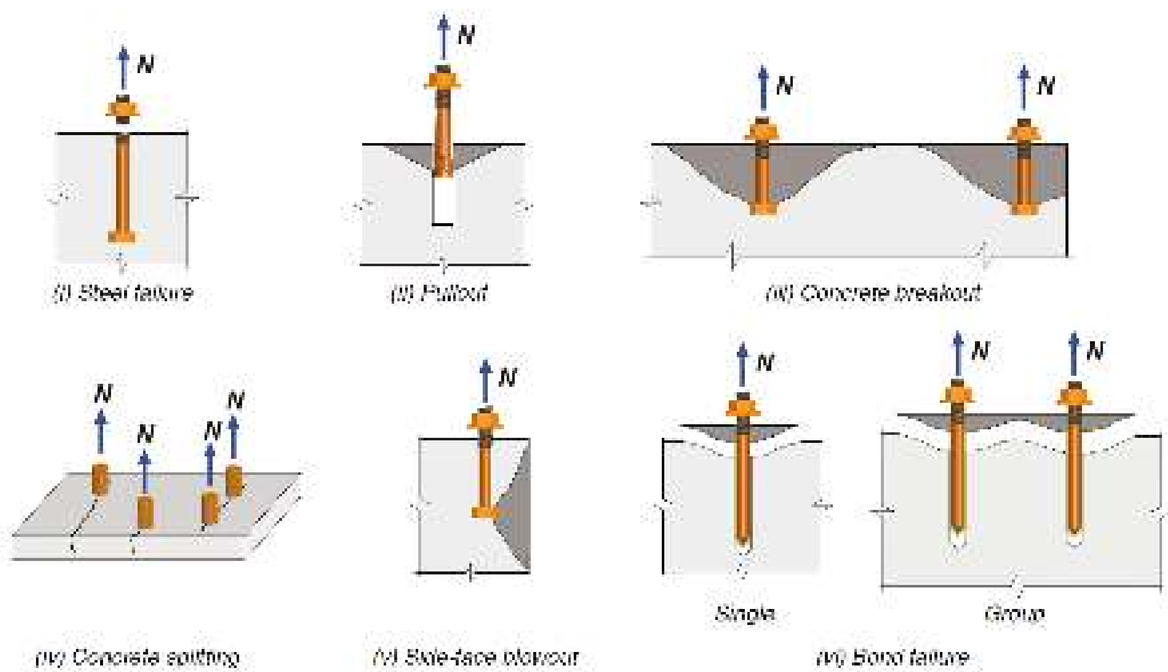

Figure 9 *Failure modes of anchors subjected to tension. Source:* (ACI Committee 318, 2019, p. 240)

2.1.2. Tangential stresses

Fastening systems have two mechanisms that contribute to resisting shear forces: dowel action and interface friction.

2.1.2.1. Dowel action.

It considers that shear is completely transferred through the cross-section area of each of the anchors that conform the connection. As the embedded part of the anchor bears against the concrete, the load is transferred between both materials. As a result, the concrete located in front of the anchor (at the region toward which the load is headed), is subjected to compressive stresses, whereas tensile stresses are prevalent at the back of the anchor. Given the low tensile resistance of concrete, as the external load increases, so does the probability of crack formation. Various equations have been proposed to account for this behavior. For instance, according to AISC 360-16 (section I8.2a.), the nominal capacity of a headed stud anchor embedded in a concrete slab or steel deck, is determined as follows (American Institute of Steel Construction, 2016):

$$\boldsymbol{Q_n = 0.5A_{sa}\sqrt{f'_c E_c} \leq R_g R_p A_{sa} f_u} \quad \text{Eq. (1)}$$

Where:

$\boldsymbol{A_{sa}}$: area of the cross-section of the headed stud.

$\boldsymbol{f'_c}$: specified concrete compressive strength.

$\boldsymbol{E_c}$: modulus of elasticity of concrete.

$\boldsymbol{f_u}$: specified minimum tensile resistance of the anchor.

$\boldsymbol{R_g}$ and $\boldsymbol{R_p}$: these parameters account for the number of anchors, their position on the rib of the deck, and the orientation of the latter with respect to the support beam. These factors only apply when steel deck is used.

Equation 1 considers the concrete breakout mode of failure on the left of the inequality, while the possibility of anchor rupture is considered in the term on the right. This equation has proved being useful in composite construction (steel and concrete), hence the inclusion of modifying factors $\boldsymbol{R_g}$ and $\boldsymbol{R_p}$. However, shear connectors employed in steel construction are usually cast-in, therefore, the approach given by AISC was not considered for this project.

In parallel, the concrete industry has also developed a theoretical basis to represent the mechanical behavior of anchors embedded in concrete. ACI 318-19 (section 17.7) provides the guidelines for the evaluation of the shear capacity of single anchors and anchor groups. Similar to the analysis when subjected to axial loads, the capacity of shear loaded anchors is computed for each failure mode, prevailing the most critical value. The failure modes contemplated in this standard are illustrated in Figure 10:

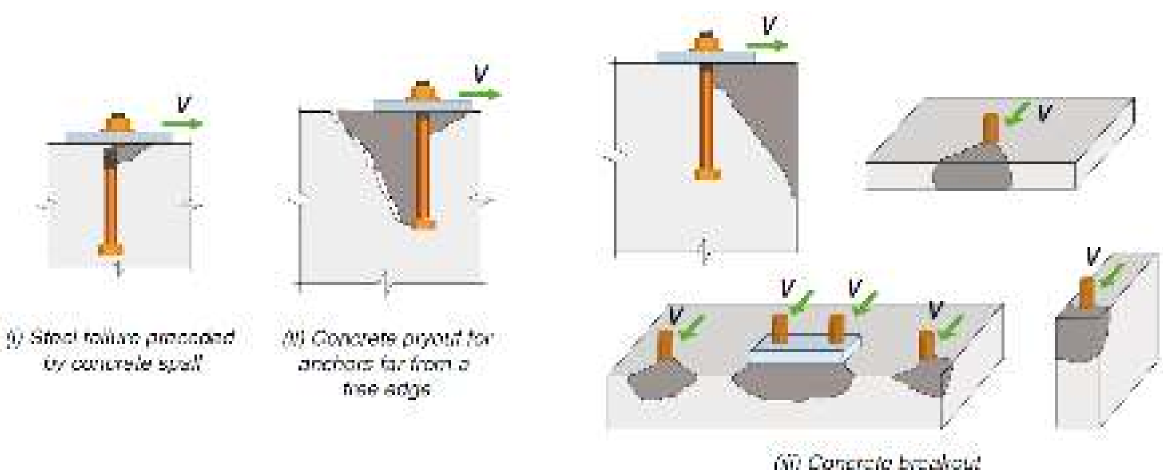

Figure 10 *Failure modes of anchors subjected to shear. Source:* (ACI Committee 318, 2019, p. 240)

- ***Steel failure***

This failure mode is entirely dependent on the material and geometrical properties of the steel that conforms the anchor. Theoretically, due to the external load, the anchor bears against the surrounding concrete. As a consequence of the limited deformation in the embedded part of the anchor, the unrestricted portion deforms in the same direction of the load, up to a point in which the material capacity is exceeded, resulting in the rupture of the anchor. The effect of this process on the concrete substrate, as well as the level of deformation attained by the anchor, are dependent on the ductility of the anchor and the mechanical properties of the concrete substrate

For cast-in headed anchors, hooked anchors, or post-installed anchors for which sleeves do not interfere with the shear plane, the shear capacity is computed as follows:

$$\boldsymbol{V_{sa} = 0.6 A_{se,V} f_{uta}} \quad \text{Eq. (2)}$$

Where:

$\boldsymbol{A_{se,V}}$: effective cross-sectional area of the shear-loaded anchor.

$\boldsymbol{f_{uta}}$: specified minimum tensile resistance of the anchor. For calculation purposes, it cannot exceed $\boldsymbol{1.9 f_{ya}}$ or $\boldsymbol{860\ MPa}$.

If a grout pad is used, the calculated nominal strength shall be multiplied by 0.80.

- ***Concrete breakout***

As the anchor bears against the concrete, the latter is subjected to tensile stresses in the region behind the anchor. The behavior of concrete in tension is dependent on the following, as reviewed by Mallée et al., pp. (2012, pp. 34–37):

- ✓ **Modulus of elasticity:** As concrete is loaded in tension, the first part of its behavior is considered linear elastic until maximum load is achieved.
- ✓ **Tensile capacity:** When stresses on concrete exceed its tensile capacity, cracks begin to form, resulting in the loss of load-bearing capacity.
- ✓ **Crack width:** In narrow cracks, mechanical interlock between both portions is the mechanism that allows for load-transfer. As the cracks widen, this effect reduces, leading to loss in capacity. Finally, if the crack is wide enough, there is no contact between both pieces, rendering them stress-free.
- ✓ **Type of aggregate:** The type, size and geometry of the aggregate have incidence on the crack trajectory. Normal weight aggregate has more strength than lightweight aggregate; therefore, in the former, cracks tend to border the aggregate, developing a longer path, which creates a larger failure surface, resulting in a less steep loss of capacity. Larger and irregular aggregates have a similar effect.

When anchors are close to an edge, a failure surface originates from their location, and propagates toward the edge, generating a concrete breakout body. The equations prescribed in ACI for this mode of failure are based in the Concrete Capacity Design (CCD) method, developed by Fuchs et al. (1995). For single anchors that support shear loads directed toward the edge, it is supposed that the failure surface resembles half of a square pyramid. One slant height of this pyramid originates at the anchor and spreads in depth with an angle close to 35° with respect to a line parallel to the anchor. The other two slant heights originate at the anchor and are supposed to spread on the surface of the member with the same angle of 35°, with respect to a line parallel to the edge. This means that on the lateral face of the concrete member, the base of this half pyramid is revealed. If the distance between the anchor and the free edge is called C_{a1}, then the measures of this failure surface are those displayed in Figure 11:

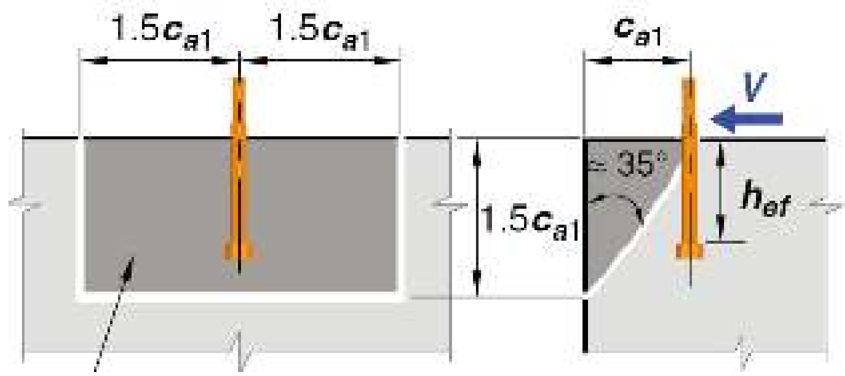

Figure 11 *Basic failure surface for concrete breakout. Source:* (ACI Committee 318, 2019, p. 265)

If the fastening system consists of various anchors, or there is proximity to other edges, or if the depth of the concrete member is insufficient, the theoretical failure surface changes correspondently, as illustrated in Figure 12:

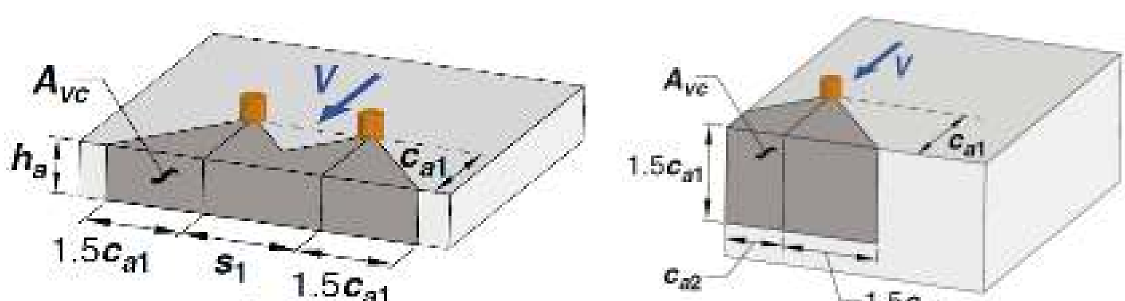

Figure 12 *Variations in the concrete breakout failure surface, due to the existence of various anchors or free edges. Source:* (ACI Committee 318, 2019, p. 266)

Considering the above, the theoretical load at which concrete breakout occurs is defined by Equation 3:

$$\boldsymbol{V_{cbg} = \frac{A_{Vc}}{A_{Vco}}\psi_{ec,V}\psi_{ed,V}\psi_{c,V}\psi_{h,V}V_b} \qquad \text{Eq. (3)}$$

Where:

$\boldsymbol{A_{Vc}/A_{Vco}}$: ratio between the actual breakout lateral area, which considers the effect of nearby anchors or free edges, and the basic failure surface lateral area.

$\boldsymbol{\psi_{ec,V}}$: accounts for eccentricities in the shear load. This parameter only applies when torsional moments are expected.

$\boldsymbol{\psi_{ed,V}}$: parameter that considers proximity to other edges.

$\boldsymbol{\psi_{c,V}}$: factor related to cracking. Its value depends on the presence or absence of supplementary reinforcement in the concrete member; as well as if the concrete surface is cracked or could crack under service conditions.

$\boldsymbol{\psi_{h,V}}$: accounts for the influence of the depth of the concrete member in which the anchor is embedded.

$\boldsymbol{V_b}$: basic single anchor breakout strength.

Thus, the nominal capacity of a single anchor or anchor group is calculated from the basic strength, which is affected by various modification factors. The basic strength of a single anchor embedded in cracked concrete is the minimum value obtained from equations 4 and 5:

$$\boldsymbol{V_b = \left(0.6\left(\frac{l_e}{d_a}\right)^{0.2}\sqrt{d_a}\right)\lambda_a\sqrt{f'_c}(c_{a1})^{1.5}} \qquad \text{Eq. (4)}$$

$$V_b = 3.7\lambda_a\sqrt{f'_c}(c_{a1})^{1.5} \qquad \text{Eq. (5)}$$

Where:

l_e: load-bearing length. For post-installed anchors, it corresponds to the minimum value between h_{ef} and $8d_a$.

d_a: anchor diameter.

λ_a: parameter that accounts for the influence of lightweight concrete.

f'_c: specified concrete compressive strength.

C_{a1}: distance from the geometric center of the anchor to the concrete edge.

- ***Concrete pryout***

This failure mode has a higher probability of occurring in regions far from any edge. If concrete pryout occurs, the ultimate capacity of an anchoring system is given by Equation 6:

$$V_{cpg} = k_{cp}N_{cpg} \qquad \text{Eq. (6)}$$

Where:

k_{cp}: depends on the anchor embedment depth.

N_{cpg}: for bonded anchors, it is the lower value between N_{cbg} and N_{ag}, which are the capacities of the anchor under tension loads, for the failure modes of concrete breakout and debonding, respectively.

2.1.2.2. Interface friction.

A commonly overlooked mechanism that participates in the load-bearing mechanism for shear loads is the friction that develops between the plate (which makes part of the anchoring system) and the concrete member on which it is supported. Considering this action would imply acknowledging that some part of the external load is taken by friction, while the other is taken by the dowel action of the fastener. Thus, not considering it leads to results that lie on the conservative side.

The friction force developed on the plate-concrete interface is calculated as follows:

$$\boldsymbol{V_n = \mu N} \qquad \text{Eq. (7)}$$

Where:

$\boldsymbol{\mu}$: Coefficient of static friction between steel and concrete.

$\boldsymbol{N}$: Normal load exerted on the steel plate. It could be generated by any action (force or moment) that makes the concrete support the plate.

The contribution of friction is considered by ACI (section 22.9) (ACI Committee 318, 2019, p. 430), as well as the Eurocode EN 1992-4:2018 (European Committee for Standardization, 2018). According to Mallée et al., p. (2012, p. 103), once the friction force is exceeded, a small displacement of the plate occurs. Then, as the plate contacts the anchor, the force is predominantly taken by the fastener, rendering any friction contribution as insignificant. The above is illustrated in Figure 13:

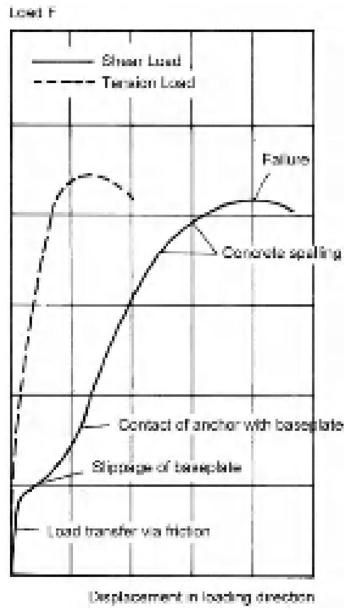

Figure 13 *Load-transfer mechanisms in shear-loaded anchors. Source:* (Mallée et al., 2012, p. 103)

2.2. Fiber-reinforced polymer (FRP)

FRP can be found in the form of bars or laminates; it can be constituted by different materials, which may include aramid, glass, carbon; and its applications range from the aviation industry to the rehabilitation of buildings. However, for this research, only the aspects related to tensile behavior of cured carbon fiber laminates (CFRP) were considered. This is because even if an anchor is subjected to a shear load, the function of the carbon fiber is to take the stresses that result from crack formation and propagation. It is the same concept that applies for steel stirrups taking shear loads of reinforced concrete members.

In this regard, the document ACI 440.2 section 12.4 addresses the design of tension-loaded FRP systems. It mentions that the strain on the laminate is critical to determine its strength, given that large strains may not be achieved due to bonding limitations. This effective strain is then associated with an effective stress, due to the linear-elastic properties of the material, and then it is computed with the force acting on the fiber, to obtain the required area of reinforcement.

Overall, as any other design, the amount of CFRP reinforcement depends on the external load taken by the laminate (which may be calculated via strut-and-tie models), and the capacity of the system. Concerning this latter aspect, ACI 440.2 establishes that the strength of a tension-loaded FRP system may be determined using the criteria for shear reinforcement. Thus, the nominal tensile capacity of the system is:

$$T_n = \psi_f A_f f_{fe} \quad \text{Eq. (8)}$$

Where:

$\boldsymbol{\psi_f}$**:** It is a reduction factor that depends on the scheme of reinforcement.

$\boldsymbol{A_f}$**:** Corresponds to the transverse area of FRP reinforcement.

$\boldsymbol{f_{fe}}$**:** It is the effective stress in the FRP at nominal strength.

The effective stress is calculated employing Hooke's Law:

$$f_{fe} = E_f \varepsilon_{fe} \qquad \text{Eq. (9)}$$

Where:

$\boldsymbol{E_f}$**:** Tensile modulus of elasticity of FRP.

$\boldsymbol{\varepsilon_{fe}}$**:** Effective strain in FRP reinforcement at failure.

For three-sided reinforcements, the effective strain is computed as follows:

$$\varepsilon_{fe} = \kappa_v \varepsilon_{fu} \leq 0.0040 \quad \text{Eq. (10)}$$

Where:

$\boldsymbol{\kappa_v}$**:** It is a bond-reduction coefficient.

$\boldsymbol{\varepsilon_{fu}}$**:** Design rupture strain of FRP.

In SI units, the bond-reduction coefficient is found per the following formula:

$$\kappa_v = \frac{\kappa_1 \kappa_2 L_e}{11\,900 \varepsilon_{fu}} \leq 0.75 \quad \text{Eq. (11)}$$

Where:

$\boldsymbol{\kappa_1}$**:** Accounts for concrete strength.

$\boldsymbol{\kappa_2}$**:** Incorporates other effects due to the scheme of reinforcement.

$\boldsymbol{L_e}$**:** Length over which most of the bond stress is maintained.

In SI units:

$$\kappa_1 = \left(\frac{f_c'}{27}\right)^{2/3} \quad \text{Eq. (12)}$$

And:

$$L_e = \frac{23\,300}{\left(n t_f E_f\right)^{0.58}} \quad \text{Eq. (13)}$$

Section 12.4 of ACI 440.2 establishes that κ_2 can be taken as 1.0 for tension-loaded FRP systems.

It is important to highlight that the design ultimate tensile strength f_{fu} and the design rupture strain ε_{fu} are obtained by affecting the values reported by the manufacturer ($f_{fu}{}^{*}$ and $\varepsilon_{fu}{}^{*}$), by the corresponding environmental reduction factor C_E, which can be found in Table 9.4 of ACI 440.2. For carbon fiber in an interior exposure setting, this factor is 0.95.

Knowing the mechanisms involved in the behavior of post-installed anchors loaded in shear, and CFRP laminates subjected to tensile stresses, it was possible to focus the literature review on investigations that addressed the strengthening of anchored connections. Thus, a state-of-the-art was elaborated.

3. STATE-OF-THE-ART

Aiming to develop a pertinent, relevant and novel project, it is essential to gather the most recent developments that cover the topic of interest. As a result, the following state-of-the-art encompasses various aspects of great utility for this work.

Bokor et al. (2020) evidenced a limitation in the applicability of current anchor design procedures, as they lack clarity in providing guidance on the behavior of group anchors arranged in a geometry different from a rectangle. As a result, the authors assessed the shear capacity of post-installed bonded anchor groups arranged in triangular, rectangular and hexagonal geometrical configurations. They used threaded anchors of 20 mm in diameter, an embedment depth of 120 mm and a specified tensile capacity of 1200 MPa. Likewise, they employed an epoxy with a bond strength of 30 MPa and concrete elements with a compressive strength of 31 MPa. It is important to note that the research focused in the shear concrete breakout capacity, with edge distances that varied between 80 mm and 240 mm.

Additionally, the test setup used in that research is presented in Figure 14. This information is of great importance, as it served as the basis for the test setup proposed in the experimental program of this document.

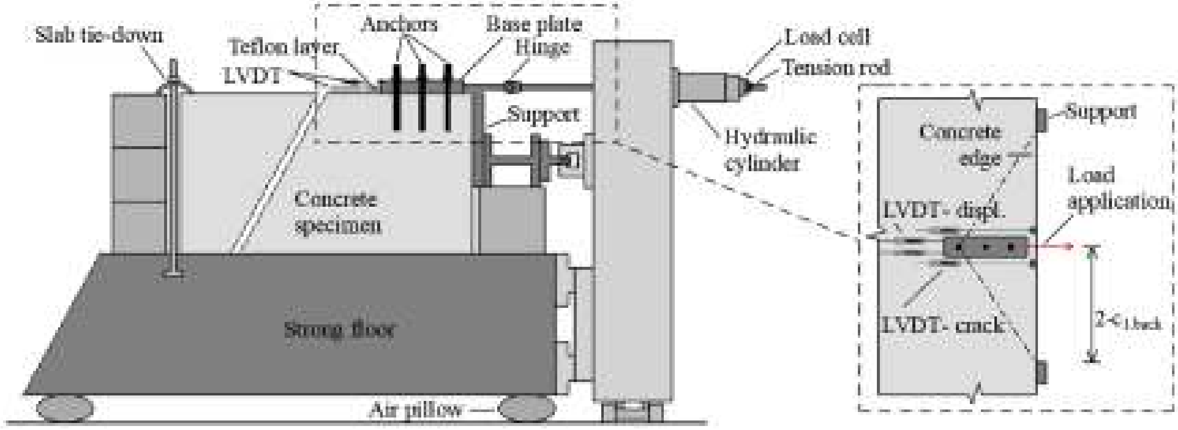

Figure 14 *Test setup for shear-loaded anchors. Source:* (Bokor et al., 2020, p. 8)

The authors found that the maximum load of single anchors could be associated with that of anchor groups, if the last row of anchors is placed with a distance to the edge equal to that of the single anchor. This demonstrates a strong correlation between the response of single and group anchors.

Beyond the test setup, Vita et al. (2022) focused on the possibility of reinforcing bonded anchors using post-installed rebars, to increase their tensile capacity. The hypothesis was that this supplementary post-installed reinforcement would take part of the external load, while mitigating crack propagation once the concrete breakout mode of failure developed. With this objective, the authors assessed the influence of using baseplates, the effect of prestressing anchors (simulating a service condition), and the incidence of the orientation of the post-installed reinforcement, as illustrated in Figure 15.

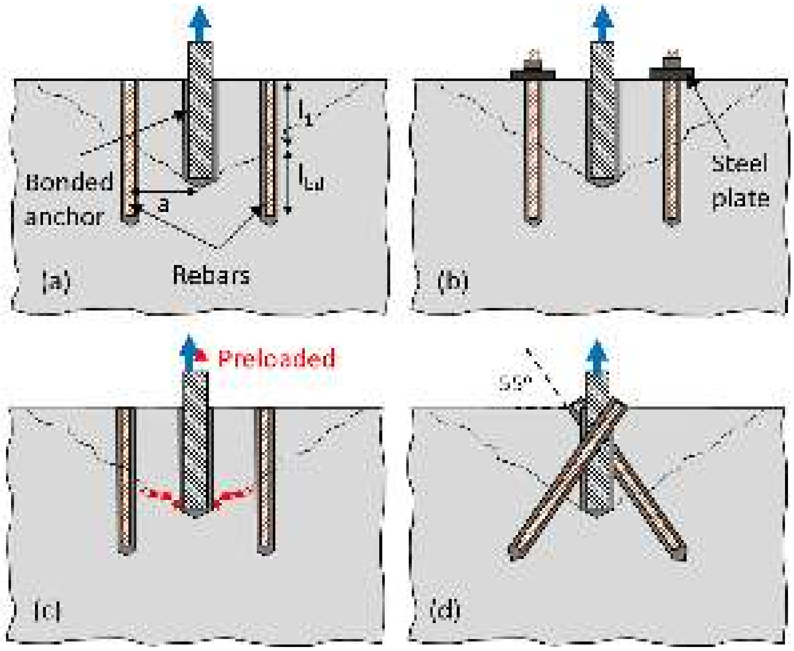

Figure 15 *Evaluated parameters. Source:* (Vita et al., 2022, p. 4)

The authors found encouraging results, as the post-installed reinforcement did increase the capacity of the anchoring system, managing to even change the failure mode to one in which concrete struts failed in compression. As a result, once the mode of failure changed, increasing the area of reinforcement did not have significant consequences on the capacity. On the other hand, they found that preloading the anchors up to 75% of their strength did not have a significant effect on the response of the anchoring system. Furthermore, the increase in capacity was accompanied by a higher ductility, as shown in Figure 16:

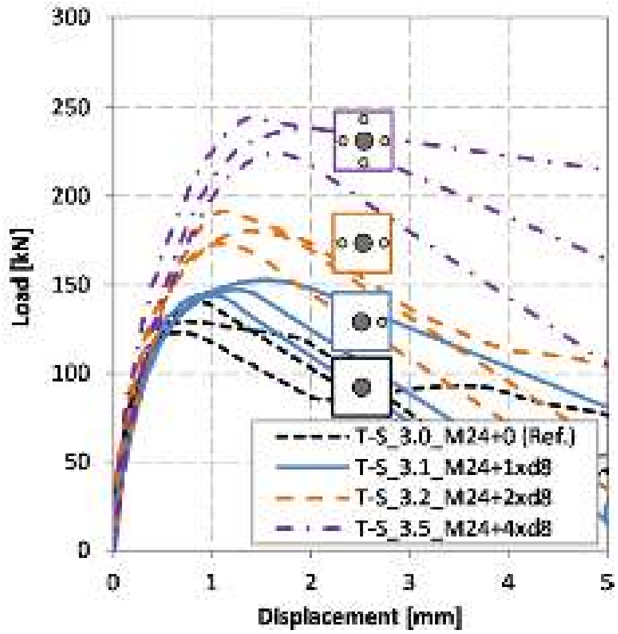

Figure 16 *Strength and ductility improvements when increasing the area of post-installed reinforcement. Source:* (Vita et al., 2022, p. 10)

This research demonstrates that there could be different alternatives for retrofitting post-installed anchors. Also, it is possible to achieve higher capacities while mitigating the probability of obtaining a brittle failure mode, such as concrete breakout.

Considering this literature review, it is evident that it is possible to propose a retrofitting alternative for post-installed anchors subjected to shear loads. The idea is to take advantage of the benefits of CFRP and use this material as if it was a post-installed external hairpin, adhered to the concrete surface so it takes the internal stresses associated with crack formation and loss of capacity. As a result of this research opportunity, an experimental program was conducted in the laboratory of structures and materials, located at Universidad Escuela Colombiana de Ingeniería Julio Garavito, in Bogota, Colombia.

4. RESEARCH OBJECTIVES

4.1. General objective

Assess the shear behavior of post-installed anchor connections strengthened with CFRP laminates, through the collection and analysis of the data obtained in the execution of an experimental program.

4.2. Specific objectives

- Investigate, through a literature review, the theoretical foundations and recent advances related to the use and response of post-installed anchors and FRP laminates, compiling the most relevant aspects in a state-of-the-art.
- Obtain, through data collection and processing, parameters associated with the response of the tested specimens, such as failure mode, ultimate capacity, energy absorption capacity, reinforcement efficacy, and load – strain behavior.
- Evaluate different strengthening configurations, identifying the nuances in their behavior, with the objective of recognizing the most effective one, according to the expected results.
- Contrast the results of CFRP-reinforced specimens, hairpin-reinforced specimens, and unreinforced specimens, emphasizing in their failure mechanism, and the advantages and disadvantages of each reinforcement alternative.

5. METHODOLOGY

The assessment of strengthened shear-loaded anchors comprises various parameters and variables that need to be understood in order to formulate an adequate experimental program. The first step in this process was consulting multiple academic sources. This involved four main objectives: recognizing the load-bearing mechanisms involved in unreinforced shear-loaded anchors; understanding the properties and behavior of fiber-reinforced polymers (FRP); getting to know the provisions detailed in current standards; and following recent investigation advances that deal with this topic.

Once this framework was established, next stage consisted of carrying out an analytical work, to identify the incidence of each parameter on the theoretical response of the fastening system. The result of this process was to select the parameters that would prove the test specimens as representative of real conditions, and that would lead to expected results.

After that, the unreinforced specimens were elaborated, tested and analyzed. This is identified as "*Phase I*" of this project. The results obtained in these control samples would become the basis for designing the conventional cast-in anchor reinforcement (hairpin), as well as the main focus of this project, which is the post-installed CFRP laminate reinforcement. The stage that involves the construction, testing and analysis of reinforced specimens, is identified as "*Phase II*".

Lastly, according to the findings of this study, some conclusions and recommendations were elaborated, to further encourage the research in this topic.

6. PHASE I – UNREINFORCED SPECIMENS

6.1. Analytical work

As the first experimental stage of this project, some parameters had to be set. First, as the idea of this study was to strengthen anchoring systems that would normally fail due to concrete breakout, the control specimens had to be elaborated so they achieved this failure mode.

Analyzing the equation related to concrete breakout capacity, the following observations were made:

- As the ratio between the effective and the basic failure surface depends on the thickness of the member and the proximity to other edges, given the wide range of possibilities, it was decided to set it to a value of 1. This means that only one edge of the concrete element would affect the response of the anchor, and that it would have enough depth so the basic failure surface could be developed. This is also evidenced in other two parameters that depend on the geometric configuration of the member.
- As only single anchors were being studied, the parameter that accounts for eccentricity of the shear load, was not considered.
- Uncracked concrete would be considered, to keep cohesion between the samples.

Finally, the basic concrete breakout strength depends on the material properties of concrete, the geometric properties of the anchor, and the most critical parameter: edge distance C_{a1}. In this regard, the election of edge distance depends on the values adopted for the other parameters. The material and geometric properties of the anchor and the concrete slab are detailed in a further section. However, it is important to highlight that their values were adopted as they are typical in real life applications.

The importance of setting those values first, is that they were necessary in the election of the concrete edge distance. As a result, considering every shear-related failure mode contemplated by ACI, the capacity of a single anchor was calculated as a function of edge distance. In this manner, it would be possible to select an adequate edge distance that ensures the concrete breakout failure mode. Figure 17 illustrates the relation between ultimate load an edge distance for the selected material and geometric properties of the specimens:

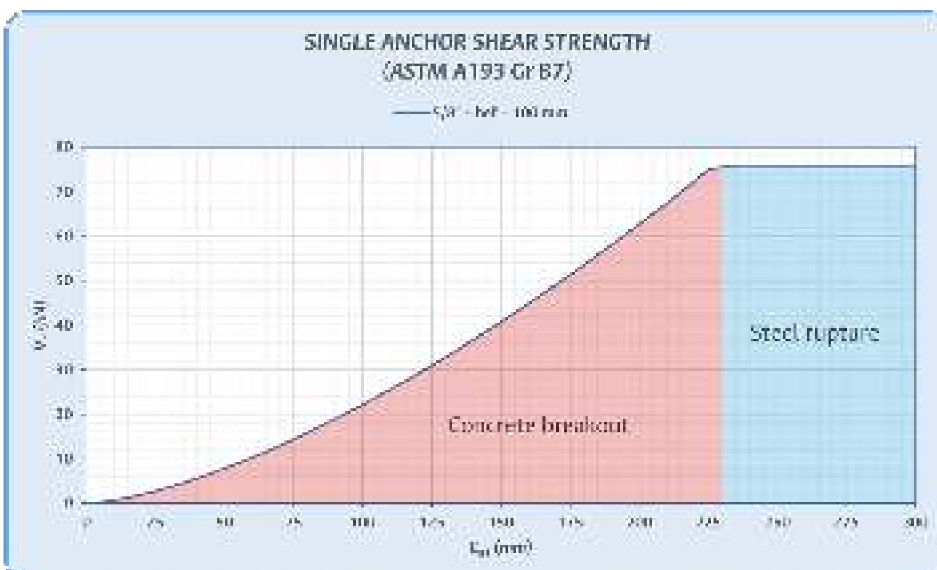

Figure 17 *Nominal strength of a single sear-loaded anchor, with respect to its distance to the edge. Source: Own.*

It is observed that as the anchor is placed farther from the edge, its capacity increases, maintaining the concrete breakout failure mode. However, in correspondence with the conditions of this study, there is a point from which the distance to the edge does not have an influence on the anchor's strength behavior. In this region, the capacity remains constant, depending only on the material and geometric characteristics of the anchor. Thus, the expected failure mode in this zone corresponds to anchor rupture.

As it was desired for control specimens to display a concrete breakout failure, two edge distances were selected: 50 mm and 100 mm. The reason behind these values is that they are common in new construction, as well as in retrofitting. For example, in balconies, railings are installed as close to the edge as possible, to maximize habitable space. Similarly, in structural rehabilitation, if a steel bracing is anchored to an existing concrete frame, it could be possible that the members that conform the frame have small dimensions; thus, the anchors need to be installed close to the edge.

The selection of these parameters, led to the development of the experimental program for unreinforced specimens, which is detailed in the following section.

6.2. Experimental program

6.2.1. Overview

A total of six (6) specimens were elaborated in total, three (3) for each edge distance. All of them were accommodated in a single concrete slab which dimensions were 2400 mm long, 800 mm wide and 300 mm thick. These dimensions guaranteed the formation of the total concrete breakout body, while preventing the intersection of cracks from different specimens.

6.2.2. Materials and properties

6.2.2.1. Reinforced concrete

6.2.2.1.1. Concrete.

A normal weight concrete with a specified compressive strength of 21 MPa (3000 psi) was used in this research.

6.2.2.1.2. Reinforcement.

The influence of rebar on the capacity of shear-loaded anchors was not within the scope of this research. Therefore, the only reinforcement of the slabs consisted of a 7 mm in diameter wire mesh with a spacing of 150 mm in both directions. The role of this wire mesh was to support the loads induced by lifting and moving the slabs, as well as for shrinkage and temperature purposes. This reinforcement was placed on the bottom of the slab, with a concrete cover of 25 mm (1 in). Due to its positioning, it would not interfere with the failure surfaces produced by testing.

6.2.2.2. Post-installed anchoring system

6.2.2.2.1. Fastening system.

The anchors consisted of threaded rods of the following specified characteristics:

- Material: ASTM A193 Grade B7.
- Tensile strength (f_{uta}): 860 MPa (125 ksi).
- Yield strength (f_{ya}): 720 MPa (105 ksi).
- Diameter (d_a): 15.9 mm (⅝ in).
- Length: 165.1 mm (6 ½ in).
- Embedment depth (h_{ef}): 100 mm (4 in)
- Pitch: 0.43 threads per millimeter (11 threads per inch).

Disclaimer: Most specimens of this investigation were elaborated with a first batch of anchors that complied with the aforementioned mechanical properties. However, during an additional test stage (that belongs to phase II of this project), a new batch of anchors was received. At the moment of testing these new threaded rods, their mechanical properties did not achieve the minimum values required for ASTM A193 Gr B7 steel. Yet, it was decided to use these anchors for those final tests. For an appropriate identification, specimens that belonged to the first batch of anchors are not marked, whereas anchors that incorporated the second type of steel are marked with a star (*). This difference is reminded to the reader each time one of these specimens is analyzed.

The mechanical properties of the second batch of anchors are listed below. The geometric characteristics of both batches of anchors were, however, the same:

- Tensile strength (f_{uta}^{*}): 761 MPa (110 ksi).
- Yield strength (f_{ya}^{*}): 709 MPa (103 ksi).

To securely fasten each anchor to the test setup, a hexagonal nut (ASTM A194 Grade 2H) and a structural washer (ASTM F436) were employed.

6.2.2.2.2. Epoxy.

A two-part injectable epoxy adhesive was used to bond the threaded rods to the concrete.

6.2.2.2.3. Installation procedure.

The installation of the anchors was done by certified technicians, following the recommendations given in the technical specifications of the epoxy. Figure 18 illustrates this process.

Figure 18 *Installation of a bonded anchor. Source: Own.*

6.2.3. Instrumentation and equipment

6.2.3.1. Steel plate

It was used to transfer the external load to the anchor through shear.

- Material: ASTM A572 Grade 50.
- Dimensions: PL 100 x 150 x 15.9 mm (PL 4 x 6 x 5/8 in).

6.2.3.2. Hydraulic jack

A 300 kN hydraulic jack was employed to generate the external shear load (Figure 19):

Figure 19 *Hydraulic jack used for testing. Source: Own.*

6.2.3.3. Load cell

Force values were collected continuously in time by a load cell with a capacity of 500 kN.

6.2.3.4. LVDTs

A total of five (5) LVDTs were used to register the displacements in various points of the setup, as illustrated in Figure 20. The data was collected with a frequency of 0.1 Hz.

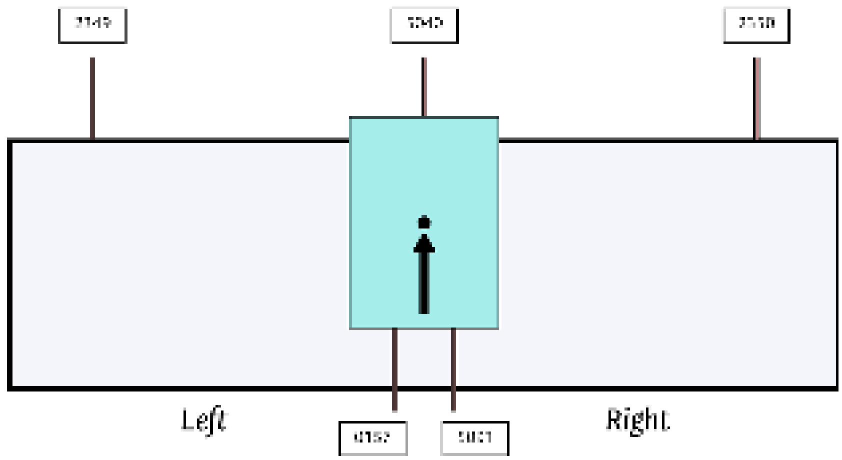

Figure 20 *LVDTs placement. Source: Own.*

LVDTs 0157 and 5091 measured the displacement of a metallic angle attached to the steel plate. The information collected by these instruments represented the anchor displacement. LVDT 5040 was placed on the lateral side of the slab, in the line of action of the external load, at mid-height of the slab. It collected data regarding the formation of breakout bodies. Finally, LVDTs 2349 and 2350 measured the overall displacement of the slab; their data verified that all displacements were relative to the position of the slab.

6.2.4. Test setup

The setup consisted of a hydraulic jack connected to the steel plate through a metallic rod that passed through a reaction wall 1500 mm thick. The concrete slab was positioned over a concrete element 650 mm thick, leaving an air pocket to simulate an isolated member. This slab was also supported in two points on the reaction wall. A lateral view of the test setup is displayed in Figure 21, while an overall schematic view of the slab that contained the unreinforced specimens is shown in Figure 22:

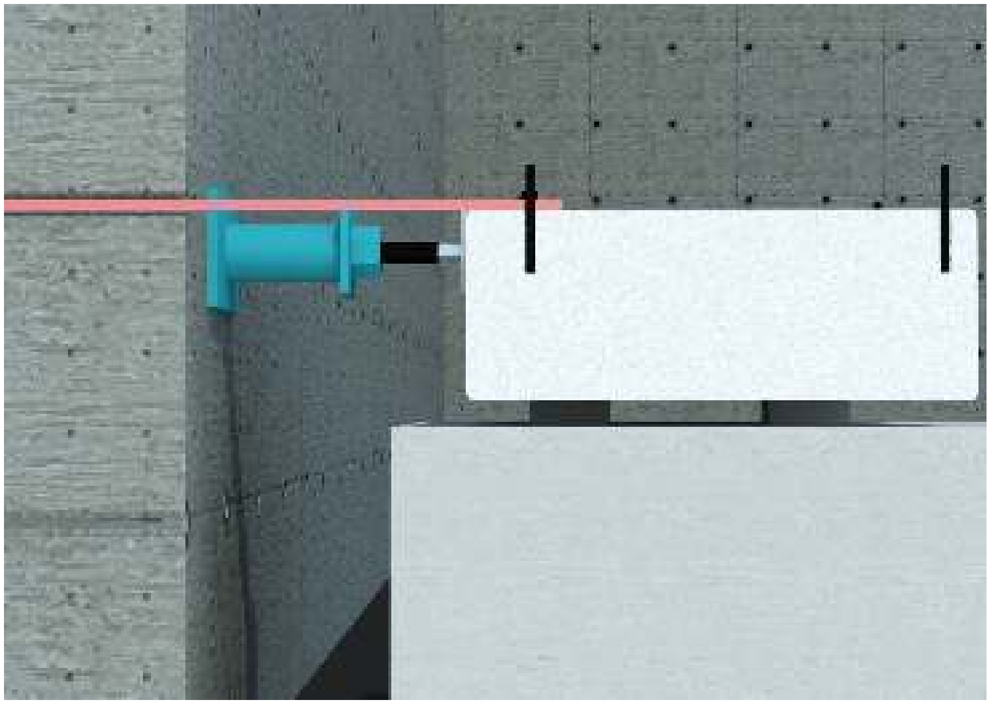

Figure 21 *Schematic representation of a tested slab. Source: Own.*

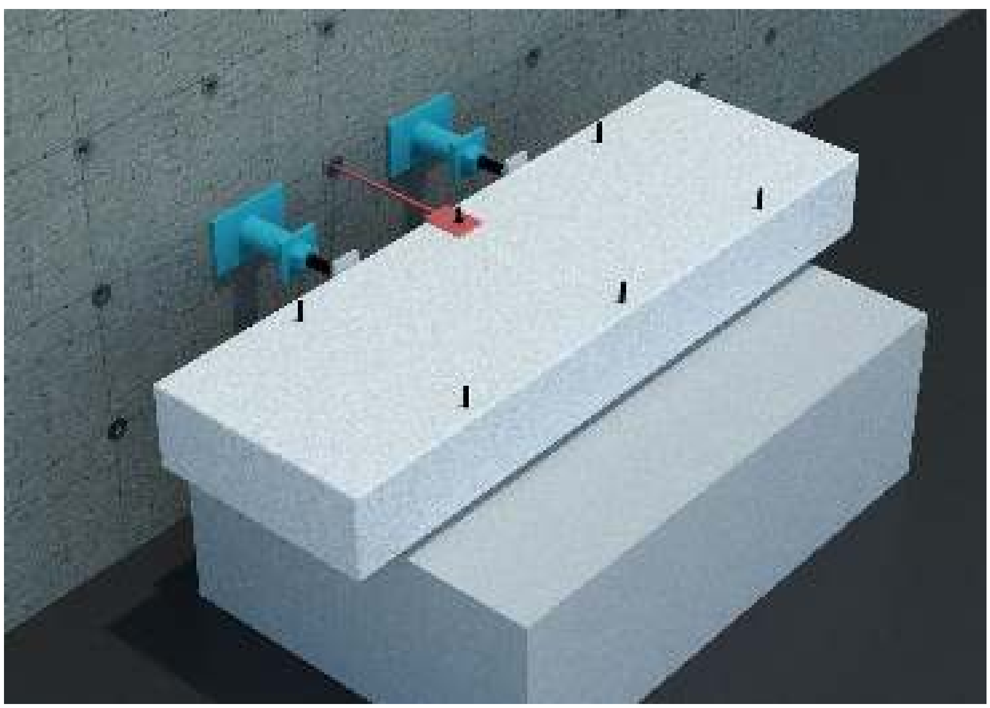

Figure 22 *Schematic representation of a slab containing unreinforced specimens. Source: Own.*

6.2.5. Labeling

All unreinforced specimens were labeled using the following format:

C0 – YY – Z

Where:

C0: Indicates that the specimen belongs to the control unreinforced samples.

YY: Edge distance.

- **50:** 50 mm distance from the center of the anchor to the edge of the slab.
- **100:** 100 mm distance from the center of the anchor to the edge of the slab.

Z: Specimen identification.

- **A:** Specimen 1.
- **B:** Specimen 2.
- **C:** Specimen 3.

6.2.6. Test matrix

The specimens tested in this phase of the experimental program are presented in Table 2:

Table 2 *Phase I specimens. Source: Own.*

PHASE I SPECIMENS		
Type	**Edge distance**	
	100 mm	***50 mm***
C0	*C0 – 100 – A*	*C0 – 50 – A*
	C0 – 100 – B	*C0 – 50 – B*
	C0 – 100 – C	*C0 – 50 – C*

6.2.7. Test conditions

- Relative humidity: 41% – 57%
- Temperature: 17 °C – 22 °C
- Load rate: 245 N/s – 363 N/s

6.3. Theoretical values

For comparison purposes, the theoretical values associated with every contemplated failure mode were calculated for each edge distance, according to the provisions given in ACI 318.

6.3.1. Edge distance: 100 mm

6.3.1.1. Concrete breakout strength (CB – 100)

The theoretical breakout strength predicted for single anchors located at 100 mm from the edge is 22.17 kN (Table 3):

Table 3 *Concrete breakout associated load (100 mm). Source: Own.*

CONCRETE BREAKOUT (SHEAR)	
Parameters	
Direction	Perpendicular
A_{Vc} (mm^2)	45000
A_{Vco} (mm^2)	45000
Factors	
A_{Vc}/A_{Vco}	1.00
$\psi_{ec,V}$	1.00
$\psi_{ed,V}$	1.00
$\psi_{c,V}$	1.40
$\psi_{h,V}$	1.00
V_b (kN)	15.84
Nominal strength	
V_{cb} (kN)	22.17

6.3.1.2. Concrete pryout strength (CP – 100)

Although concrete pryout is a mode of failure related to shear loads, its calculation depends on the tension-related concrete breakout and bond strength limit states. Once again, considering the geometric properties, as well as the adherence attributes given by the epoxy, for a distance to the edge of 100 mm, the concrete pryout failure mode would theoretically happen at a load of 51.55 kN (Table 4):

Table 4 *Concrete pryout associated load (100 mm). Source: Own.*

CONCRETE BREAKOUT (TENSION)	
Parameters	
k_c	10
A_{Nc} (mm^2)	75000
A_{Nco} (mm^2)	90000
Factors	
A_{Nc}/A_{Nco}	0.83
$\psi_{ec,N}$	1.00
$\psi_{ed,N}$	0.90
$\psi_{c,N}$	1.00
$\psi_{cp,N}$	0.75
N_b (kN)	45.83
Nominal strength	
N_{cb} (kN)	25.78

BOND STRENGTH (TENSION)	
Parameters	
c_{Na} (mm)	205
A_{Na} (mm^2)	124911
A_{Nao} (mm^2)	167876
Factors	
A_{Na}/A_{Nao}	0.74
$\psi_{ec,Na}$	1.00
$\psi_{ed,Na}$	0.85
$\psi_{cp,Na}$	1.00
N_{ba} (kN)	63.02
Nominal strength	
N_a (kN)	39.69

CONCRETE PRYOUT (SHEAR)	
Parameters	
k_{cp}	2.0
N_{cp} (kN)	25.78
Nominal strength	
V_{cp} (kN)	51.55

6.3.1.3. Anchor shear strength (SR)

Finally, steel rupture only depends on the anchor properties, resulting in a value of 75.51 kN for the first batch of anchors and of 66.82 kN for the second batch (Table 5):

Table 5 *Steel rupture associated loads (100 mm). Source: Own.*

STEEL RUPTURE (SHEAR)	
Type	Adhesive
f_{uta} (MPa)	860
d_a (mm)	15.9
n_t (/mm)	0.43
A_{se} (mm^2)	146
Nominal strength	
V_{sa} (kN)	75.51

STEEL RUPTURE* (SHEAR)	
Type	Adhesive
f_{uta} (MPa)	761
d_a (mm)	15.9
n_t (/mm)	0.43
A_{se} (mm^2)	146
Nominal strength	
V_{sa} (kN)	66.82

6.3.2. Edge distance: 50 mm

6.3.2.1. Concrete breakout strength (CB – 50)

On the other hand, for anchors located at 50 mm to the edge, the calculated concrete breakout strength value was 7.84 kN (Table 6):

Table 6 *Concrete breakout associated load (50 mm). Source: Own.*

CONCRETE BREAKOUT (SHEAR)	
Parameters	
Direction	Perpendicular
A_{Vc} (mm^2)	11250
A_{Vco} (mm^2)	11250
Factors	
A_{Vc}/A_{Vco}	1.00
$\psi_{ec,V}$	1.00
$\psi_{ed,V}$	1.00
$\psi_{c,V}$	1.40
$\psi_{h,V}$	1.00
V_b (kN)	5.60
Nominal strength	
V_{cb} (kN)	7.84

6.3.2.2. Concrete pryout strength (CP – 50)

For 50 mm specimens, concrete pryout would theoretically happen at a load of 36.66 kN (Table 7):

Table 7 *Concrete pryout associated load (50 mm). Source: Own.*

CONCRETE BREAKOUT (TENSION)	
Parameters	
k_c	10
A_{Nc} (mm^2)	60000
A_{Nco} (mm^2)	90000
Factors	
A_{Nc}/A_{Nco}	0.67
$\psi_{ec,N}$	1.00
$\psi_{ed,N}$	0.80
$\psi_{c,N}$	1.00
$\psi_{cp,N}$	0.75
N_b (kN)	45.83
Nominal strength	
N_{cb} (kN)	18.33

BOND STRENGTH (TENSION)	
Parameters	
c_{Na} (mm)	205
A_{Na} (mm^2)	104121
A_{Nao} (mm^2)	167876
Factors	
A_{Na}/A_{Nao}	0.62
$\psi_{ec,Na}$	1.00
$\psi_{ed,Na}$	0.77
$\psi_{cp,Na}$	1.00
N_{ba} (kN)	63.02
Nominal strength	
N_a (kN)	30.31

CONCRETE PRYOUT (SHEAR)	
Parameters	
k_{cp}	2.0
N_{cp} (kN)	18.33
Nominal strength	
V_{cp} (kN)	36.66

6.3.2.3. Anchor shear strength (SR)

The strength of the anchor does not vary with edge distance; thus, the values remain for both anchor batches (Table 8):

Table 8 *Steel rupture associated loads. Source: Own.*

STEEL RUPTURE (SHEAR)	
Type	Adhesive
f_{uta} (MPa)	860
d_a (mm)	15.9
n_t (/mm)	0.13
A_{se} (mm^2)	146
Nominal strength	
V_{sa} (kN)	75.51

STEEL RUPTURE* (SHEAR)	
Type	Adhesive
f_{uta} (MPa)	761
d_a (mm)	15.9
n_t (/mm)	0.13
A_{se} (mm^2)	146
Nominal strength	
V_{sa} (kN)	66.82

6.3.3. Overall values

It is observed that for anchors located closer to the edge, concrete breakout and concrete pryout would theoretically occur at a lower load than if they were placed farther from the edge. The summary of these values is presented in Table 9, as well as the abbreviation for failure modes that will be used for this document.

Table 9 *Modes of failure and their correspondent theoretical loads. Source: Own.*

Mode of failure	ID	Nominal strength (kN)	
		C_{a1} = 100 mm	C_{a1} = 50 mm
Concrete breakout	***CB***	22.17	7.84
Concrete pryout	***CP***	51.55	36.66
Steel rupture	***SR***	75.51	75.51
Steel rupture*	***SR****	66.82	66.82

6.4. Experimental results and analysis

6.4.1. Control specimens

6.4.1.1. C0 – 100

- ***Strength and failure mode***

Information associated with ultimate strength and failure mode of specimens installed at a distance of 100 mm to the edge, is presented in Table 10:

Table 10 *Strength and failure mode C0 – 100. Source: Own.*

STRENGTH & FAILURE MODE C0 – 100					
Specimen	**V_u (kN)**	**Avg. V_u (kN)**	**V_u / $V_{Theo.}$**	**Avg. V_u / $V_{Theo.}$**	**Failure mode**
A	35.02	35.64	1.58	1.61	***CB***
B	36.79		1.66		***CB***
C	35.12		1.58		***CB***

First and foremost, it is evident that all specimens displayed the expected mode of failure (concrete breakout). Nevertheless, their experimental capacity exceeded the calculated one, on average, in 61%. Recalling that no strength reduction factors were employed, these values represent the margin of safety involved in anchor design. The coefficient of variation of these results is 2.3%, which demonstrates an acceptable reliability.

On the other hand, Figure 23 evidences the load – displacement behavior of the tested specimens:

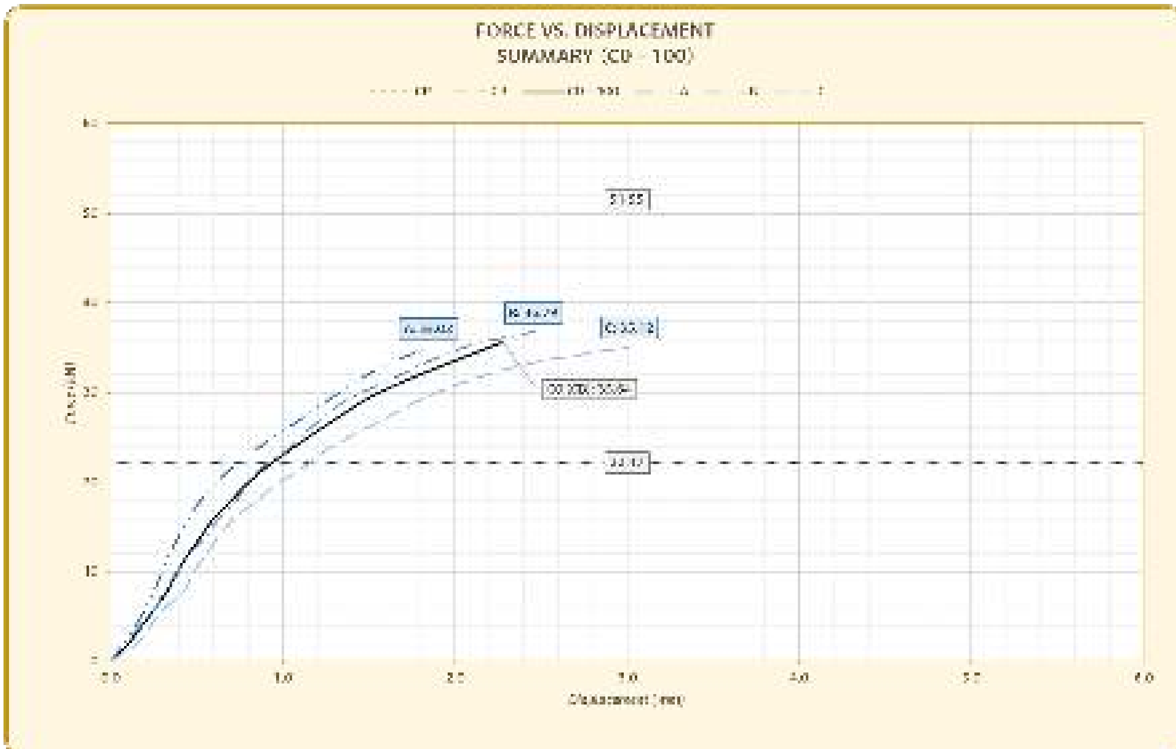

Figure 23 *Force vs. displacement C0 – 100. Source: Own.*

Clearly, the three curves follow similar paths, reaching failure at a similar load. The degradation of stiffness observed in the curves is attributed to the crack formation process, which is explained in further detail in the "*Failure mechanism*" section.

- ***Energy absorption***

Total energy absorbed by each specimen was calculated as the area below the load – displacement curve. The results are summarized in Table 11:

Table 11 *Absorbed energy C0 – 100. Source: Own.*

ABSORBED ENERGY C0 – 100		
Specimen	**W_u (J)**	**Avg. W_u (J)**
A	41.3	56.7
B	58.7	
C	70.0	

These values serve as reference for analyzing the increase in energy absorption for strengthened specimens. An increase in dispersion is evidenced in these values, in comparison to capacity results, with a coefficient of variation of 21%. This is attributed to the fact that energy absorption is linked to achieved displacements. As crack formation is a process that varies for each specimen, this effect is evidenced in its absorbed energy value.

- ***Failure mechanism***

As mentioned before, all specimens demonstrated concrete breakout. Moreover, the load – displacement curves displayed a progressive loss in rigidity of the specimens. This behavior was attributed to the process of crack formation. As cracks propagate, less concrete surface can support the internal stresses transferred by the anchor, overloading the remaining load-bearing surface. Also, narrow cracks can only transfer load via interlocking; it these cracks widen, this interlocking mechanism is no longer possible, resulting in a further reduction of rigidity, and therefore, in the total formation of the concrete breakout body. This type of failure is sudden and brittle, as no significant time passes since the formation of observable cracks, to the failure of the anchor.

Figure 24 shows the crack formation process while specimen A was being tested:

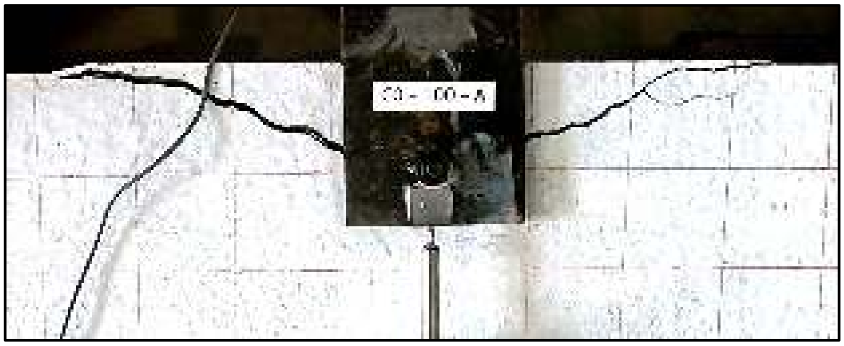

Figure 24 *Crack formation C0 – 100 – A. Source: Own.*

Furthermore, Figure 25 shows the failure surface after specimen A reached failure:

Figure 25 *Failure surface C0 – 100 – A. Source: Own.*

It is possible to affirm that the slab thickness was optimal, as its depth did not affect the total formation of the concrete breakout body.

On the other hand, Figure 26 shows the concrete breakout body and the final state of the anchor that corresponded to specimen A:

Figure 26 *Concrete breakout body C0 – 100 – A. Source: Own.*

It was decided to measure the angles in which the cracks propagated on the top surface of the concrete, to corroborate them with the theoretical 35° angle adopted by the CCD method. Part of the crack orientation analysis for specimen A is illustrated in Figure 27:

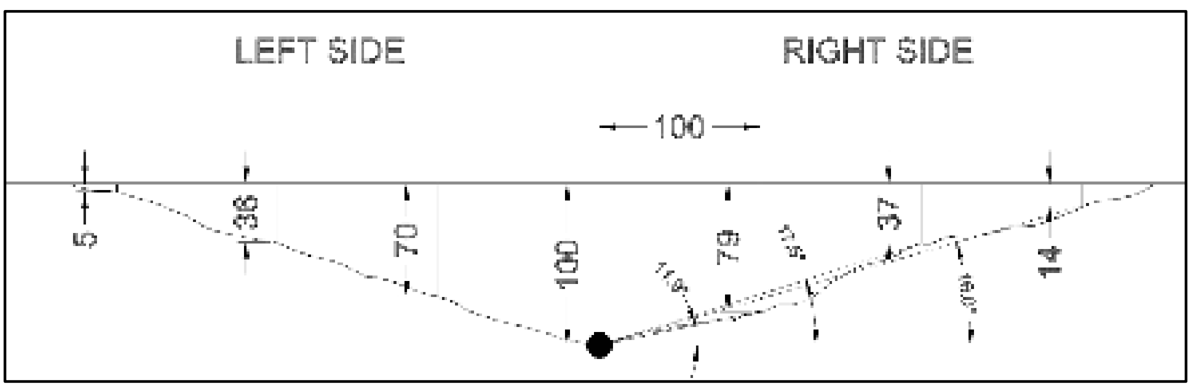

Figure 27 *Crack orientation analysis C0 – 100 – A. Source: Own.*

Each 100 mm, the distance from the edge to the crack was measured. After that, the angle of the cracks was calculated considering horizontal dimensions that increased in intervals of 100 mm. Then, the resulting angles were averaged. For specimen A, this analysis is shown in Table 12:

Table 12 *Crack orientation analysis C0 – 100 – A. Source: Own.*

CRACK ORIENTATION ANALYSIS C0 – 100 – A			
Measurement	**Left side**	**Right side**	**Average per measurement**
Each 100 mm	17.6°	15.9°	*16.7°*
Each 200 mm	17.9°	17.7°	*17.8°*
Each 300 mm	17.6°	16.0°	*16.8°*
Average per side	*17.7°*	*16.5°*	**17.1°**

As a result, the average crack angle for specimen A was 17.1°. This process was repeated for specimens B and C. The results obtained from the analysis of the three breakout bodies are shown in Table 13:

Table 13 *Crack orientation analysis C0 – 100. Source: Own.*

CRACK ORIENTATION ANALYSIS C0 – 100	
Specimen	**Average angle**
C0 – 100 – A	17.1°
C0 – 100 – B	17.5°
C0 – 100 – C	15.3°
C0 – 100	**16.6°**

Therefore, an experimental angle of 17° was obtained for control specimens with anchors placed at 100 mm from the edge. This angle is approximately half of the theoretical angle of failure adopted by the CCD method. The fact that the experimental angle is lower implies that the crack must travel a longer distance to reach the edge of the member. Consequently, more concrete surface participates in the load-bearing mechanism, which contributes to explain why the experimental ultimate loads were higher than the theoretical ones.

6.4.1.2. C0 – 50

- ***Strength and failure mode***

The strength and failure mode results collected from anchors located at 50 mm from the edge, are presented in Table 14:

Table 14 *Strength and failure mode C0 – 50. Source: Own.*

STRENGTH & FAILURE MODE C0 – 50					
Specimen	**V_u (kN)**	**Avg. V_u (kN)**	**V_u / $V_{Theo.}$**	**Avg. V_u / $V_{Theo.}$**	**Failure mode**
A	12.56	13.28	1.60	1.69	***CB***
B	12.85		1.64		***CB***
C	14.42		1.84		***CB***

Similar to the 100 mm specimens, all 50 mm specimens evidenced concrete breakout, with an average experimental ultimate load 69% higher than the theoretical one. In this case, the safety margin given by the concrete breakout equations is slightly larger than for the specimens installed farther from the edge. However, given that the coefficient of variation increased as well, with a value of 6.2%, it is possible that this increased safety margin is not representative.

Moreover, Figure 28 shows the load – displacement curves of C0 – 50 specimens:

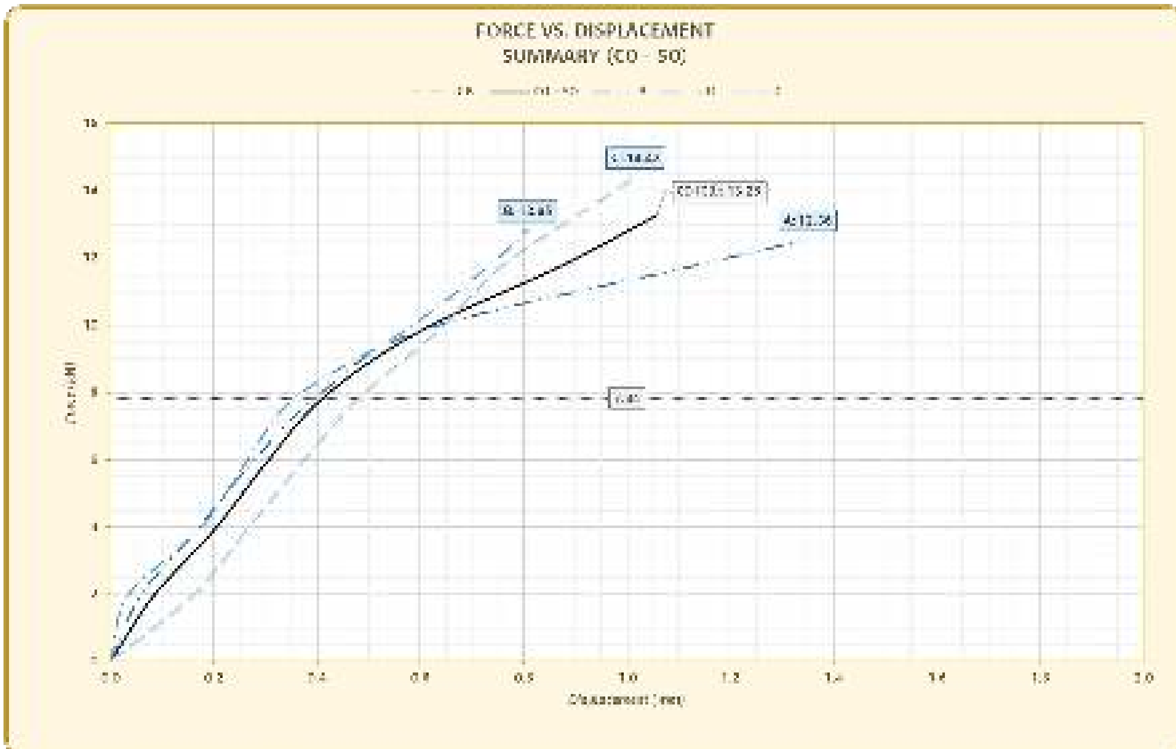

Figure 28 *Force vs. displacement C0 – 50. Source: Own.*

It is observed that for these specimens, the behavior is almost linear in its entirety. This could be attributed to the fact that as the anchors are located closer to the edge, the failure mechanism occurs faster. Therefore, as cracks do not have enough time to transfer stresses through mechanical interlocking, this nonlinear behavior is not significantly displayed in the response of the specimens. In conclusion, this type of concrete breakout failure is more sudden and brittle than that observed in the configuration at 100 mm to the edge.

- ***Energy absorption***

Regarding energy absorption capacity, the results are summarized in Table 15:

Table 15 *Absorbed energy C0 – 50. Source: Own.*

ABSORBED ENERGY C0 – 50		
Specimen	**W_u (J)**	**Avg. W_u (J)**
A	12.0	8.63
B	6.11	
C	7.83	

As a result of the process described in the "*Strength and failure mode*" section, the absorbed energy of these specimens was significantly lower in comparison to 100 mm specimens. This is, the average ultimate load of 50 mm specimens was 37% of that of the 100 mm specimens. In parallel, the average energy absorbed by configuration C0 – 50 was 15% of the energy absorbed by C0 – 100 samples. This evidences that the nuances in the response of shear-loaded anchors are deeply related to their failure mechanism, especially, the process that involves crack formation.

- ***Failure mechanism***

Most of the details related to the failure mechanism of these specimens have been discussed in the previous sections, this section will evidence the state of the specimens after failure, as well as the crack orientation analysis. Figure 29 shows the breakout body of specimen A:

Figure 29 *Concrete breakout body C0 – 50 – A. Source: Own.*

On the other hand, the crack orientation analysis for specimens situated at 50 mm from the edge, is exhibited in Table 16:

Table 16 *Crack orientation analysis C0 – 50. Source: Own.*

CRACK ORIENTATION ANALYSIS C0 – 50	
Specimen	**Average angle**
C0 – 50 – A	20.4°
C0 – 50 – B	26.3°
C0 – 50 – C	22.6°
C0 – 50	**23.1°**

It is of great significance that the average angle orientation for the 50 mm specimens (23°) was higher than for the 100 mm specimens (17°). First, it shows that crack angle is not a variable that follows always the same tendency. With these results, it is demonstrated that crack angle is dependent on the location of the anchor, as it would seem that the closer the angle is from the edge, the steeper the cracks become. Also, a higher angle implies a shorter trajectory from the anchor to the edge. This means less load-bearing surface and less energy absorption capacity. Overall, these crack trajectory results explain why the behavior of these anchors was more brittle than the 100 mm one.

7. PHASE II – REINFORCED SPECIMENS

7.1. Experimental program

In this case, the experimental program is presented before the analytical work, so the labeling of the specimens is already known when addressing the design of the cast-in and post-installed reinforcement systems.

7.1.1. Overview

In this phase, a total of 32 anchors were tested, 16 for each edge distance typology. Of the total of anchors tested for each edge distance, three (3) corresponded to hairpin-reinforced specimens, while the other 13 were strengthened with CFRP laminates. For this purpose, eight (8) concrete slabs were constructed. Their dimensions were the same as for phase I (2400 x 800 x 300 mm).

7.1.2. Materials and properties

The basic material properties mentioned in phase I were the same for phase II. It should be pointed out that this phase used some anchors constituted by the second type of steel. The new material properties listed in this phase correspond to the type of anchor reinforcement employed. These are described in the following sections.

7.1.2.1. Cast-in anchor reinforcement

7.1.2.1.1. Hairpin.

Hairpins consisted of a deformed reinforcement bar of the following specified characteristics:

- Material: ASTM A706 Grade 60.
- Specified tensile strength (f_u): 550 MPa (80 ksi).
- Specified yield strength (f_y): 420 MPa (60 ksi).
- Nominal diameter: 12.7 mm (1/2 in).
- Length: 750 mm (29.5 in).

7.1.2.1.2. *Installation procedure.*

The installation of hairpins involved great attention to detail. As reviewed in the theoretical framework, the response of hairpin-reinforced anchors depends on great measure, of the quality of the installation. Minimum top cover of 25 mm (1 in) was guaranteed, as well as contact between the anchor and the specimen. It was also verified that the hairpin was leveled within the concrete mass. Evidence of this work is illustrated in Figures 30 and 31:

Figure 30 *Hairpin installation to guarantee contact with the anchor. Source: Own.*

Figure 31 *Hairpin installation guaranteeing minimum concrete cover. Source: Own.*

7.1.2.2. Post-installed anchor reinforcement

7.1.2.2.1. CFRP laminates.

Cured laminate properties for the CFRP laminates used are displayed in Table 17:

Table 17 *Cured properties of CFRP laminates. Source: Own.*

Cured laminate property	Average values	Design values
Tensile strength	1241 MPa (180 ksi)	1068 MPa (155 ksi)
Modulus of elasticity	98 181 MPa (14 240 ksi)	96 527 MPa (14 000 ksi)
Elongation	1.27%	1.10%
Thickness	2.03 mm (0.08 in)	

7.1.2.2.2. Epoxy.

A two-part epoxy adhesive was used for bonding the CFRP laminates to the concrete substrate. It was verified that the epoxy and the laminates were compatible, to guarantee a proper bond, and to achieve an appropriate mix design, due to its use as primer, filler, and saturant.

7.1.2.2.3. Installation procedure.

All CFRP laminates were installed by certified technicians, following the procedures recommended by the manufacturer and exercising good practice techniques (Figures 32 and 33):

Figure 32 *Application of filling putty to guarantee uniformity of the concrete region in contact with the CFRP. Source: Own.*

Figure 33 *CFRP installation. Source: Own.*

7.1.3. Instrumentation and equipment

All instruments and equipment used in phase II were the same as in phase I. The only additional instrumentation corresponded to strain gauges.

7.1.3.1. Strain gauges

Various 10 mm long quarter bridge strain gauges were used for measuring the unit strains on the CFRP laminates. Their data was collected by a recording system and then analyzed correspondently.

7.1.4. Test setup

The test setup for phase II had no changes with respect to that employed in phase I. A schematic view of a slab containing reinforced specimens is shown in Figure 34:

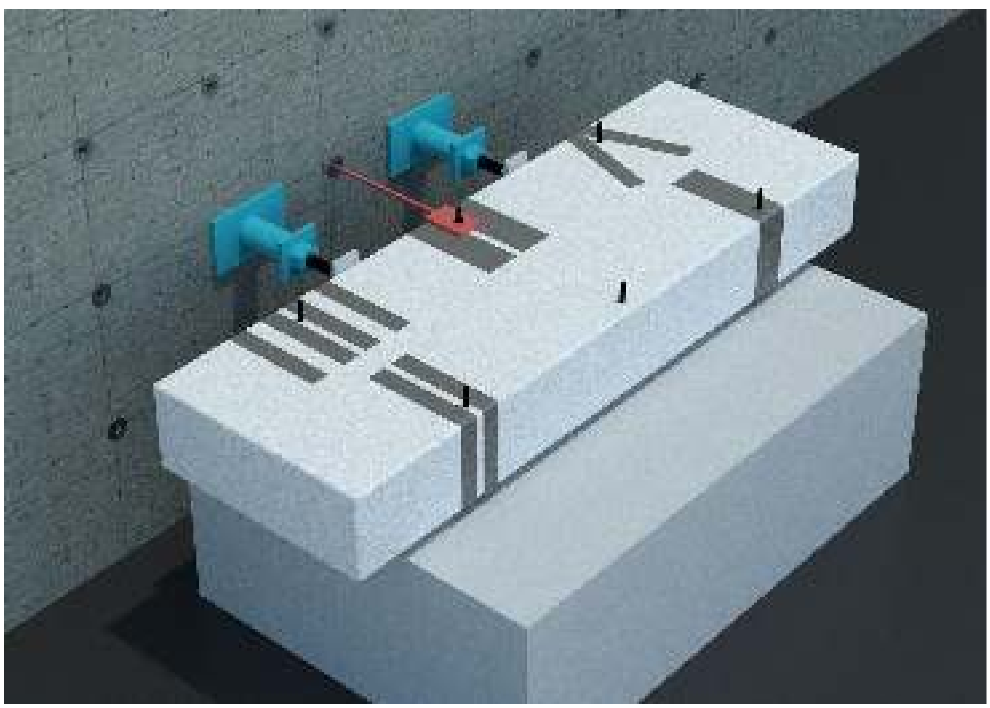

Figure 34 *Schematic representation of a slab containing reinforced specimens. Source: Own.*

7.1.5. Labeling

All **hairpin-reinforced** specimens were labeled using the following format:

CH – YY – Z

Where:

CH: Indicates that the specimen uses cast-in anchor reinforcement (hairpin).

YY: Edge distance.

- **50:** 50 mm distance from the center of the anchor to the edge of the slab.
- **100:** 100 mm distance from the center of the anchor to the edge of the slab.

Z: Specimen identification.

- **A:** Specimen 1.
- **B:** Specimen 2.
- **C:** Specimen 3.

On the other hand, all **CFRP-reinforced** specimens were labeled using the following format:

RV – W – X – YY – Z

Where:

R: Indicates that the anchor is reinforced with CFRP laminates.

V: Corresponds to the number of CFRP laminates installed on each side of the anchor.

- **0:** No individual laminates were installed on each side. A single laminate was employed to cover the entire reinforcement surface, allowing the passage of the anchor through the fiber.
- **1:** One laminate on each side.
- **2:** Two laminates on each side.

W: Related to the width of each laminate, in inches.

- **2.5:** CFRP laminates 2.5 in (64 mm) wide.
- **5:** CFRP laminates 5.0 in (127 mm) wide.

X: Refers to a particular reinforcement configuration. If this part does not appear in the label, it means that the specimen does not belong to this reinforcement scheme.

- **X:** The specimen belongs to the X reinforcement scheme.

YY: Edge distance.

- **50:** Distance from the centerline of the anchor to the edge of 50 mm.
- **100:** Distance from the centerline of the anchor to the edge of 100 mm.

Z: Specimen identification.

- **A:** Specimen 1.
- **B:** Specimen 2
- **C:** Specimen 3.
- **D:** Specimen 4.

7.1.6. Test matrix

The specimens tested in this phase of the experimental program are presented in Table 18:

Table 18 *Phase II specimens. Source: Own.*

PHASE II SPECIMENS		
Type	**Edge distance**	
	100 mm	***50 mm***
CH	*CH – 100 – A**	*CH – 50 – A**
	*CH – 100 – B**	*CH – 50 – B**
	*CH – 100 – C**	*CH – 50 – C**
R1 – 5	*R1 – 5 – 100 – A*	*R1 – 5 – 50 – A*
	R1 – 5 – 100 – B	*R1 – 5 – 50 – B*
	R1 – 5 – 100 – C	*R1 – 5 – 50 – C*
	R1 – 5 – 100 – D	–
R2 – 2.5	*R2 – 2.5 – 100 – A*	–
	R2 – 2.5 – 100 – B	–
	R2 – 2.5 – 100 – C	–
R1 – 2.5	*R1 – 2.5 – 100 – A*	*R1 – 2.5 – 50 – A*
	R1 – 2.5 – 100 – B	*R1 – 2.5 – 50 – B*
	R1 – 2.5 – 100 – C	*R1 – 2.5 – 50 – C*
R1 – 2.5 – X	*R1 – 2.5 – X – 100 – A**	*R1 – 2.5 – X – 50 – A**
	*R1 – 2.5 – X – 100 – B**	*R1 – 2.5 – X – 50 – B**
	*R1 – 2.5 – X – 100 – C**	*R1 – 2.5 – X – 50 – C**
R0 – 5	–	*R0 – 5 – 50 – A**
	–	*R0 – 5 – 50 – B**
	–	*R0 – 5 – 50 – C**

7.1.7. Test conditions

- Relative humidity: 27% – 58%
- Temperature: 17 °C – 22 °C
- Load rate: 245 N/s – 422 N/s

7.2. Analytical work

7.2.1. CFRP laminate design

The calculation of the effective stress in the FRP at failure is summarized in Table 19:

Table 19 *CFRP parameters for effective stress calculation. Source: Own.*

EXPOSURE	
Exposure	**Interior**
Fiber	**Carbon**
C_E	0.95
MATERIALS	
f'_c (MPa)	**21**
f_{fu}^* (MPa)	**1068**
f_{fu} (MPa)	1015
ε_{fu}^*	**0.011**
ε_{fu}	0.010
E_f (MPa)	**96527**
GEOMETRY	
Scheme	**3-sided**
ψ_f	0.85
n	**1**
t_f (mm)	**2.030**
PARAMETERS	
Load	**Tension**
L_e (mm)	19.9
κ_1	0.85
κ_2	1.00
κ_v	0.14
ε_{fe}	0.0014
f_{fe} (MPa)	136

For each CFRP configuration, this effective stress was related to the acting load, in order to obtain the required area of reinforcement. Lastly, an adequate development length was provided for all laminates, according to the provisions of section 14.1.3 of ACI 440.2 (ACI Committee 440, 2017).

7.2.1.1. Reinforcement configuration R1 – 5

This configuration consisted of one (1) 5.0 in (127 mm) wide CFRP laminate on each side of the anchor.

7.2.1.1.1. Edge distance: 100 mm.

The theoretical acting load acting at the center of each laminate was calculated using a strut-and-tie-model, in which the external force corresponded to the shear load associated with steel rupture of the first batch of anchors (Figure 35):

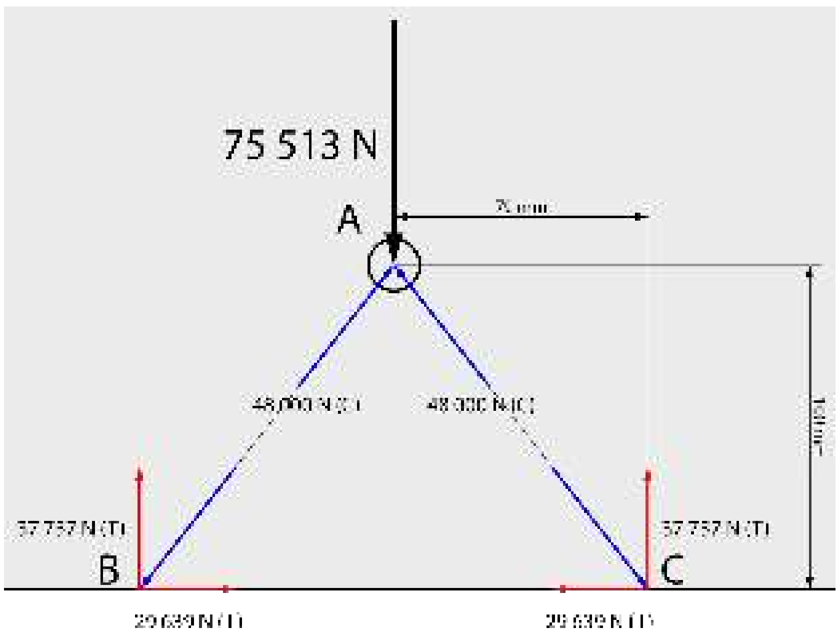

Figure 35 *Strut-and-tie model R1 – 5 – 100. Source: Own.*

Thus, a load of 37.76 kN would be theoretically acting on each laminate. Considering the effective stress at which the CFRP works while preventing debonding, the following strip width is obtained:

$$T_n = \psi_f w_f t_f f_{fe} \longrightarrow w_f = \frac{37\ 757\ \mathrm{N}}{0.85 \cdot 2.03\ \mathrm{mm} \cdot 136\ \mathrm{MPa}}$$

$$w_f = 161\ \mathrm{mm}\ [6.3\ \mathrm{in}]$$

Although the design requires a width of 161 mm (6.3 in), it was decided to set the experimental width to 127 mm (5.0 in), to evaluate the performance of reinforcement schemes that used less area than the required. It is also important to note that no strength-reduction factors were employed. This scheme is shown in Figure 36:

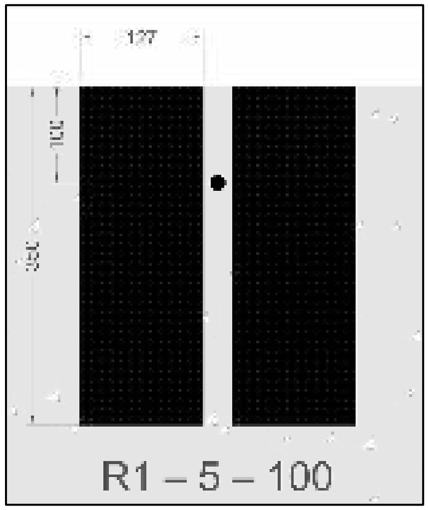

Figure 36 *R1 – 5 – 100 plan view. Source: Own.*

7.2.1.1.2. Edge distance: 50 mm.

The strut-and-tie model that applies for an edge distance of 50 mm is displayed in Figure 37:

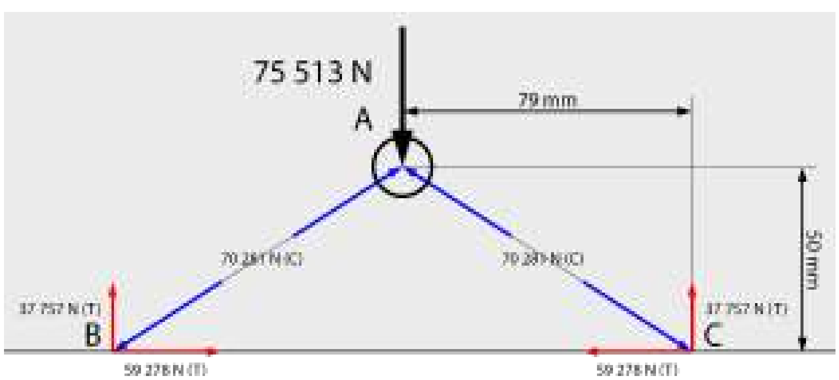

Figure 37 *Strut-and-tie model R1 – 5 – 50. Source: Own.*

For an edge distance of 50 mm the required strip width is the same as for 100 mm, due to the same external load and reinforcement scheme conditions:

$$T_n = \psi_f w_f t_f f_{fe} \longrightarrow w_f = \frac{37\,757\ \mathrm{N}}{0.85 \cdot 2.03\ \mathrm{mm} \cdot 136\ \mathrm{MPa}}$$

$$w_f = 161\ \mathrm{mm}\ [6.3\ \mathrm{in}]$$

In this case, the experimental width was also kept as 127 mm (5 in). Also, it is important to note how the tensile force acting along the edge of the member (59.28 kN) is higher than the load taken by each laminate (37.76 kN). This will be recalled when analyzing these specimens. This arrangement is presented in Figure 38:

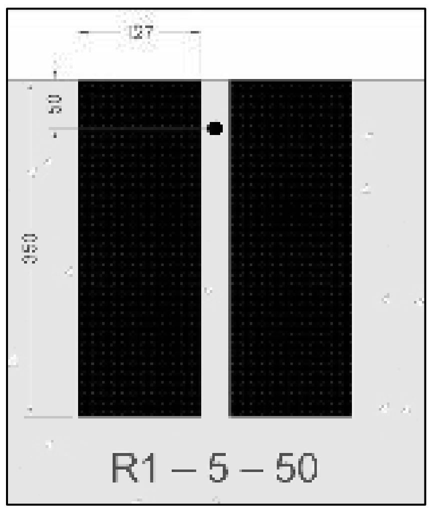

Figure 38 *R1 – 5 – 50 plan view. Source: Own.*

7.2.1.2. Reinforcement configuration R2 – 2.5

This reinforcement scheme consisted of two (2) 2.5 in (64 mm) wide laminates on each side of the anchor. This configuration only applied for anchors located at 100 mm to the edge. This was because during testing, it was concluded that this configuration would not provide any benefit to 50 mm specimens given the proximity of the anchor to the edge and the separation of the laminates.

7.2.1.2.1. Edge distance: 100 mm

The strut-and-tie model for this reinforcement configuration is shown in Figure 39:

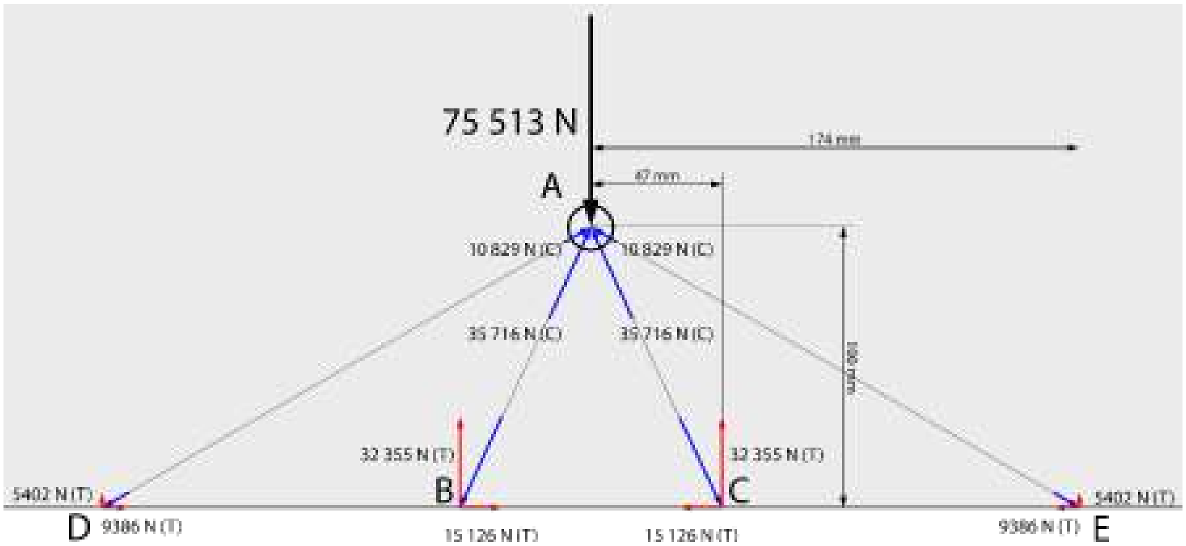

Figure 39 *Strut-and-tie model R2 – 2.5 – 100. Source: Own.*

For this edge distance, the width of CFRP reinforcement would require differentiating the load acting on the internal and external laminates. For the internal ones:

$$T_n = \psi_f w_f t_f f_{fe} \longrightarrow w_f = \frac{32\ 355\ \mathrm{N}}{0.85 \cdot 2.03\ \mathrm{mm} \cdot 136\ \mathrm{MPa}}$$

$$w_f = 138\ \mathrm{mm}\ [5.4\ \mathrm{in}]$$

On the other hand, for the external laminates:

$$T_n = \psi_f w_f t_f f_{fe} \longrightarrow w_f = \frac{5402\ \mathrm{N}}{0.85 \cdot 2.03\ \mathrm{mm} \cdot 136\ \mathrm{MPa}}$$

$$w_f = 23\ \mathrm{mm}\ [0.91\ \mathrm{in}]$$

It is important to notice the significant difference between both types of laminate. Also, this model supposes that during the totality of the test, all laminates will be acting at the same time. However, the internal laminates would be activated before the external ones, as cracking initiates on the surroundings of the anchor, and then propagates to the edges. These considerations will also be brought up when analyzing the results of these specimens.

Yet, as the idea behind this configuration was to evaluate the effectiveness of distributing the total area of reinforcement into different strips (as stirrups in a reinforced concrete member) it was decided to set the width of all the laminates on 64 mm (2.5 in). Therefore, this corresponds to the same area used in *R1 – 5* specimens but distributing it in twice the strips. This scheme is shown in Figure 40:

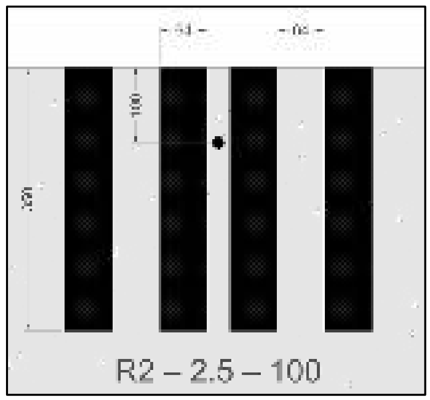

Figure 40 *R2 – 2.5 – 100 plan view. Source: Own.*

7.2.1.3. Reinforcement configuration R1 – 2.5

This reinforcement configuration employed half the area of reinforcement of the previous ones, to assess how this reduction would affect the response of the specimens. Thus, it consisted of one (1) 2.5 in (64 mm) wide laminate placed on each side of the anchor.

7.2.1.3.1. Edge distance: 100 mm.

The strut-and-tie model that corresponds to this configuration is shown in Figure 41:

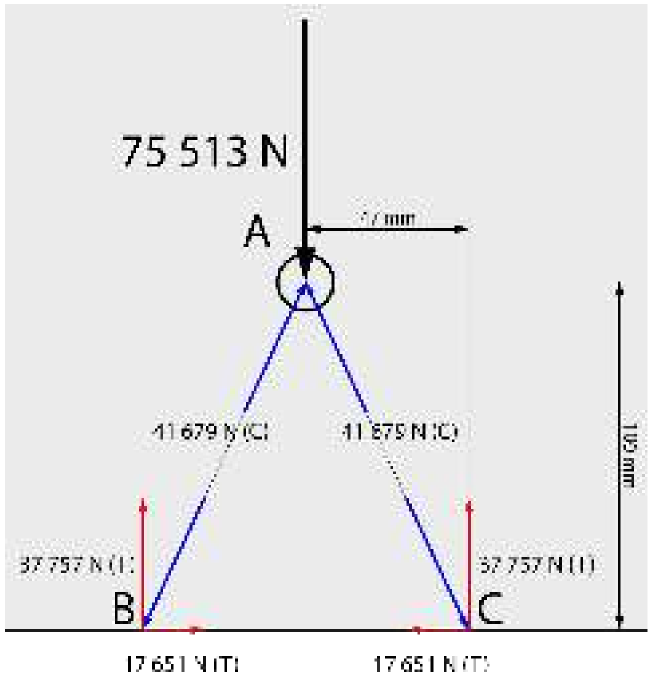

Figure 41 *Strut-and-tie model R1 – 2.5 – 100. Source: Own.*

It is observed that even if the centerline of the laminates is placed closer to the anchor, this does not have any effect on the load received by each CFRP strip (37.76 kN) when only two laminates in total are used. Therefore, the required width is the following:

$$T_n = \psi_f w_f t_f f_{fe} \longrightarrow w_f = \frac{37\ 757\ \text{N}}{0.85 \cdot 2.03\ \text{mm} \cdot 136\ \text{MPa}}$$

$$w_f = 161\ \text{mm}\ [6.3\ \text{in}]$$

For uniformity purposes, a width of 64 mm (2.5 in) was decided. This reinforcement is shown in Figure 42:

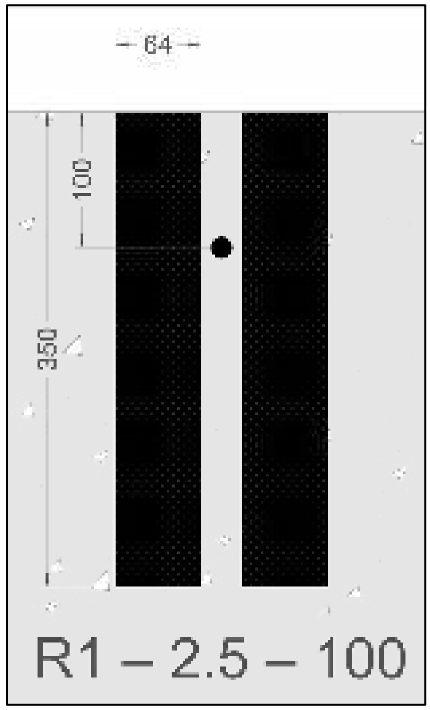

Figure 42 *R1 – 2.5 – 100 plan view. Source: Own.*

7.2.1.3.2. Edge distance: 50 mm.

In parallel, for a distance of 50 mm to the edge, the strut-and-tie model for this configuration is illustrated in Figure 43:

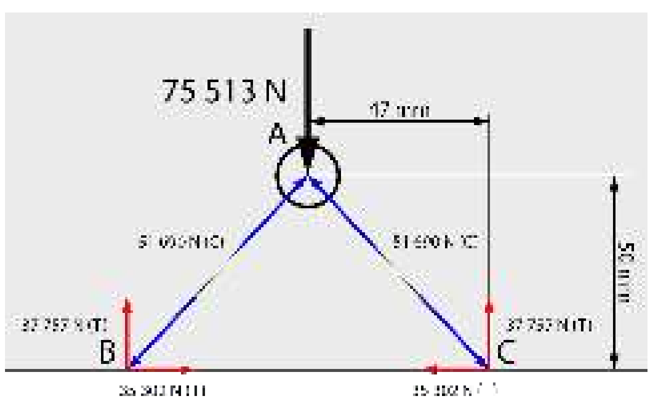

Figure 43 *Strut-and-tie model R1 – 5 – 50. Source: Own.*

As the load taken by each laminate remains the same, so does the required laminate width:

$$T_n = \psi_f w_f t_f f_{fe} \longrightarrow w_f = \frac{37\ 757\ \text{N}}{0.85 \cdot 2.03\ \text{mm} \cdot 136\ \text{MPa}}$$

$$w_f = 161\ \text{mm}\ [6.3\ \text{in}]$$

Thus, as this configuration considers half of the set reinforcement area, these laminates were also kept as 64 mm (2.5 in) wide. Once again, it is highlighted that the tensile force acting on the edge of the member is theoretically almost the same as that taken by the CFRP laminates. The plan of this configuration is presented in Figure 44:

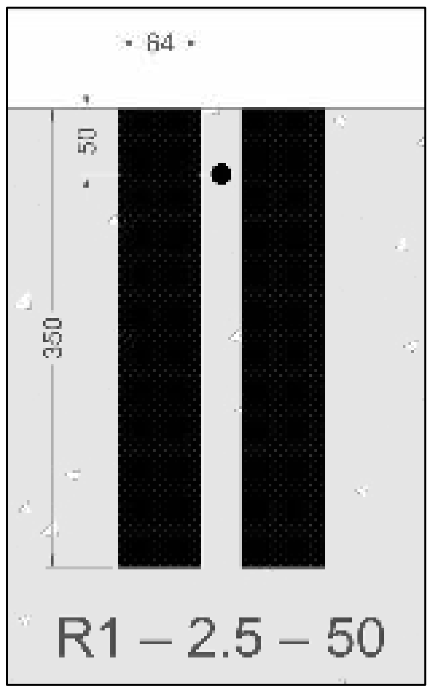

Figure 44 *R1 – 2.5 – 50 plan view. Source: Own.*

7.2.1.4. Reinforcement configuration R1 – 2.5 – X

As a consequence of the results obtained in phase I, it was decided to propose a reinforcement configuration which axis would be perpendicular to the experimental crack path. The theoretical advantage of this configuration would be that the CFRP would take the totality of stresses associated with cracking as tensile stresses, with no shear components, rendering a more efficient scheme.

Also, it was decided to use the same width as for *R1 – 2.5* specimens, to compare results and assess if orienting the laminates in a different manner would bring any significant advantage to the response of the strengthened system.

7.2.1.4.1. Edge distance: 100 mm

The plan of this configuration for an edge distance of 100 mm is shown in Figure 45:

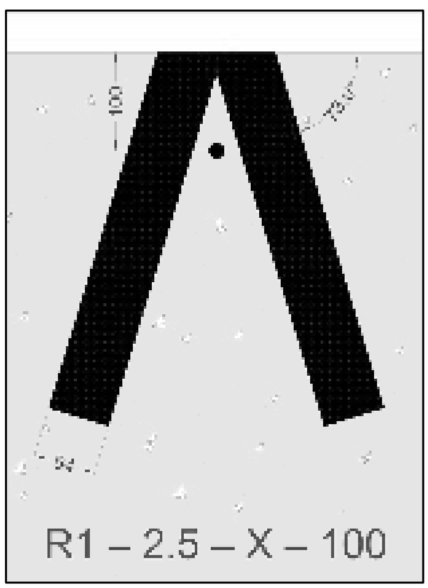

Figure 45 *R1 – 2.5 – X – 100 plan view. Source: Own.*

7.2.1.4.2. Edge distance: 50 mm

For 50 mm specimens, the geometric detail of the X-arrangement is illustrated in Figure 46:

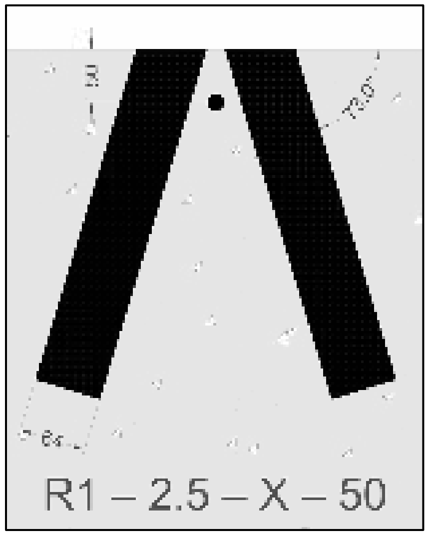

Figure 46 *R1 – 2.5 – X – 50 plan view. Source: Own.*

7.2.1.5. Reinforcement configuration R0 – 5

During testing of 50 mm specimens, it was observed that an improved reinforcement configuration would consist of only one laminate surrounding the anchor, not dividing the area into different strips on each side. Therefore, this configuration was used only for anchors located at 50 mm from the edge.

7.2.1.5.1. Edge distance: 50 mm

In this configuration, the centerline of the CFRP coincides with the action line of the external force. Thus, the total force is taken by the laminate. Thus:

$$T_n = \psi_f w_f t_f f_{fe} \longrightarrow w_f = \frac{75\ 513\ \mathrm{N}}{0.85 \cdot 2.03\ \mathrm{mm} \cdot 136\ \mathrm{MPa}}$$

$$w_f = 322\ \mathrm{mm}\ [12.7\ \mathrm{in}]$$

To keep uniformity with reinforcement schemes that used half of the reinforcement area, this width was set to 127 mm (5.0 in), as evidenced in Figure 47:

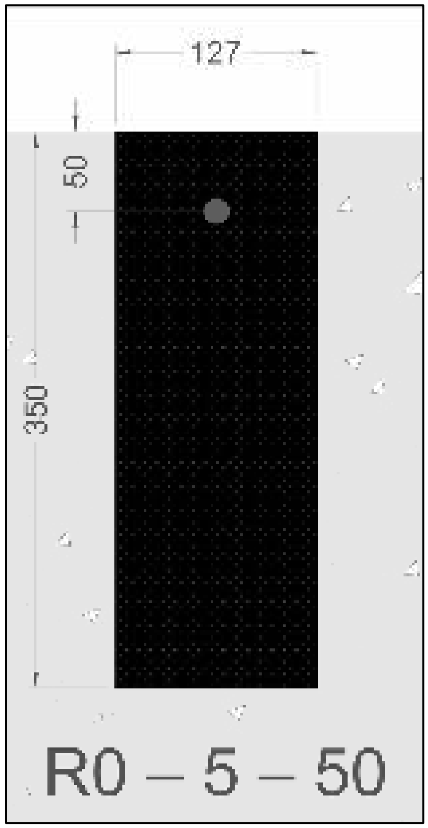

Figure 47 *R0 – 5 – 50 plan view. Source: Own.*

7.2.2. Hairpin design

ACI 318-19 establishes that concrete breakout mode of failure may be omitted if anchor reinforcement is contemplated. Thus, the internal stresses that produce cracking are taken by this reinforcement so the breakout body cannot be formed.

To elaborate the strut-and-tie model, a No. 4 bar was considered. Recalling that the hairpin consists of a 180-degree hook, the following geometry parameters were calculated per Chapter 25 of ACI 318-19.

Table 20 *Bar-to-develop properties. Source: Own.*

BAR-TO-DEVELOP PROPERTIES	
f_y (MPa)	420
Bar	No. 4
d_b (mm)	12.7
Angle	180
Amount	1
Coating	No
Spacing (mm)	
A_{hs} (mm^2)	129.00

Table 21 *Concrete properties. Source: Own.*

CONCRETE PROPERTIES	
f'_c (MPa)	21
Weight	Normal
Member	Slab
Cover (mm)	25.4

Table 22 *Confining reinforcement parameters. Source: Own.*

CONFINING REINFORCEMENT	
Confining existence	No
Bar	
Legs	
Amount	
A_{th} (mm^2)	0.00

Table 23 *Hairpin development length parameters. Source: Own.*

PARAMETERS	
λ	1.00
ψ_e	1.00
ψ_r	1.60
ψ_o	1.25
ψ_c	0.80
A_{th}/A_{hs}	0.00

Table 24 *Calculated development length for hairpin. Source: Own.*

DEVELOPMENT LENGTH	
l_{dh1} (mm)	289.5
l_{dh2} (mm)	101.6
l_{dh3} (mm)	152.4

Table 25 *Hairpin hook geometry. Source: Own.*

HOOK GEOMETRY	
l_{dh} (mm)	**289.5**
$D_{Mín.}$ (mm)	**76.2**
$l_{ext.}$ (mm)	**63.5**

Considering the minimum inside bend diameter, the geometry of the hairpin, and the distance from the anchor to the edge, the strut-and-tie model is constructed. It is important to highlight that the tensile forces that act upon the hairpin legs correspond in the model to the ties that are located and oriented on their same axis. In this case, for both edge distances, each leg takes half of the shear force acting on the anchor. As the desired mode of failure is steel rupture of the anchor, this external force is considered in the model.

However, before designing the reinforcement, R17.5.2.1 of ACI 318 states that as anchor reinforcement is located below the anchor fixture where the load is applied, this eccentricity results in a larger force that needs to be taken by the reinforcement. ACI does not give a deeper insight into how to calculate this effect. However, Eurocode asserts that for shear-loaded anchors, the force acting on the hairpin shall be modified as follows (European Committee for Standardization, 2018):

$$N_{Ed,re} = \left(\frac{e_s}{z} + 1\right) V$$

Where:

$\boldsymbol{N_{Ed,re}}$**:** Factored design force.

$\boldsymbol{e_s}$**:** Distance between axis of reinforcement and line of shear force acting on the fixture.

$\boldsymbol{z \approx 0.85d}$, with d no larger than the minimum value between $2h_{ef}$ and $2C_{a1}$.

$\boldsymbol{V}$**:** Force taken by each leg of the hairpin.

By means of the previous equation, the required area of reinforcement was calculated for each case.

7.2.2.1. Edge distance: 100 mm

The strut-and-tie model for this case is shown in Figure 48:

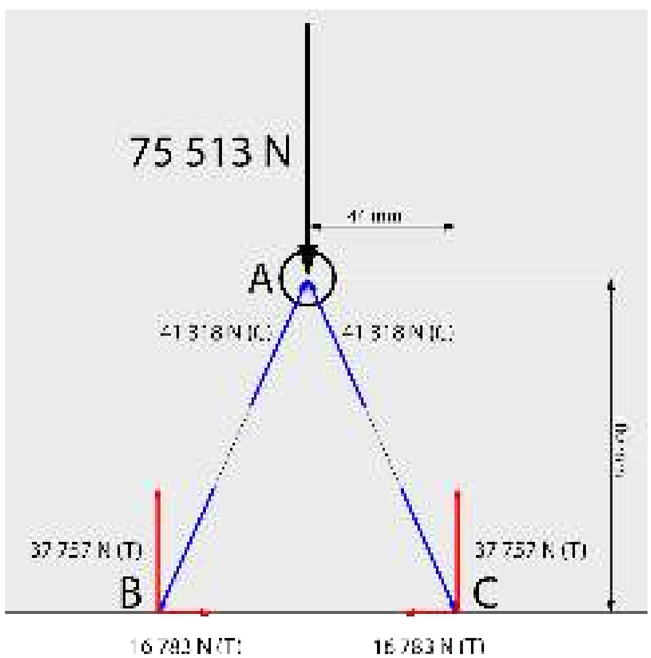

Figure 48 *Strut-and-tie model CH – 100. Source: Own.*

As discussed before, each hairpin leg would be taking half of the shear load acting upon the anchor. In addition, the geometry necessary for calculating the increased load due to eccentricity effects is presented below (Figure 49):

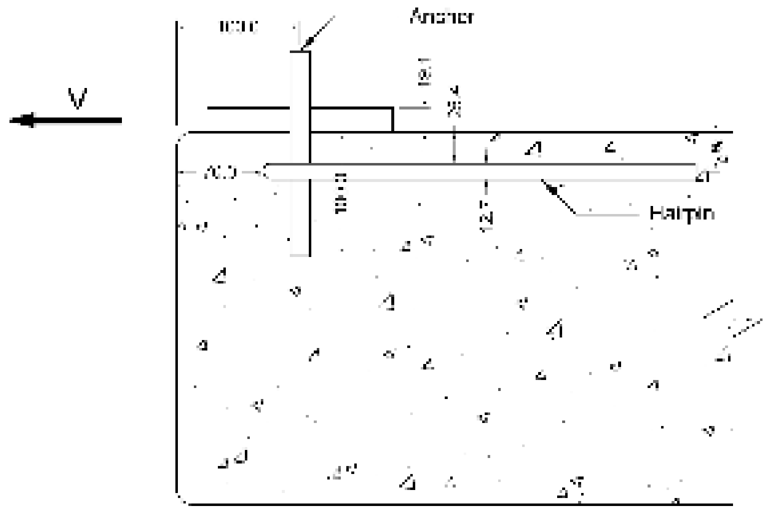

Figure 49 *Hairpin-reinforced specimen CH – 100. Lateral view. Source: Own.*

The distance from the load to the axis of the reinforcement (e_s) is 41.3 mm. Also, d takes the minimum value between $\left(2h_{ef} = 200 \text{ mm}\right)$ and $(2C_{a1} = 200 \text{ mm})$; this is 200 mm.

$$N_{Ed,re} = \left(\frac{41.3 \text{ mm}}{170 \text{ mm}} + 1\right) \cdot 37\,756 \text{ N}$$

$$N_{Ed,re} = 1.24 \cdot 37\,756 \text{ N}$$

$$N_{Ed,re} = 46\,928 \text{ N}$$

Considering the reinforcement steel yields in tension, and that the force acting on each leg of the hairpin is the one calculated previously, the required area of reinforcement is calculated:

$$f_y = \frac{N_{Ed,re}}{A_{Req.}} \longrightarrow A_{Req.} = \frac{46\,928 \text{ N}}{420 \text{ MPa}}$$

$$A_{Req.} = 112 \text{ mm}^2$$

This requirement is fulfilled by the supposed No. 4 rebar ($A = 129 \text{ mm}^2$).

7.2.2.2. Edge distance: 50 mm

The strut-and-tie model for this case is shown in Figure 50:

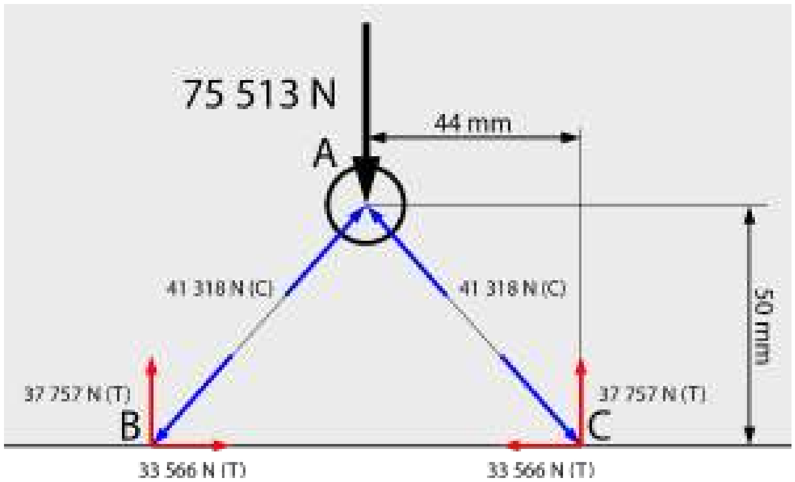

Figure 50 *Strut-and-tie model CH – 50. Source: Own.*

Equally, for the shorter edge distance, each hairpin leg also takes half of the total shear load. In the same way, the geometry necessary to consider eccentricity effects is presented in Figure 51:

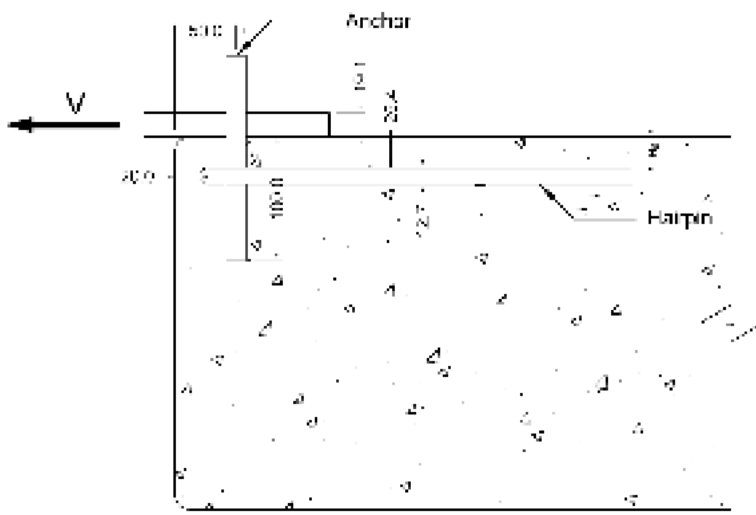

Figure 51 *Hairpin-reinforced specimen CH – 50. Lateral view. Source: Own.*

The distance from the load to the axis of the reinforcement (e_s) is 41.3 mm. Also, d takes the minimum value between $(2h_{ef} = 200\ \mathrm{mm})$ and $(2C_{a1} = 100\ \mathrm{mm})$; this is 100 mm.

$$N_{Ed,re} = \left(\frac{41.3\ \text{mm}}{85\ \text{mm}} + 1\right) \cdot 37\ 756\ \text{N}$$

$$N_{Ed,re} = 1.49 \cdot 37\ 756\ \text{N}$$

$$N_{Ed,re} = 56\ 101\ \text{N}$$

Considering the reinforcement steel yields in tension, and that the force acting on each leg of the hairpin is the one calculated previously, the required area of reinforcement is calculated:

$$f_y = \frac{N_{Ed,re}}{A_{Req.}} \longrightarrow A_{Req.} = \frac{56\ 101\ \text{N}}{420\ \text{MPa}}$$

$$A_{Req.} = 134\ \text{mm}^2$$

The area difference between the supplied No. 4 rebar ($A = 129\ \text{mm}^2$) and the required reinforcement area is considered infimum. Consequently, the same cast-in reinforcement is considered for both edge distances.

Finally, the adopted geometry for all hairpins is shown below (Figure 52):

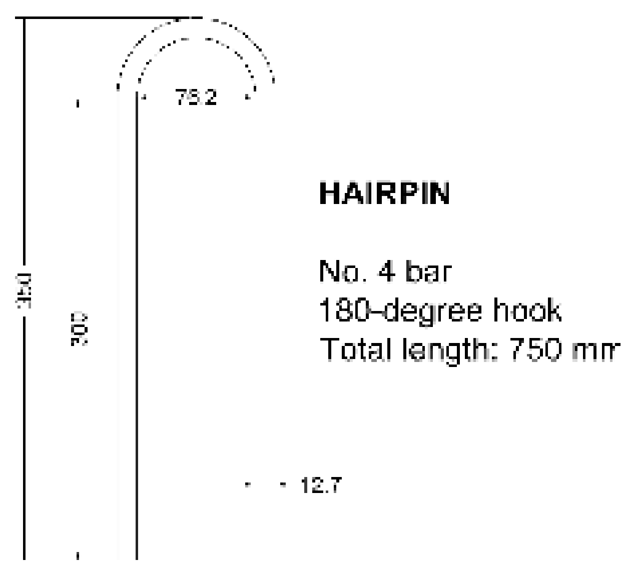

Figure 52 *Hairpin geometry. Source: Own.*

7.3. Theoretical values

No theoretical values were calculated, as there is no evidence of equations that predict the nominal strength of reinforced anchors. The results of this investigation would constitute a first step in developing design provisions related to the strengthening of anchors with cast-in and post-installed CFRP reinforcement.

7.4. Experimental results and analysis

7.4.1. Edge distance: 100 mm

7.4.1.1. Hairpin-reinforced specimens.

- ***Strength and failure mode***

The results related with capacity and failure mode, gathered for these specimens, are summarized in Table 26:

Table 26 *Strength and failure mode CH – 100. Source: Own.*

STRENGTH & FAILURE MODE CH – 100							
Specimen	**V_u (kN)**	**Avg. V_u (kN)**	**V_u / $V_{Theo.}$**	**Avg. V_u / $V_{Theo.}$**	**V_u / V_{C0}**	**Avg. V_u / V_{C0}**	**Failure mode**
A*	52.52	49.26	0.79	0.74	1.47	1.38	***CB → SR***
B*	46.00		0.69		1.29		***CB → SR***
C*	68.27	68.27	1.02	1.02	1.92	1.92	***SR***

It is important to draw attention to the fact that two different failure modes were obtained. It is evidenced that specimen C* attained an experimental load higher than the theoretical one associated with steel rupture; therefore, this specimen displayed that mode of failure. However, specimens A* and B* reached, on average, 74% of the theoretical load. This incapacity to reach the design load led to a combined mode of failure characterized by formation of a concrete breakout body, followed by rupture of the anchor. Nevertheless, all specimens demonstrated gains in strength with respect to control samples.

In parallel, Figure 53 displays the load – displacement behavior of these hairpin-reinforced anchors:

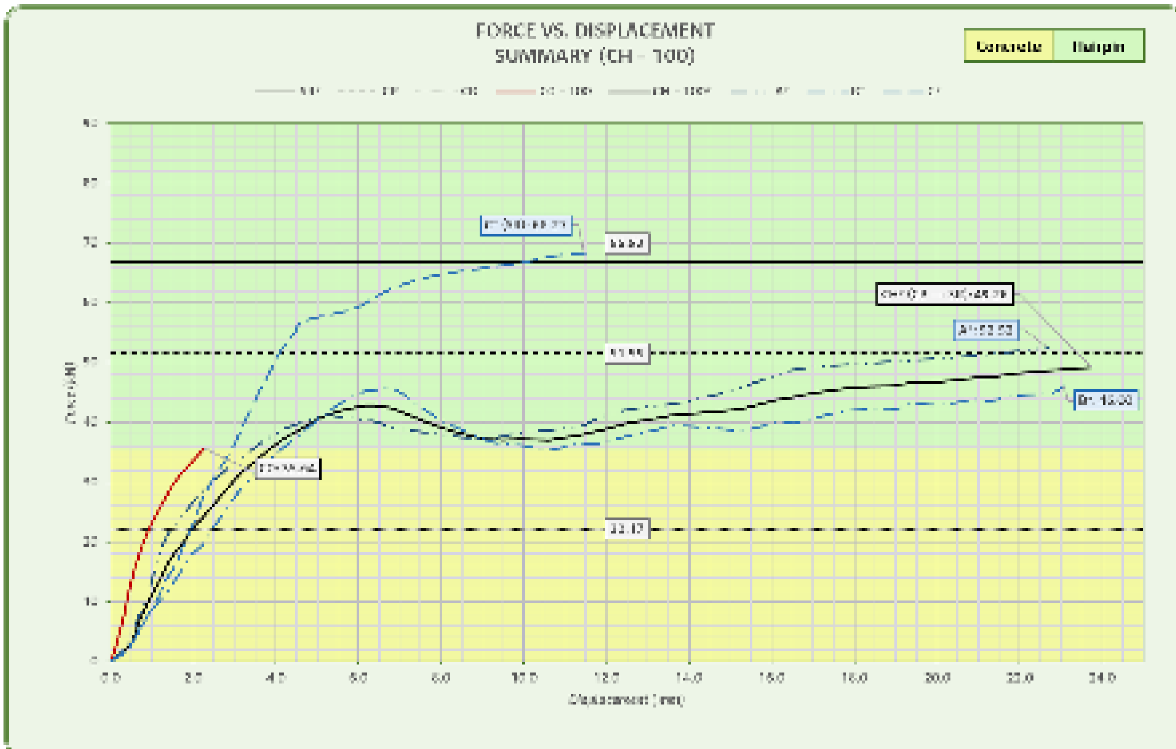

Figure 53 *Force vs. displacement CH – 100. Source: Own.*

The difference between the two failure modes obtained is also evidenced in this graph. It is observed how the specimen that developed a “pure” steel rupture (without a preceding concrete breakout) reaches a higher ultimate load, whereas the specimens that showed a combined failure mode, did not reach the expected capacity, but developed significant displacements.

The reason behind the two obtained failure modes is attributed to quality in the hairpin installation. It is observed how specimens A* and B* follow, initially, a trajectory similar to that of the control specimens, which means that micro cracking occurred within the concrete structure. During the test, it was observed that the upper part of the anchor developed a slight rotation toward the edge. This behavior is due to the eccentricity between the point of support of the anchor (hairpin) and the external load. It is possible that, in a first stage, the anchor crushed the small amount of concrete that separated it from the hairpin (even if contact between both was guaranteed during installation); this displacement could have initiated crack formation, but it also activated the hairpin. Then, given the moment generated by the external load, the anchor tended to rotate, but as the bottom part of the anchor bore against the back side concrete, only the region above the hairpin experienced notable bending deformations. This explains why the response of these anchors soften at a load slightly above the experimental concrete breakout capacity. Next, as the upper side of the anchor rotated, large deformations were achieved, but this combination of shear and bending induced significant strain on the back of the anchor's cross-section. Thus, in that region the anchor began rupturing, until two completely separated parts were obtained, indicating the total loss of load-bearing capacity of the system.

On the other hand, the positioning of specimen C's hairpin, could have guaranteed total load-transfer since the beginning of the test, preventing the formation of a concrete breakout body. If a breakout body was not generated, this implies a better confinement of the anchor, which reduces deformations associated with bending, achieving a mode of failure attributed mainly to shear action. As the hairpin could have been activated since the beginning of the test, this explains why specimen C's linear behavior reached a higher load. The inflection point is explained by yield of the steel hairpin, and the nonlinear behavior that develops afterwards is attributed to the sum of the shear deformation of the anchor, and the plastic axial deformation of the hairpin. This behavior continues until the anchor reaches shear failure.

- ***Energy absorption***

In terms of energy absorption, obtained results are arranged in Table 27:

Table 27 *Absorbed energy CH – 100. Source: Own.*

ABSORBED ENERGY CH – 100				
Specimen	**W_u (J)**	**Avg. W_u (J)**	**W_u / W_{C0}**	**Avg. W_u / W_{C0}**
A*	918	881	16.2	15.5
B*	843		14.9	
C*	562	562	9.9	9.9

The difference between failure modes is significant. Specimens that demonstrated a combined failure mode absorbed 57% more energy than the specimen that achieved a “pure” steel rupture. Nevertheless, all specimens achieved significant improvements in relation to unreinforced specimens.

- ***Failure mechanism***

The crack pattern evidenced in specimen A* is shown in Figure 54:

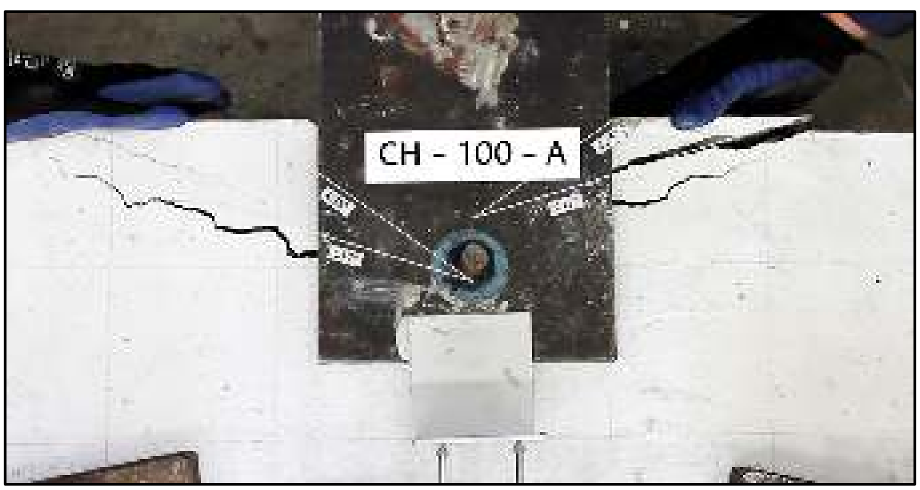

Figure 54 *Crack formation CH – 100 – A*. Source: Own.*

It is observed that even if the anchor is reinforced, concrete breakout cracks propagate with an orientation similar to the experimental 17° obtained in control specimens.

Moreover, a detail on specimen A* after failure is illustrated in Figure 55:

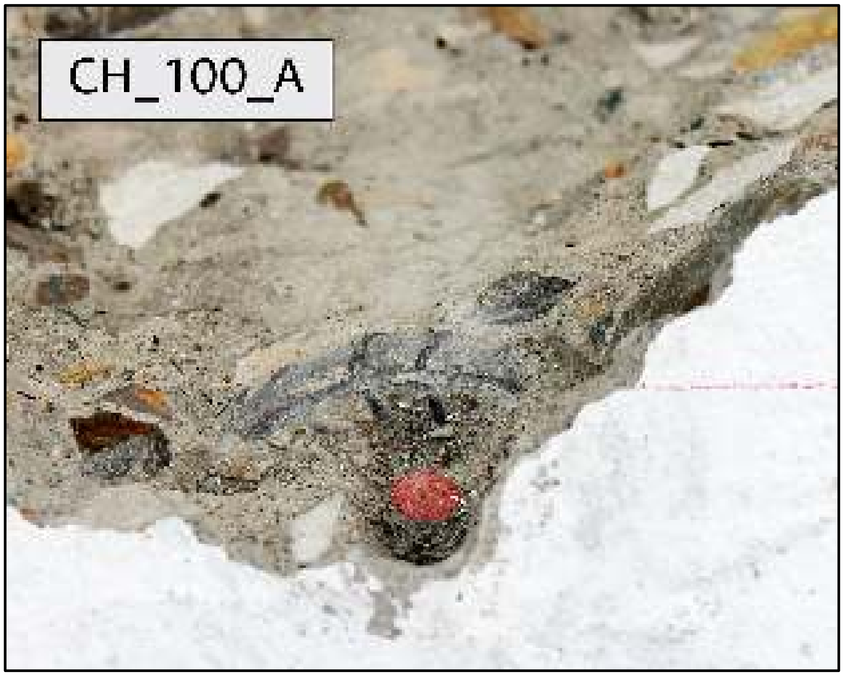

Figure 55 *Detail in specimen CH – 100 – A*. Source: Own.*

Two main aspects may be observed from the picture:

- ✓ The cross-section of the anchor resembles an ellipsoid. This is due to the angle of the anchor with respect to the lens of the camera, evidencing that bending played a significant role on the failure mechanism.
- ✓ There is a space between the anchor and the hairpin, which is filled with crushed concrete. This further supports the idea that explained the concrete breakout body formation.

Regarding specimen C, which showed “pure” steel rupture, a detail of its failure mode is evidenced in Figure 56:

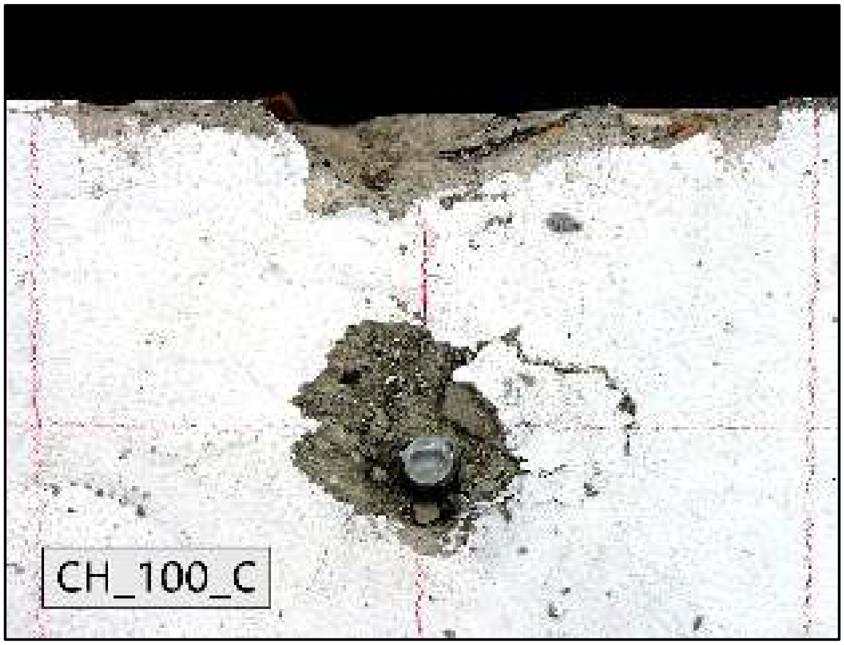

Figure 56 *Specimen CH – 100 – C* failure mode. Source: Own.*

First, it is important to note that although no concrete breakout body formed, there was evidence of concrete spalling mostly in front of the anchor. This phenomenon is typical in shear-loaded anchors, but it does not affect significantly the ultimate load, as only a superficial laminate of concrete detaches from the member. However, the most important aspect to highlight, is that the anchor’s cross-section maintained a circular shape, evidencing that the input of bending was not significant in this specimen. Lastly, it is observed that a piece of concrete detached from the edge of the slab. As the anchor bears against the concrete, some tensile stresses develop at the edge of the slab, in direction perpendicular to the force (as evidenced in the strut-and-tie models of section 7.2). These stresses produce the breakout of the concrete located on the edge of the member.

7.4.1.2. CFRP-reinforced specimens.

7.4.1.2.1. R1 – 5 – 100.

This reinforcement configuration involved one CFRP laminate on each side of the anchor. Each laminate had a width of 5.0 in (127 mm). This was equivalent to 79% of the reinforcement area obtained in design.

- ***Strength and failure mode***

A summary of strength-related parameters and failure modes of the tested specimens is shown in Table 28:

Table 28 *Strength and failure mode R1 – 5 – 100. Source: Own.*

STRENGTH & FAILURE MODE R1 – 5 – 100							
Specimen	**V_u (kN)**	**Avg. V_u (kN)**	**V_u / $V_{Theo.}$**	**Avg. V_u / $V_{Theo.}$**	**V_u / V_{C0}**	**Avg. V_u / V_{C0}**	**Failure mode**
A	80.05	76.40	1.06	1.01	2.25	2.14	***SR***
B	79.26		1.05		2.22		***SR***
C	76.62		1.01		2.15		***SR***
D	69.65		0.92		1.95		***SR***

These results show that this configuration of post-installed CFRP reinforcement does work. First, reinforced specimens achieved a strength of, on average, two times that of unreinforced specimens. Next, this increase in strength could not develop any further, as now the anchors' material properties controlled the failure mechanism, obtaining anchor rupture in all tested specimens. This shows that CFRP anchor reinforcement can be appropriately designed to obtain the desired failure mode. Furthermore, this is also reflected in the fact that, on average, the ultimate load of these specimens was similar to the theoretical load associated with steel rupture.

However, although specimen D also failed due to steel rupture, it only managed to achieve 92% of the theoretical value. This could be attributed to variability in the anchor's steel properties, but it could also be related to the properties of the concrete in which this anchor was embedded. It is important to highlight that specimens A, B and C belonged to the same concrete slab, while specimen D was included in a different one. Although the differences in compressive strength between both slabs could be deemed as insignificant (3 MPa), it was observed that the concrete in which specimen D was located contained a larger amount of air pockets. When subjected to the test, these voids could have an influence on the stiffness of the concrete substrate. This could lead to larger displacements but could also signify a difference in the support conditions of the anchor within the concrete. Although it is idealized that the concrete substrate functions as a fixed support for the anchor, in reality, and especially for specimen D, the concrete allows a certain degree of displacement and rotation of the anchor. As a result, bending is involved. Thus, the interaction between bending and shear could explain the reduction in the ultimate load of specimen D.

In fact, it was observed that even if all anchors experimented steel rupture, those with lower capacity evidenced greater deformations due to the influence of bending, as seen in Figure 57:

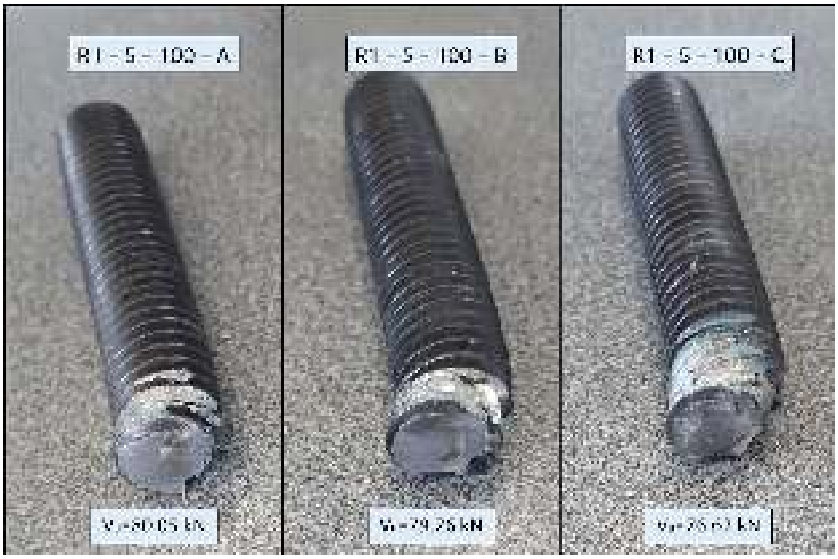

Figure 57 *Failure mode of R1 – 5 – 100 anchors. Source: Own.*

Moreover, the load – displacement behavior of these specimens is shown in Figure 58:

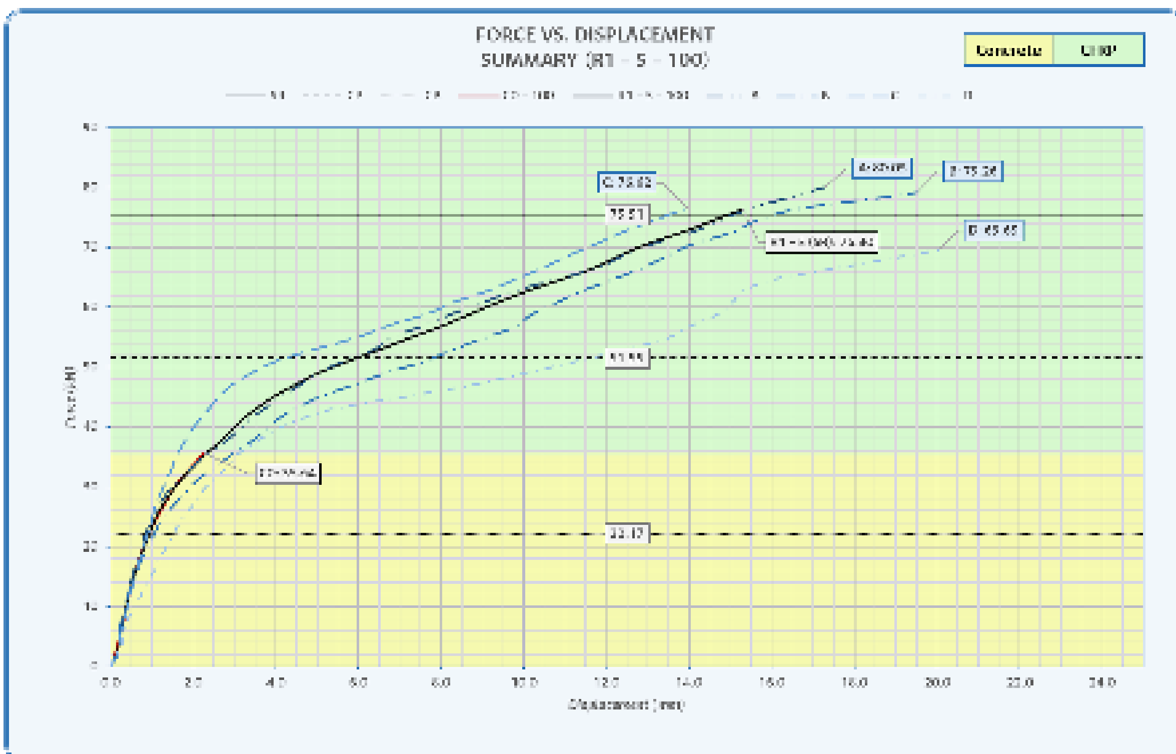

Figure 58 *Force vs. displacement R1 – 5 – 100. Source: Own.*

The most important thing to notice is the significant increase in strength and deformation capacity of reinforced specimens, in comparison to the average control behavior (C0 – 100). Additionally, it is evident that reinforced specimens A, B and C exhibited a similar behavior, whereas specimen D evidenced a lower stiffness in the zone in which the CFRP reinforcement takes the shear force. As explained before, the internal structure of the concrete slab that contained specimen D could explain this lower slope, as well as failure at a slightly lower load than the theoretical one.

The system's response is characterized by an initial region in which concrete receives the external load from the anchor and transfers it to the supports. Due to the region surrounding the anchor being subjected to high stresses, the concrete in that region reaches its tensile capacity first, leading to cracking. As concrete loses its load-bearing capacity, the slope decreases, indicating the propagation of cracks related to concrete breakout. In this moment, the CFRP is activated, controlling crack expansion. However, as load increases, bending becomes involved, hence, the formation of concrete pryout cracks. The system continues to experience stiffness degradation, until the CFRP becomes the most crucial aspect of the response. This happens at loads close to the theoretical concrete pryout one, when the behavior becomes linear until failure.

- ***Energy absorption***

Additionally, the total energy absorbed by each specimen, as well as their relation to the average energy absorbed by control specimens, is shown in Table 29:

Table 29 *Absorbed energy R1 – 5 – 100. Source: Own.*

ABSORBED ENERGY R1 – 5 – 100				
Specimen	**W_u (J)**	**Avg. W_u (J)**	**W_u / W_{C0}**	**Avg. W_u / W_{C0}**
A	971	948	17.1	16.7
B	1084		19.1	
C	767		13.5	
D	970		17.1	

Given the improvements in terms of strength and deformation of the reinforced systems, which are attributed to the mechanical properties of CFRP, it was possible to absorb almost 17 times more energy than control specimens. Nevertheless, it is important to note that these values are tightly related to the geometric and material conditions of this study.

These results, in conjunction with the load – displacement behavior and the modification of the failure mode of the anchors, reflect that even if shear-related failure modes are considered brittle, reinforced specimens evidenced a somewhat more ductile behavior. Another advantage of CFRP reinforcement is that when the composite material begins to work, the sound of the fiber being stressed could be heard, which functions as an alarm mechanism to indicate that the anchoring system is reaching its ultimate load.

- ***Failure mechanism***

Besides, to get a deeper understanding of the failure mechanism, the CFRP was retired once the test ended, as shown in Figure 59 for specimen B:

Figure 59 *Failure mechanism R1 – 5 – 100 – B. Source: Own.*

First, it is important to highlight that cracks that would be associated with concrete breakout did appear, but they did not manage to go through the total width of the laminate, indicating that the composite material was effective in taking the stresses induced by the external load, halting the propagation of these cracks.

Second, cracking was found on the border between the CFRP and the exposed concrete, in the same direction in which the fiber was installed. This is explained by the stiffness differences between the composite material and the concrete, which generates a border zone with stress concentration.

Third, approximately 50 mm behind the anchor, an important cracking scheme was also observed. These cracks are similar to those related to the concrete pryout failure mode. This indicates that after concrete breakout failed to occur, the shear load continued increasing. As mentioned before, the eccentricity between the force line and the centroid of the anchor generates a moment, so these higher loads induced a greater basculation tendency on the anchor, up to a point in which the concrete behind the anchor reached its tensile strength, hence, the formation of the aforementioned cracks. However, the CFRP was also effective in containing the propagation of these cracks, ensuring even higher loads, up to the point in which steel ultimately failed. This same pattern was observed in all *R1 – 5* specimens.

- ***Stress – unit strain behavior***

Finally, an analysis of the unit strain behavior of the CFRP was conducted. Regarding specimen D, the location of the strain gauges is shown below (Figure 60):

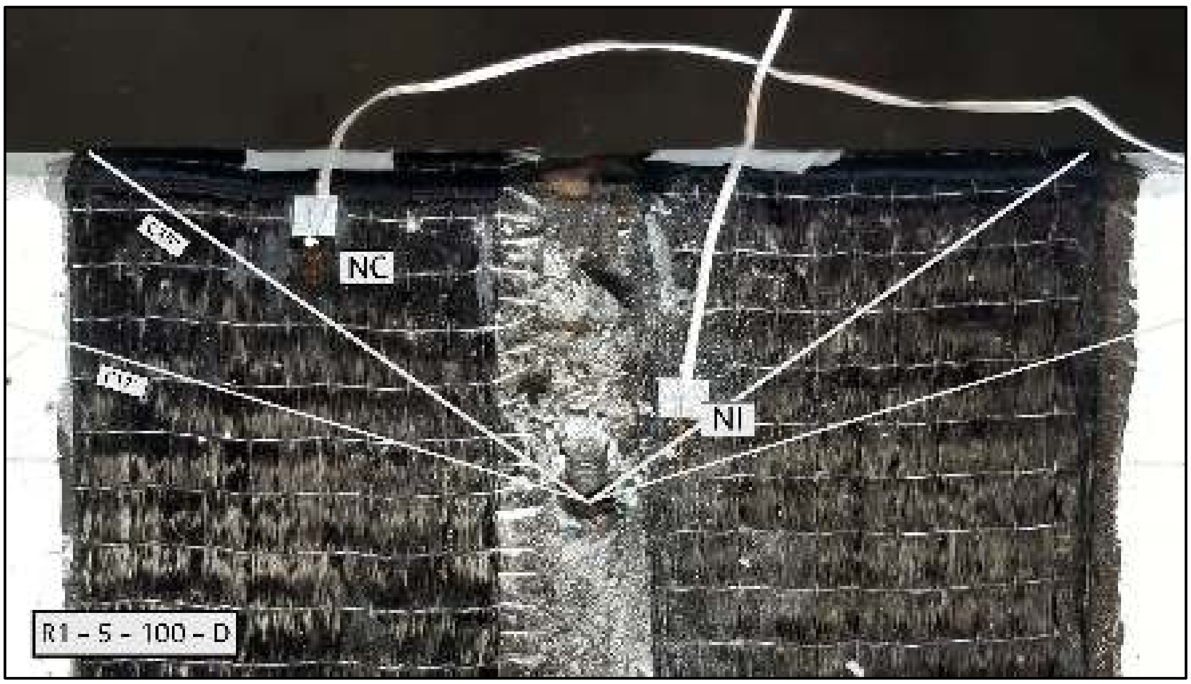

Figure 60 *Strain gauges location R1 – 5 – 100 – D. Source: Own.*

It is important to note that the strain gauges were installed near the theoretical concrete breakout crack path, which has an orientation of 35°, although the control specimens showed that the most prominent cracks appear at an orientation of around 17°.

The unit strain measured by each gauge is shown in Figure 61:

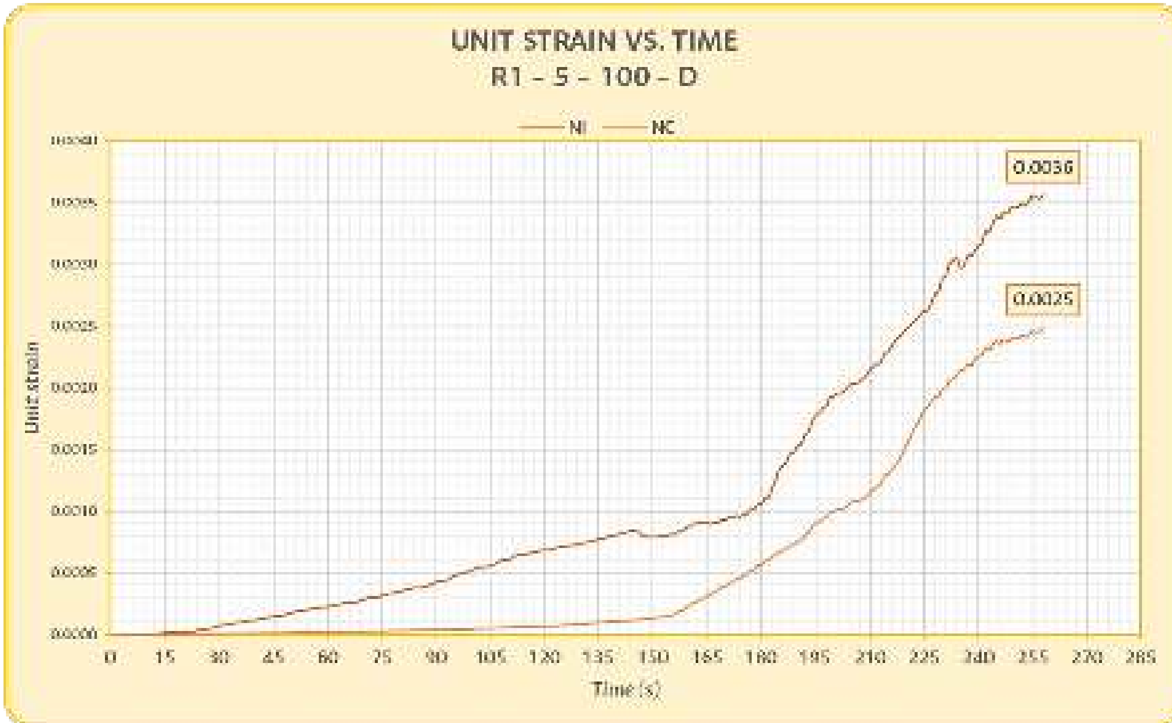

Figure 61 *Unit strains R1 – 5 – 100 – D. Source: Own.*

Evidently, the gauge located closest to the anchor, over the most probable concrete breakout crack path, sustained a higher strain than the one placed outside the crack path, farther from the anchor.

Recalling the linear behavior of CFRP, it was possible to calculate how close to failure was the fiber when the system reached its ultimate load. These values are shown in Table 30:

Table 30 *CFRP exigency ratio R1 – 5 – 100 – D. Source: Own.*

CFRP EXIGENCY PROPORTION R1 – 5 – 100 – D			
Strain gauge	$\varepsilon_{f_{Máx.}}$	$\varepsilon^*_{f_u}$	$\varepsilon_{f_{Máx.}}/\varepsilon^*_{f_u}$
NI	0.0036	0.011	32.7%
NC	0.0025		22.7%

This information is relevant, as it means that considering that debonding did not occur and taking into consideration the material properties of the steel employed, the CFRP was subjected to a maximum strain (or stress) equivalent to 32.7% of its ultimate capacity. However, it is important to emphasize that a unit strain of 0.0036 is higher than the effective strain that was employed for designing the CFRP reinforcement $(\varepsilon_{fe} = 0.0014)$. This could imply that although the region closer to the anchor was experimenting higher unit strains than expected, on average, over the total width of the laminate, the strain was not enough to cause debonding. Yet, this maximum test unit strain reached 85.7% of the debonding strain as defined in section 10.1.1 of ACI 440 $(\varepsilon_{fd} = 0.0042)$.

Lastly, Figure 62 evidences the force – unit strain behavior (until maximum load) registered by the strain gauges installed on specimen D:

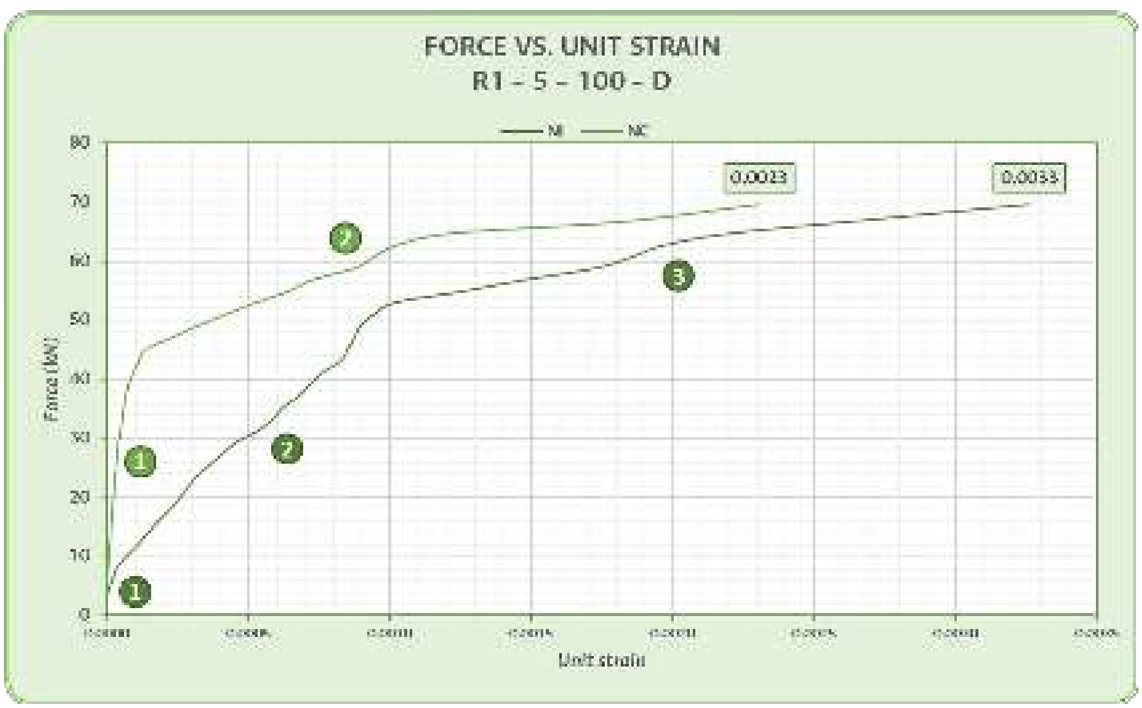

Figure 62 *Force vs. unit strain R1 – 5 – 100 – D. Source: Own.*

This graph shows that the gauge placed near the anchor (NI) registered a linear behavior up to a shear load of around 4 kN (zone 1); which reflects uncracked concrete and CFRP working together. After that, the stiffness degradation is attributed to the formation of micro fissures (zone 2). Next, the cracks associated with concrete breakout induce higher displacements on the system. As the crack widens, the stress transferred through surface interlocking decreases, decreasing once more the stiffness and leaving CFRP as the main load bearing mechanism until the anchor fails (zone 3).

On the other hand, the gauge placed over the fiber on the edge of the slab (NC) demonstrated a first linear behavior (zone 1) that extended further than that of the gauge installed closer to the anchor (NI). This is because concrete and CFRP work together for a longer time, as no significant fissures form in this region. After that, a second linear region develops (zone 2), which behavior corresponds to that of zone 3 of the gauge located near the anchor. However, the strains developed in this region are lower, as most of the bond stress is concentrated near the main cracking region.

7.4.1.2.2. R2 – 2.5 – 100.

This reinforcement configuration involved two CFRP laminates on each side of the anchor. Each laminate had a width of 2.5 in (64 mm). This scheme also involved employing 79% of the design reinforcement area.

- ***Strength and failure mode***

Table 31 summarizes the most important information regarding strength and mode of failure of the tested specimens:

Table 31 *Strength and failure mode R2 – 2.5 – 100. Source: Own.*

STRENGTH & FAILURE MODE R2 – 2.5 – 100							
Specimen	**V_u (kN)**	**Avg. V_u (kN)**	**V_u / $V_{Theo.}$**	**Avg. V_u / $V_{Theo.}$**	**V_u / V_{C0}**	**Avg. V_u / V_{C0}**	**Failure mode**
A	73.77	73.77	0.98	0.98	2.07	2.07	***SR***
B	63.96	64.26	0.85	0.85	1.79	1.80	***CP → DB***
C	64.55		0.85		1.81		***CP → DB***

First of all, it is evident that two different failure modes were obtained, as specimen A exhibited steel rupture, whereas specimens B and C showed CFRP debonding caused by concrete pryout. Indeed, if debonding occurred, it happened at a load lower than that related to steel rupture. A more detailed analysis of this variable behavior may be found on the “Failure mechanism” section. However, even if a different behavior was observed, the CFRP did increase the ultimate strength of the anchoring system, displaying improvements of 107% and 80% with respect to control specimens, for the modes of failure of steel rupture and debonding generated by concrete pryout, respectively.

Variability in the failure mode and the overall reduction in the capacity of the strengthened systems implied that distributing the required area of reinforcement in various strips of less width was less effective than concentrating it in a single ply on each side.

The load – displacement behavior of these specimens is shown in Figure 63:

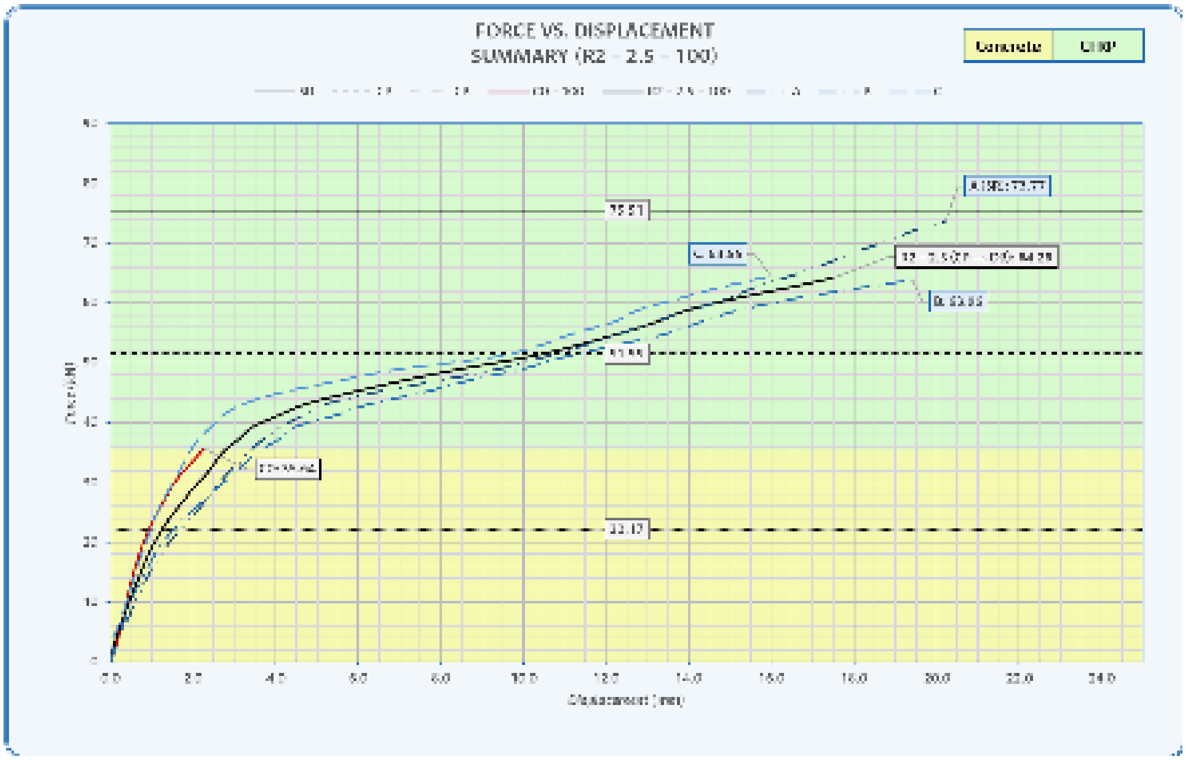

Figure 63 *Force vs. displacement R2 – 2.5 – 100. Source: Own.*

The graph shows that all curves have a similar behavior, but the specimens that presented debonding failed at a lower load than the specimen that displayed steel rupture. Similar to *R1 – 5*, the curves exhibit how the system loses rigidity as the load increases, passing through the formation of concrete breakout and concrete pryout cracks. However, specimens B and C display additional stiffness degradation toward their ultimate load, while specimen A’s behavior remains linear. This could indicate that specimens B and C developed wider cracks, which led to larger strains on the CFRP, and finally, to a higher probability of debonding.

Overall, the CFRP is effective in increasing the strength and the deformation capacity of the anchoring system, as well as preventing the concrete breakout mode of failure. Despite this, there is more variability in the possible failure outcomes, in comparison to concentrating the reinforcement area in just one strip on each side of the anchor.

- ***Energy absorption***

The parameters associated with energy absorption for this reinforcement configuration are shown in Table 32:

Table 32 *Absorbed energy R2 – 2.5 – 100. Source: Own.*

ABSORBED ENERGY R2 – 2.5 – 100				
Specimen	**W_u (J)**	**Avg. W_u (J)**	**W_u / W_{C0}**	**Avg. W_u / W_{C0}**
A	996	996	17.6	17.6
B	898	834	15.9	14.7
C	769		13.6	

The results show specimen A as the one with more absorbed energy until failure due to steel rupture. On the other hand, as specimens B and C did not achieve the ultimate expected load, their energy absorption capacity was lower. Nevertheless, all specimens showed a significantly better behavior than unreinforced ones.

- ***Failure mechanism***

The failed anchor and the crack analysis of specimen A are presented in Figures 64 and 65, respectively.

Figure 64 *Anchor failure R2 – 2.5 – 100 – A. Source: Own.*

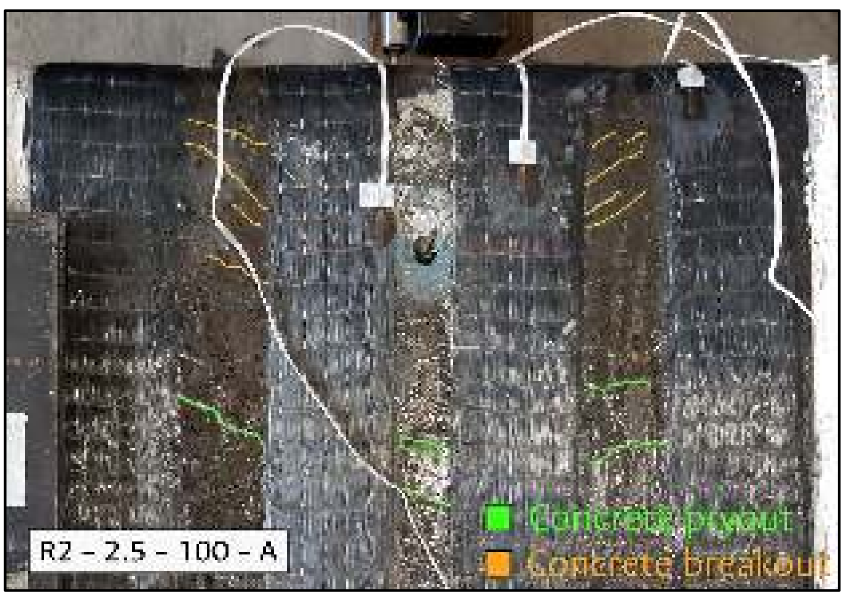

Figure 65 *Failure mechanism R2 – 2.5 – 100 – A. Source: Own.*

Specimen A's anchor shows great deformation on the failure plane. As commented before, this could hint the incidence of bending toward the last stages of the test. Also, the evidence of concrete spalling on the front part of the anchor is the result of the anchor bearing against the concrete, which is common in shear tests. Besides, it is evident that concrete breakout cracks managed to get through the internal CFRP laminates. This once again indicates that arranging the reinforcement in a stirrup-like manner with all laminates of the same width does mitigate crack propagation but is not sufficient to effectively control them. In parallel, concrete pryout cracks were also observed approximately 120 mm behind the anchor. Similar to concrete breakout cracks, some concrete pryout cracks also reached the external laminates. It is important to highlight that as the concrete pryout body develops and rotates, the CFRP gets pulled away from the substrate (Figure 66). As a result, given the advanced state of the concrete pryout cracks, it is possible that if the anchor did not fail, debonding of the composite material could have been close from happening.

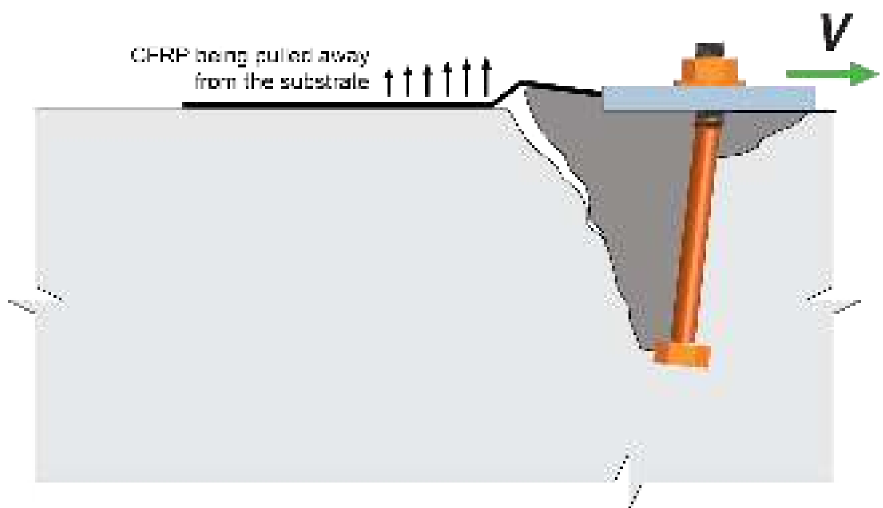

Figure 66 *Concrete pryout effect on CFRP laminates. Adapted from:* (ACI Committee 318, 2019)

Regarding specimens B and C, their failure mode is shown in Figure 67:

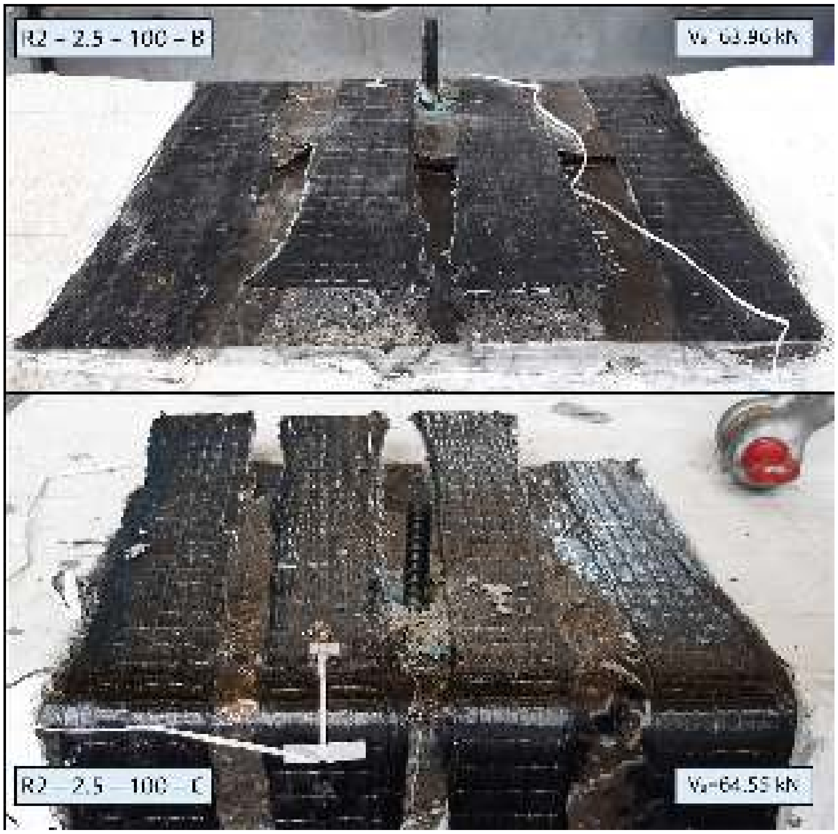

Figure 67 *Failure mode R2 – 2.5 – 100 – (B, C). Source: Own.*

Both specimens exhibited a similar ultimate load and failure mode; the difference lay in the number of strips that debonded from the concrete: two (2) for specimen B and three (3) for specimen C.

For specimen B, the concrete pryout pulled the CFRP with such force, that the internal left laminate debonded first. Part of the force that was being transferred by this strip was redistributed to the internal right laminate, which debonded almost immediately after the first one. Finally, some cracks advanced and went through the CFRP-concrete interface of the external laminates, generating bulges on them. However, given the stiffness differences between concrete and CFRP, some cracks remained on the border region between the external laminates and the concrete, advancing toward the edge of the slab. Once these cracks intersected with some concrete breakout cracks formed previously, the concrete pryout body could rotate freely, thus, the system could not bear any significant load. The crack pattern of specimen B is presented in Figure 68:

Figure 68 *Failure mechanism R2 – 2.5 – 100 – B. Source: Own.*

An important note regarding the observed failure mechanism, is that the external laminates help mitigate the propagation of cracks beyond them; concentrating them in the region in which the reinforcement is installed.

Concerning specimen C, its failure mode was similar to that of specimen B. Even so, the debonding occurred with such a force, that at least one concrete breakout crack advanced through the external right laminate, which also debonded from the substrate. An important observation is that this crack had an orientation of approximately 17°, which corresponds with the experimental angles obtained in the control specimens, contrary to the theoretical 35° angle that belongs to the CCD method. This crack pattern is shown in Figure 69:

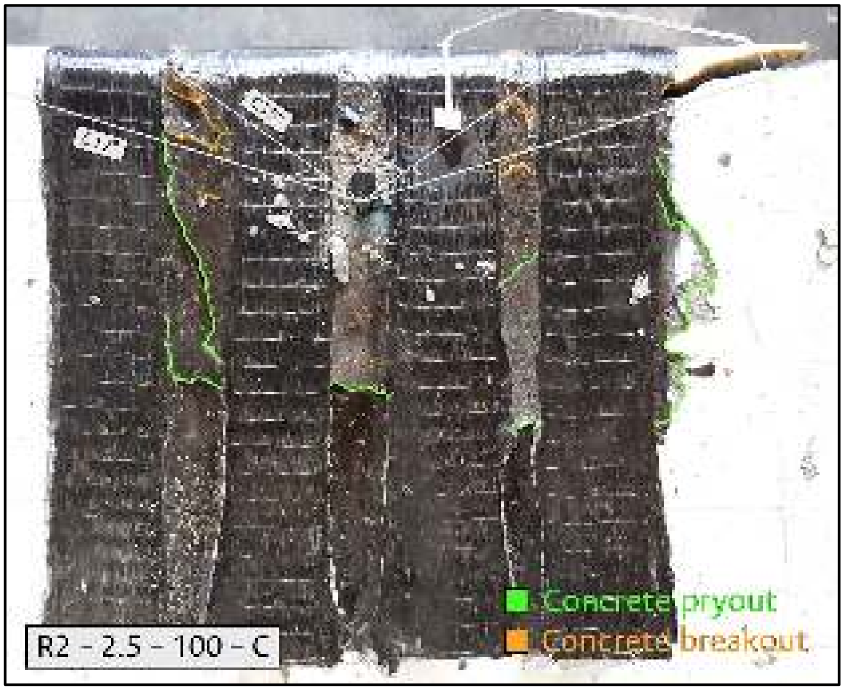

Figure 69 *Failure mechanism R2 – 2.5 – 100 – C. Source: Own.*

To conclude, recalling the observations of the "*Strength and failure mode*" section, even if the total reinforcement area of this configuration was the same as for *R1 – 5*, distributing the CFRP leads to a different behavior. The strut-and-tie model that corresponds to *R2 – 2.5 –* 100 shows that initially, the internal laminates would be those subjected to a higher load, while the external ones would not be bearing any significant stress. Therefore, the width of each laminate should correspond to the force acting on them, which would result in wider internal laminates and narrow external laminates. However, this would lead to a one-laminate-on-each-side design, due to the external laminates being so thin that it would be a better approach to concentrate all the reinforcement as in *R1 – 5 – 100*. Thus, in these applications, distributing the reinforcement in various strips is not recommended. If the design requires an impractical width, overlapping plies of reinforcement could lead to effective results. Also, employing different strips renders a less rigid system, which results in more cracking, and leading to a higher probability of CFRP debonding.

- ***Stress – unit strain behavior***

Specimen A's strain gauges were installed as shown in Figure 70. Once again, the strain gauges were installed close to the theoretical 35° crack path.

Figure 70 *Strain gauges placement R2 – 2.5 – 100 – A. Source: Own.*

The unit strains measured by these gauges over time are represented in Figure 71:

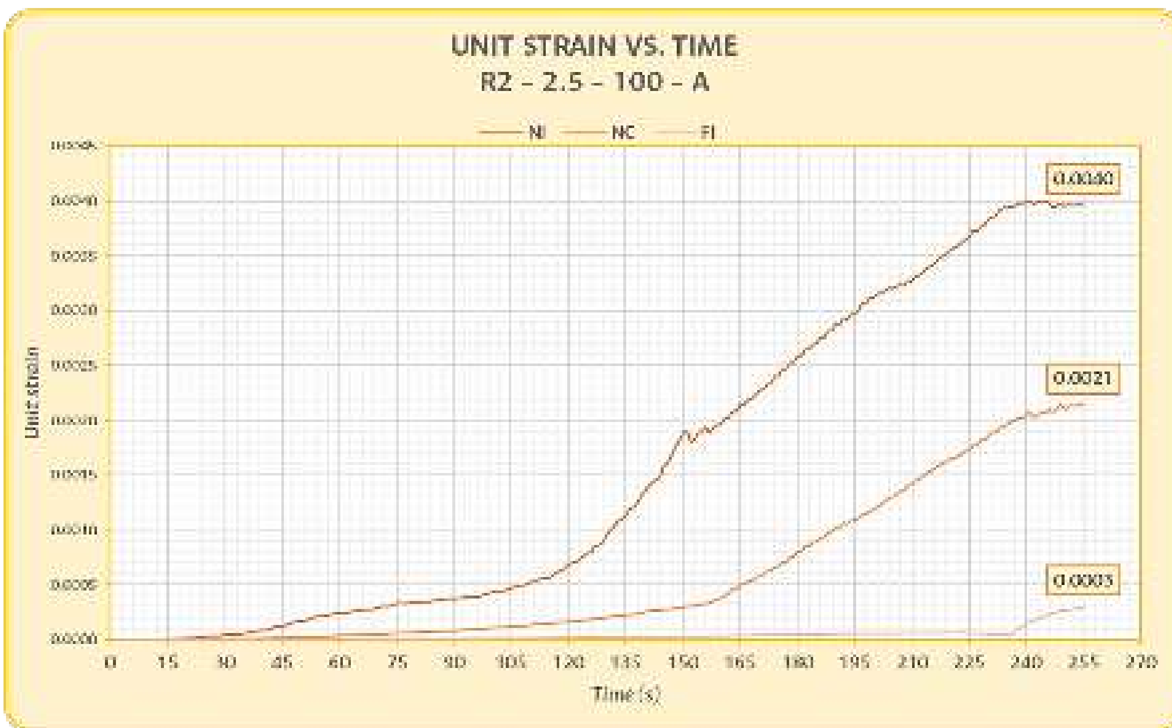

Figure 71 *Unit strains R2 – 2.5 – 100 – A. Source: Own.*

This graph shows how the unit strain decreases as the distance between the anchor and the gauge becomes larger. For instance, when the anchor failed, the strain decreases to almost half (47.5%) between the internal and central regions of the same laminate (between NI and NC). Regarding the external plies, their strains are insignificant in comparison to those registered near the anchor.

Resorting once again to the strut-and-tie model, it is observed that, theoretically, a force of 32.35 kN would be acting on the center of the internal laminates, while the external laminates would be carrying a force of 5.40 kN. This means a reduction of 83.3%. On the other hand, from the unit strain of 0.0021 registered at the center of the internal laminate, to the unit strain of 0.0003 measured at the center of the external laminate, there is a decrease of 85.7%. This exhibits the accuracy of the strut-and-tie model, emphasizing that there is some difference due to the unit strain of the external fiber being measured on the internal part, while the theoretical force was supposed acting on the center.

Overall, these results indicate that the maximum recorded strain (0.0040) was approximately 95.2% of the theoretical debonding strain $\left(\varepsilon_{fd} = 0.0042\right)$, which is evidence that the CFRP could have been close to debonding from the concrete substrate. Table 33 shows how demanded was the CFRP at failure, in relation to its ultimate strain:

Table 33 *CFRP exigency ratio R2 – 2.5 – 100 – A. Source: Own.*

CFRP EXIGENCY RATIO R2 – 2.5 – 100 – A			
Strain gauge	$\boldsymbol{\varepsilon_{f_{Máx.}}}$	$\boldsymbol{\varepsilon^*_{f_u}}$	$\boldsymbol{\varepsilon_{f_{Máx.}}/\varepsilon^*_{f_u}}$
NI	0.0040	0.011	36.4%
NC	0.0021		19.1%
FI	0.0003		2.7%

These values prove that if debonding could be effectively controlled, the laminate could bear even higher stresses, given that approximately only 36% of its ultimate capacity was required. Thus, for some applications, the use of CFRP anchors could lead to a more effective reinforcement design.

Finally, the force – unit strain behavior (until maximum load) of specimen A is registered in Figure 72:

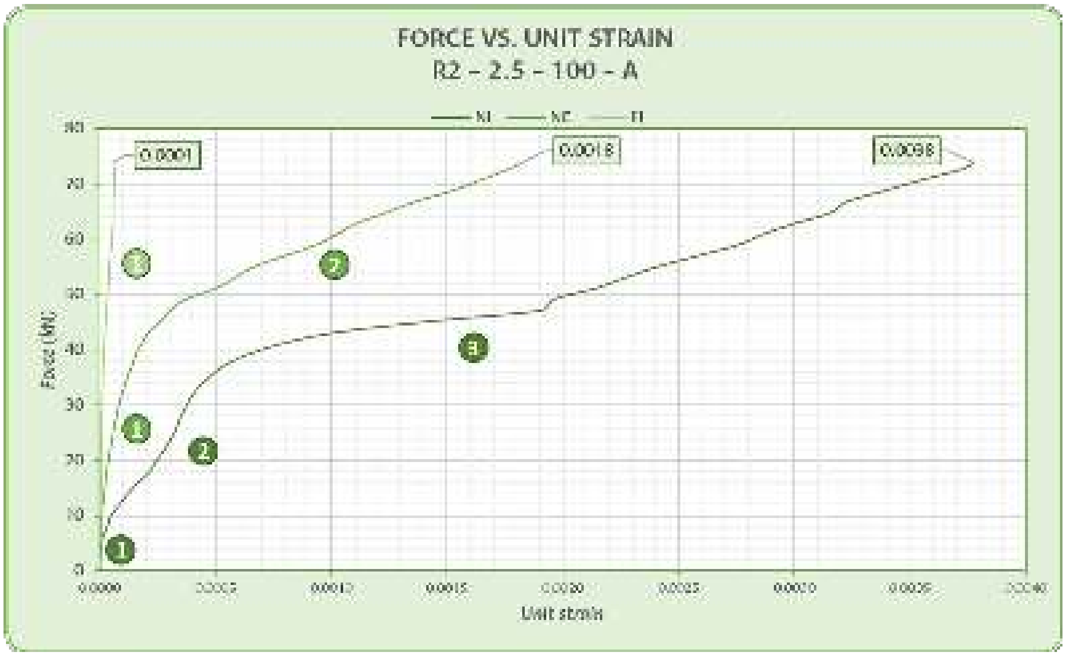

Figure 72 *Force vs. unit strain R2 – 2.5 – 100 – A. Source: Own.*

In this graph, it is corroborated that unit strains are larger close to the anchor, as in this zone cracking is more prominent, thus, the nonlinear behavior registered by gauges NI and NC. On the other hand, the behavior on the external fiber, represented by gauge FI, was linear during the whole test, as almost no observable cracking developed in that region. This is more evidence that supports the idea that more laminates represent no improvement on the behavior. On the contrary, there is more uncertainty in regard to the failure mode and the ultimate achieved strength.

Lastly, strains were also measured in specimens B and C. However, in specimen B, the gauge was installed in an NC position. As a result, the values did not reflect the maximum strains on the fiber, which occur in an NI position. Nevertheless, this specimen's unit strain at failure was 0.0010. Although this value is significantly lower than the one obtained in specimen A on the same position, this variability is attributed to the randomness of crack propagation. Yet, it was possible that the most stressed fiber on specimen B reached a strain larger than the maximum of specimen A, thus, leading to the debonding of the laminate. On the other hand, concerning specimen C, its gauge was damaged during the test, resulting in no registered values during failure.

7.4.1.2.3. R1 – 2.5 – 100.

This reinforcement configuration consisted of one CFRP laminate on each side of the anchor. Each laminate had a width of 2.5 in (64 mm). As a result, this scheme uses 40% of the design reinforcement area.

- ***Strength and failure mode***

Strength related information is presented in Table 34:

Table 34 *Strength and failure mode R1 – 2.5 – 100. Source: Own.*

STRENGTH & FAILURE MODE R1 – 2.5 – 100							
Specimen	**V_u (kN)**	**Avg. V_u (kN)**	**V_u / $V_{Theo.}$**	**Avg. V_u / $V_{Theo.}$**	**V_u / V_{C0}**	**Avg. V_u / V_{C0}**	**Failure mode**
A	79.46	74.69	1.05	0.99	2.23	2.10	***CP → DB***
B	72.40		0.96		2.03		***CP → DB***
C	72.21		0.96		2.03		***CP → DB***

Initially, no significant differences are appreciated between the three specimens. Their mode of failure was characterized by debonding due to the propagation of concrete pryout cracks. Also, the span between ultimate loads was 9.7% of the average load, which is deemed as an acceptable dispersion of the data.

In spite of the obtained mode of failure, the capacity of the specimens was very similar to the theoretical steel rupture one. In fact, specimen A achieved a load higher than the theoretically necessary to obtain anchor failure, but it still failed due to debonding of the CFRP laminates.

The fact that steel rupture was not obtained in any specimen could be attributed to two main reasons: variability in the materials properties, and less stiffness of the reinforcement system, which allowed the formation of wider cracks, resulting in a higher probability of debonding. Nevertheless, these results indicate that it could be possible to obtain the desired mode of failure, with less than half of the required reinforcement area. Also, the effectiveness of CFRP in improving the behavior is evident, increasing, in average, the system’s capacity in 110% in relation to unreinforced specimens.

Figure 73 summarizes the load – displacement behavior of this reinforcement configuration:

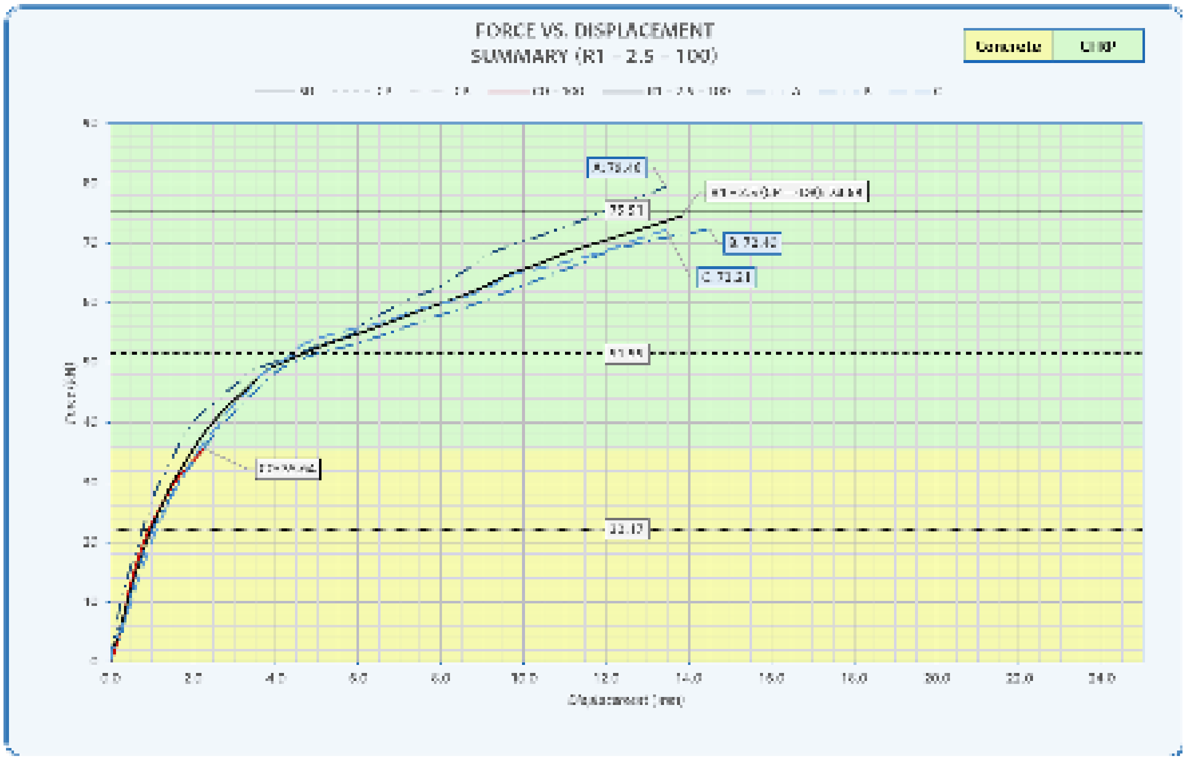

Figure 73 *Force vs. displacement R1 – 2.5 – 100. Source: Own.*

These curves show that, in terms of strength, all specimens were close to achieving steel rupture. In addition, in relation to the curve that represents control specimens, the enhanced behavior given by CFRP to the anchoring system, is also visible.

Finally, these curves also display how the response becomes approximately linear around the theoretical concrete pryout load, indicating the full effect of CFRP.

- ***Energy absorption***

Table 35 shows the most relevant information concerning the energy absorption capacity of this reinforcement configuration:

Table 35 *Absorbed energy R1 – 2.5 – 100. Source: Own.*

ABSORBED ENERGY R1 – 2.5 – 100				
Specimen	**W_u (J)**	**Avg. W_u (J)**	**W_u / W_{C0}**	**Avg. W_u / W_{C0}**
A	757	743	13.4	13.1
B	765		13.5	
C	707		12.5	

These results point out that, although debonding is a brittle mode of failure, this reinforcement system has a higher ductility than an unreinforced one. It is also important to recall that all calculations were done considering the behavior until the maximum load was achieved, but the nonlinear behavior continued until failure, thus, resulting in more absorbed energy. Once again, the sound emitted by the CFRP during the test became a warning sign that indicated proximity to failure.

- ***Failure mechanism***

The mode of failure of these anchors could be explained similarly as for *R2 – 2.5* specimens. However, *R1 – 2.5* samples contained 50% less reinforcement area. This agrees with the hypothesis that if reinforcement is distributed, the strips closer to the anchor will do most of the load-bearing work. The failure mechanism of specimen A is illustrated in Figure 74:

Figure 74 *Crack formation in specimen R1 – 2.5 – 100 – A. Source: Own.*

The most noticeable effect of not using external laminates, is that cracks (especially concrete pryout ones) extend beyond the CFRP, until they reach the edge of the slab, completing the concrete pryout body and leading to debonding. All specimens exhibited debonding of both laminates, so this mode of failure was also observed in specimens B and C.

- ***Stress – unit strain behavior***

No strain gauges were installed on these specimens. However, it could be expected that the fibers located closer to the anchor experimented strains similar or larger than the theoretical unit strain associated with debonding $\left(\varepsilon_{fd} = 0.0042\right)$.

7.4.1.2.4. R1 – 2.5 – X – 100.

This reinforcement configuration consisted of one CFRP laminate on each side of the anchor, but in X configuration, i.e., the laminates were oriented perpendicular to the average experimental concrete breakout crack path. Each laminate had a width of 2.5 in (64 mm). This configuration employed the second type of steel used in this project. Due to the mechanical differences between both types of steel, although the geometry of the laminates was the same, the reinforcement area corresponded to 45% of the required area by design, which is 13% more area than for configuration *R1 – 2.5*.

- ***Strength and failure mode***

Failure mode and strength results are summarized in Table 36. As all specimens from this reinforcement configuration employed the latter steel, all of them are marked with a star (*). The theoretical rupture load related to this steel is 66.82 kN.

Table 36 *Strength and failure mode R1 – 2.5 – X – 100. Source: Own.*

STRENGTH & FAILURE MODE R1 – 2.5 – X – 100							
Specimen	**V_u (kN)**	**Avg. V_u (kN)**	**V_u / $V_{Theo.}$**	**Avg. V_u / $V_{Theo.}$**	**V_u / V_{C0}**	**Avg. V_u / V_{C0}**	**Failure mode**
A*	67.57	67.98	1.01	1.02	1.90	1.91	***SR***
B*	66.71		1.00		1.87		***SR***
C*	69.65		1.04		1.95		***SR***

The results are satisfactory, as steel rupture was obtained in all tested specimens, showing ultimate loads 2% higher, in average, than the theoretical load required to obtain this failure mode. Also, in comparison to unreinforced specimens, the capacity increased in 91%. These are significant response improvements, considering the amount of reinforcement employed, and that no strength reduction factors were employed.

Also, the dispersion between ultimate load values was not significant, as the span between maximum and minimum strength was 2.94 kN, which is 4.3% of the average maximum load.

Graphically, the load – displacement response curves are displayed in Figure 75:

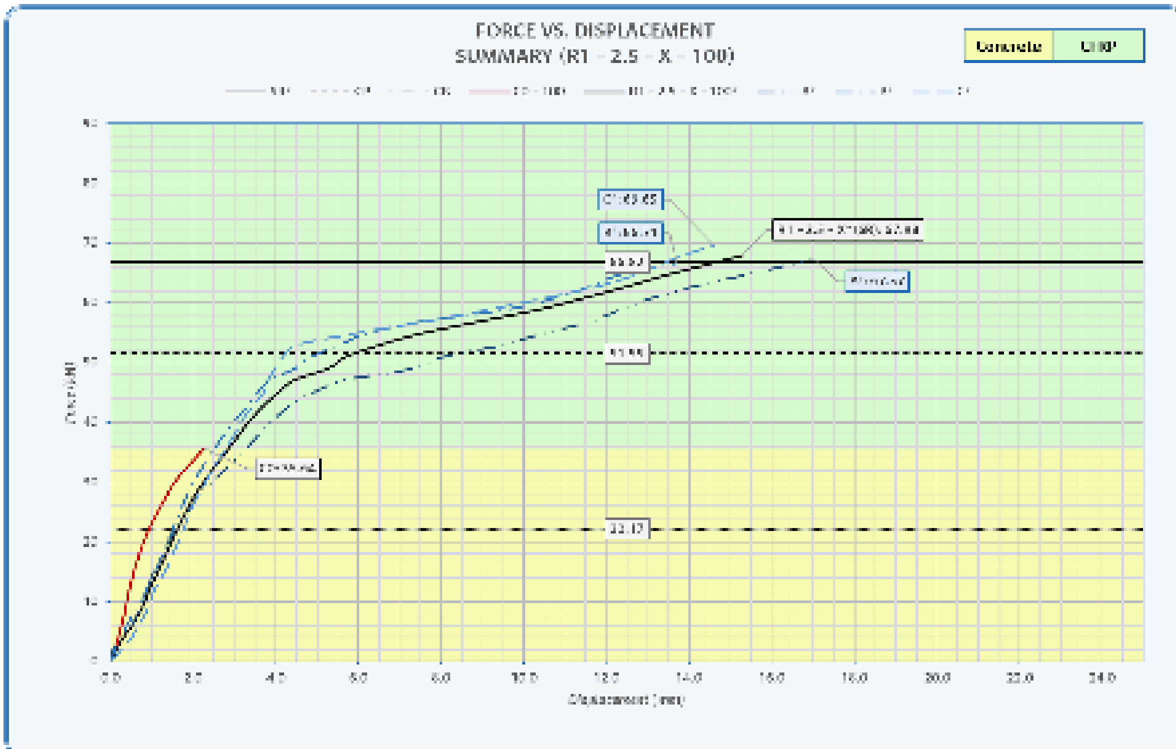

Figure 75 *Force vs. displacement R1 – 2.5 – X – 100. Source: Own.*

The overall behavior of this configuration is similar to that of the other CFRP-reinforced specimens. It illustrates the progressively decreasing load-bearing capacity of the concrete, and the subsequent contribution of the composite material, which provides enough additional strength to guarantee steel rupture. However, at the beginning, there is a slight discordance with the experimental control curve. In this regard, as tests were carried out, the baseplate employed for applying load displayed signs of wear in the region in contact with the backside of the anchor (Figure 76). Therefore, this variation could be attributed to a slippage of the baseplate so it could be in full contact with the anchor. Finally, it is observed that all specimens achieved ultimate loads that surpassed the theoretical steel rupture one.

Figure 76 *Wear on the steel plate due to accumulated tests. Source: Own.*

- ***Energy absorption***

Results related to absorbed energy are presented in Table 37:

Table 37 *Absorbed energy R1 – 2.5 – X – 100. Source: Own.*

ABSORBED ENERGY R1 – 2.5 – X – 100				
Specimen	**W_u (J)**	**Avg. W_u (J)**	**W_u / W_{C0}**	**Avg. W_u / W_{C0}**
A*	812	740	14.3	13.0
B*	675		11.9	
C*	732		12.9	

All specimens exhibited similar behaviors, achieving 13 times more energy absorption capacity than the control specimens, which is a significant improvement, considering that the desired failure mode was achieved with less than half of the required area of reinforcement.

- ***Failure mechanism***

As steel rupture was obtained in all specimens, failure was characterized by the complete fracture of the anchor. However, the laminates were retired from the concrete, to assess how advanced was cracking when failure occurred.

Figure 77 illustrates the most noticeable cracks observed in specimen A*:

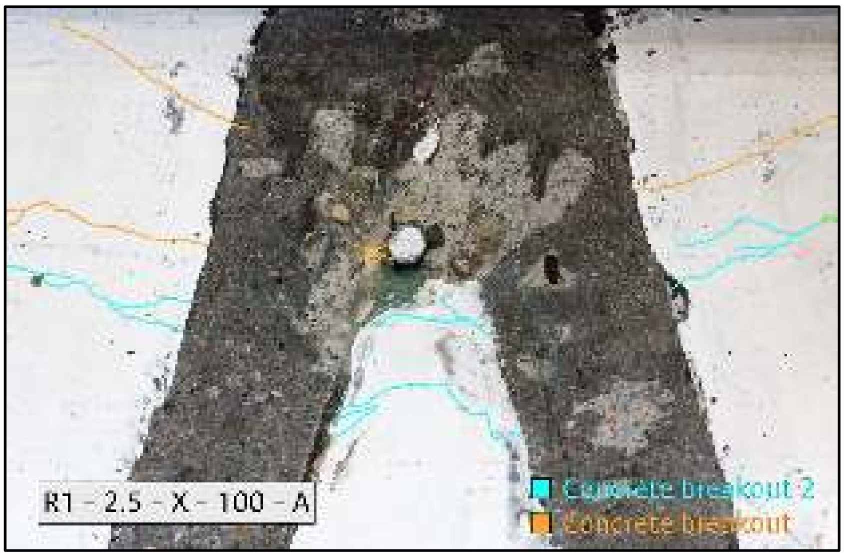

Figure 77 *Failure mechanism R1 – 2.5 – X – 100 – A*. Source: Own.*

It is evident that various cracks extended beyond the fiber; some of them even reaching the edge of the member. This indicates that some concrete could have been close to detaching from the slab, even if anchor failure was obtained.

In addition, what would normally be categorized as concrete pryout cracks, displayed a particular behavior. First, these cracks were usually observed in a range between 80 to 120 mm behind the anchor, but in this case, they were located at approximately half of that distance. Also, the concavity of the arch between the laminates was different than usual. In this case, it is possible that the orientation of the fibers was effective in mitigating concrete pryout, guaranteeing an optimal confinement of the concrete. As a result, if the reinforced system deformed as a unity, it would be feasible for concrete breakout cracks to form progressively farther from the edge, as if the anchoring system was being torn from its placement. Therefore, these cracks are catalogued as concrete breakout cracks that appear at higher loads, given certain confinement conditions.

On the other hand, specimen B* exhibited less cracking than specimen A*. Actually, it was observed that no cracks extended beyond the CFRP, and none reached the concrete's edge, as shown in Figure 76:

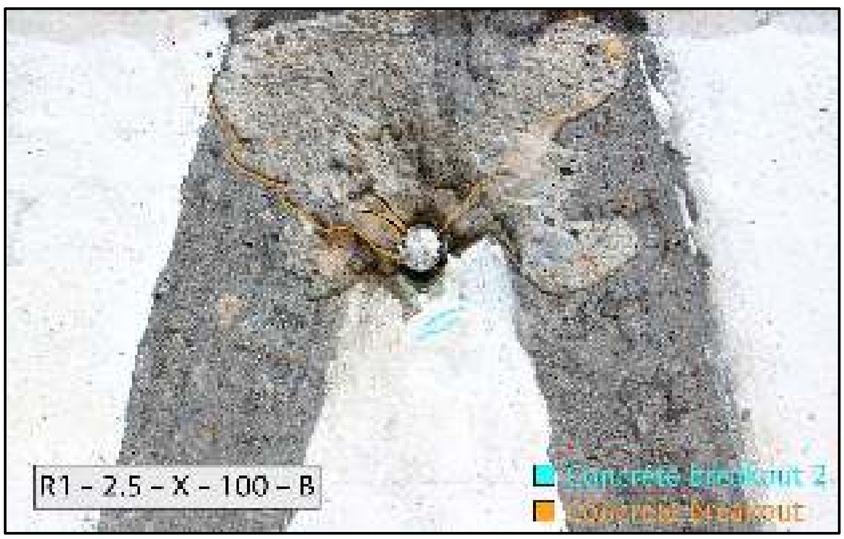

Figure 78 *Failure mechanism R1 – 2.5 – X – 100 – B*. Source: Own.*

According to this picture, it is possible to assert that as the X configuration concentrates a higher amount of CFRP near the anchor, crack control is more effective. This is supported by the measured crack width, as none of them was wider than 0.10 mm. Moreover, no cracks related to concrete pryout were observed.

Lastly, specimen C displayed a behavior similar to specimen B, with no significant cracking on the vicinity of the fractured anchor.

- ***Stress – unit strain behavior***

Strain gauges were installed on specimens A* and B*. They were placed on the internal region of the laminate, and as close to the concrete breakout crack path as possible. The location of these gauges on each specimen is shown in Figure 79:

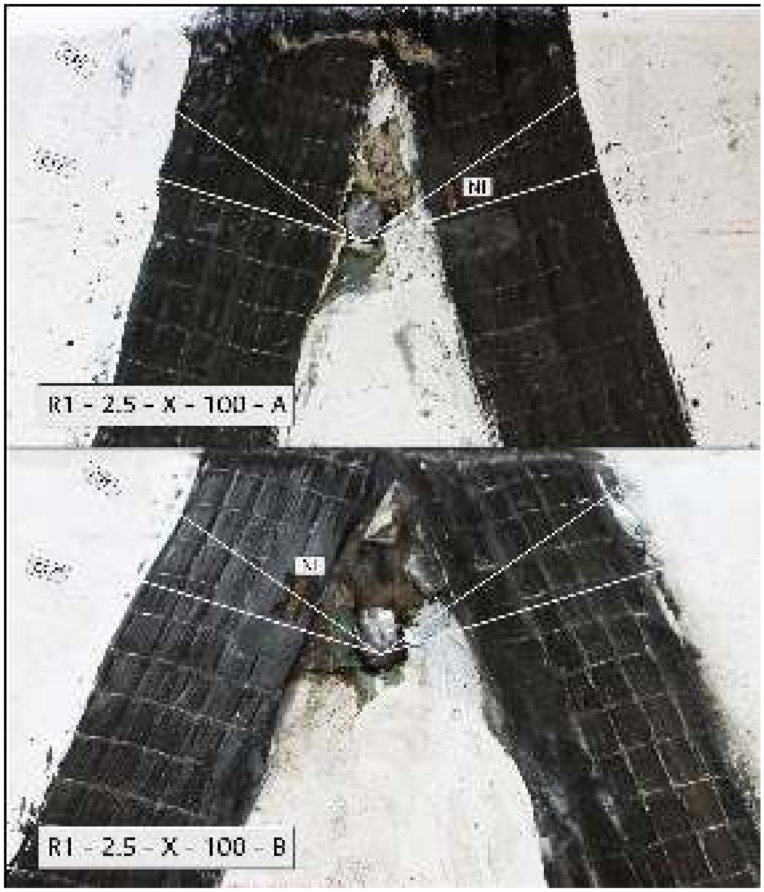

Figure 79 *Strain gauges placement R1 – 2.5 – X – 100 – (A*, B*). Source: Own.*

Maximum registered unit strains registered for both specimens, as well as the CFRP efficiency ratio are shown in Table 38:

Table 38 *CFRP exigency ratio R1 – 2.5 – X – 100. Source: Own.*

CFRP EXIGENCY RATIO R1 – 2.5 – X – 100				
Specimen	**Strain gauge**	$\varepsilon_{f_{Máx.}}$	$\varepsilon_{f_u}^{*}$	$\varepsilon_{f_{Máx.}}/\varepsilon_{f_u}^{*}$
A*	NI	0.0042	0.011	38.2%
B*	NI	0.0031		28.2%

Specimen A* shows a higher maximum unit strain than specimen B*. This could be attributed to the placement of the anchor within the laminates. As shown in Figure 77, the location of specimen A*'s anchor was somewhat to the left. This may have induced cracking at the right of the anchor, due to the absence of CFRP on that immediate region. As a result, wider cracks led to higher unit strains registered by the gauge. In addition, for specimen A*, the strain gauge recorded a maximum unit strain of 0.0042, which is 1.05 times the theoretical debonding unit strain. Similar to specimen *R2 – 2.5 – 100 – A*, even if steel rupture was obtained, the fiber could have been close to debonding from the concrete substrate. However, the absence of significant cracks may imply that even higher loads would have been necessary to cause debonding of the laminates. This proves the efficacy of the geometry of this reinforcement configuration.

Finally, the force – unit strain behavior of specimens A* and B* is presented in Figure 80. These curves show the response just until the maximum load was achieved.

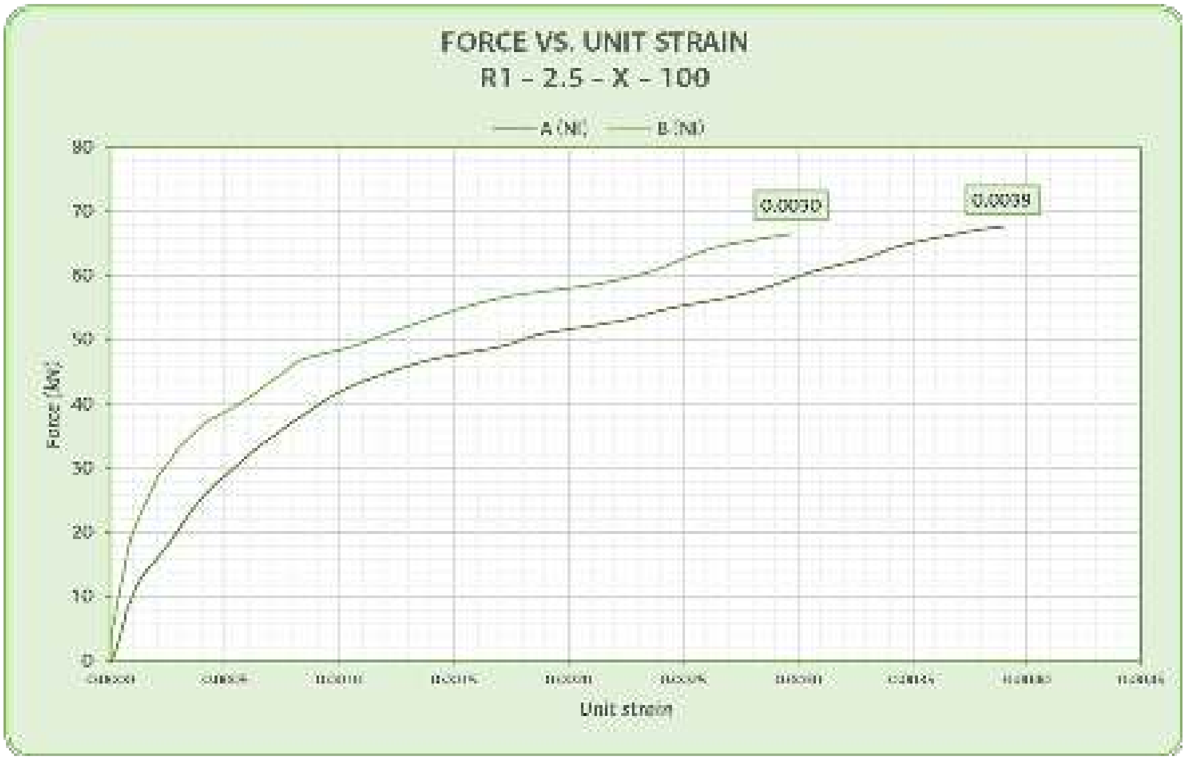

Figure 80 *Force vs. unit strain R1 – 2.5 – X – 100. Source: Own.*

This graph supports the hypothesis that the region in which specimen A*'s gauge was located sustained more fissure formation, leading to a degradation in stiffness of that area.

7.4.1.2.5. Overall analysis (100 mm)

- ***Strength and failure mode***

Table 39 summarizes all information associated with strength and modes of failure for specimens located at 100 mm from the edge.

Table 39 *Strength and failure mode summary (100 mm). Source: Own.*

STRENGTH AND FAILURE MODE SUMMARY C_{a1} = 100 mm						
ID	**Specimens**	**Avg. V_u (kN)**	**Avg. V_u / $V_{Theo.}$**	**Avg. V_u / V_{C0}**	**$A_{Reinf.}$ / $A_{Des.}$**	**Failure mode**
C0	A, B, C	35.64	1.61	–	–	***CB***
CH	A*, B*	49.26	0.74	1.38	1.30	***CB → SR***
	C*	68.27	1.02	1.92		***SR***
R1 – 5	A, B, C, D	76.40	1.01	2.14	0.79	***SR***
R2 – 2.5	A	73.77	0.98	2.07	0.79	***SR***
	B, C	64.26	0.85	1.80		***CP → DB***
R1 – 2.5	A, B, C	74.69	0.99	2.10	0.40	***CP → DB***
R1 – 2.5 – X	A*, B*, C*	67.98	1.02	1.91	0.45	***SR***

In parallel, overall load – displacement behavior is illustrated in Figure 81:

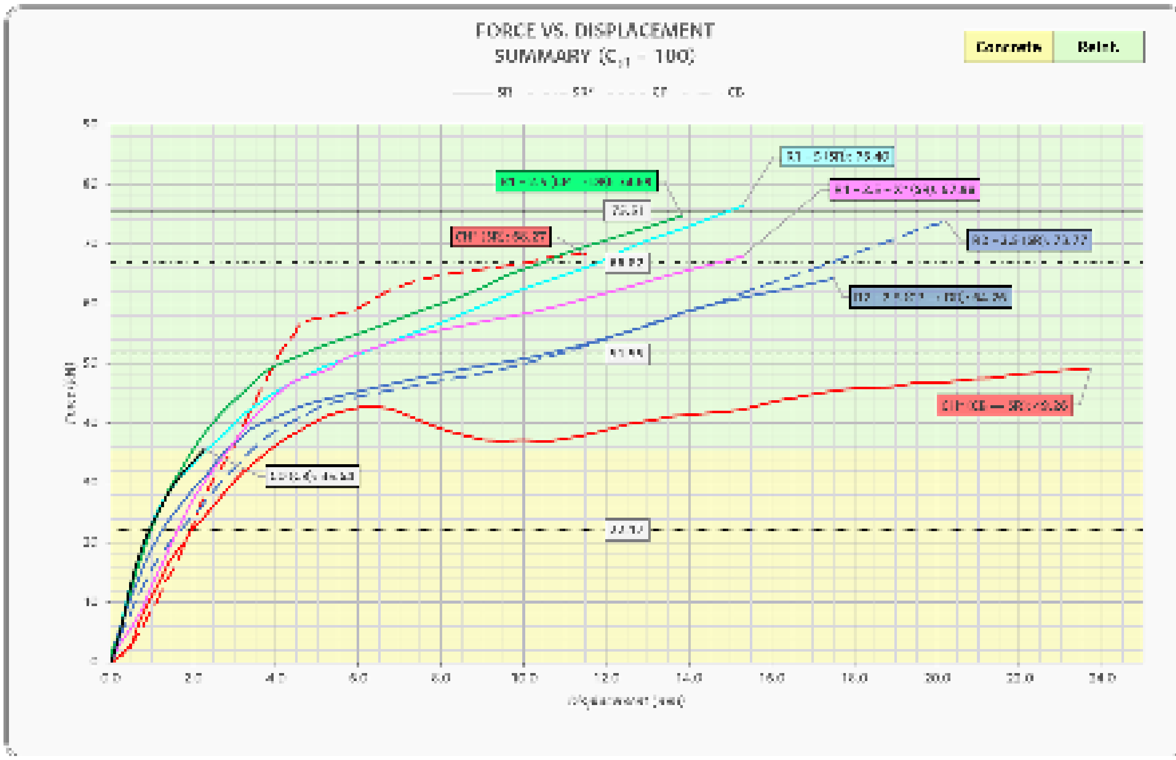

Figure 81 *Force vs. displacement summary (100 mm). Source: Own.*

All reinforcement schemes demonstrated strength improvements when compared to unreinforced specimens. Regarding CFRP-reinforced specimens, configuration *R1 – 5 – 100* proved the best behavior in this aspect. Despite consisting of 79% of the design reinforcement area, steel rupture was obtained in every anchor, increasing the ultimate load in 114% in relation to unreinforced anchors. Furthermore, this increase could have been greater, if not limited by the ultimate mechanical properties of the anchor.

Next, is reinforcement scheme *R2 – 2.5 – 100*. Even if this configuration also consisted of 79% of the area dictated by design, it displayed uncertainty in its mechanical response, revealing two failure modes. As commented in its corresponding section, distributing the reinforcement into various strips affects the mechanical response of the system. Most importantly, internal laminates take most of the force initially, due to cracks intersecting them first. Also, as their width is smaller, their capacity of controlling fissures decreases; therefore, wider cracks develop. These cracks induce large strains on the fiber, which in conjunction with concrete pryout lead to a higher probability of debonding. Nevertheless, it was observed that external laminates do serve a purpose, as they act as a barrier that concentrates most cracks within the reinforced region. Finally, in comparison to other curves, specimens that belonged to this configuration demonstrated less rigidity, which could be attributed to differences in the internal concrete structure, ranging from compaction deficiencies to pre-existing micro fissures.

Concerning reinforcement type *R1 – 2.5 – 100*, with 40% of the required reinforcement, these specimens experimented debonding, but were close to achieving steel rupture. This proves that controlling crack propagation is crucial on preventing debonding of the laminates. It is possible that a slight increase area of reinforcement could guarantee the required stiffness to effectively mitigate the effect associated with concrete pryout, increasing the probability of anchor failure.

Regarding configuration *R1 – 2.5 – X – 100*, the biggest remark is that steel rupture was obtained in every specimen, with just 45% of the calculated required reinforcement. In comparison to *R1 – 2.5 – 100*, these results could be attributed to the slightly higher area of reinforcement. However, placing the laminates perpendicular to the cracks did show improvements in crack control, as no evidence of concrete pryout was observed on the concrete surface. Therefore, this configuration displayed the best strength-related behavior, next to *R1 – 5 – 100*.

Finally, regarding hairpin-reinforced specimens, their behavior was highly dependent on the installation of the anchor reinforcement. As noted by (Mallée et al., 2012, p. 122), the depth of the hairpin within the concrete member, as well as its closeness to the anchor, have significant influence on the strength and the mechanical behavior of the system. If full contact is guaranteed between the anchor and the hairpin, stresses can effectively be transferred between both elements. Also, if the hairpin is placed near the concrete surface, higher loads can be achieved, due to a reduction in the eccentricity between the reinforcement and the external load. However, a minimum concrete cover should be given, to comply with durability requirements. Small differences in these construction parameters can reduce the effectiveness of the reinforcement in approximately 50% (Mallée et al., 2012, p. 124). Considering the above, even if both types of reinforcement (cast-in and post-installed) require adequate design, installation and supervision, hairpin-reinforced anchoring systems show a higher sensitivity in this aspect.

- ***Energy absorption***

The energy absorption capacity of all systems is presented in Table 40:

Table 40 *Energy absorption summary (100 mm). Source: Own.*

ENERGY ABSORPTION SUMMARY C_{a1} = 100 mm					
ID	**Specimens**	**Avg. W_u (J)**	**Avg. W_u / W_{C0}**	**$A_{Reinf.}$ / $A_{Des.}$**	**Failure mode**
C0	A, B, C	56.7	–	–	***CB***
CH	A*, B*	881	15.5	1.30	***CB → SR***
	C*	562	9.9		***SR***
R1 – 5	A, B, C, D	948	16.7	0.79	***SR***
R2 – 2.5	A	996	17.6	0.79	***SR***
	B, C	834	14.7		***CP → DB***
R1 – 2.5	A, B, C	743	13.1	0.40	***CP → DB***
R1 – 2.5 – X	A*, B*, C*	740	13.0	0.45	***SR***

All reinforcements improved the response of the anchoring system with respect to unreinforced specimens. The minimum gain was shown by specimen *CH – 100 – C**, increasing absorption capacity in almost 10 times. On the other hand, the biggest improvement was displayed by specimen *R2 – 2.5 – 100 – A*, which absorbed 17.6 times more energy than unreinforced specimens. Overall, huge improvements are achieved when reinforcing anchors susceptible to failure due to concrete breakout.

It is important to notice that the lowest improvement was observed in the hairpin-reinforced specimen that achieved a higher ultimate load (*CH – 100 – C**). In contrast, the other samples that incorporated cast-in reinforcement, showed an exchange between ultimate load and deformation capacity. The systems that displayed a preliminary concrete breakout failure followed by steel rupture (*CH – 100 – A*, CH – 100 – B**), achieved, on average, 56.7% more energy absorption than their counterpart that demonstrated “pure” shear anchor failure (*CH – 100 – C**). Yet, these same specimens achieved only 72% of the ultimate load attained by specimen C*.

- ***Reinforcement effectiveness***

To make a comparison that involves both ultimate load and energy absorbed, the relation between these two parameters was calculated. Clearly, these values are not supposed to be taken as definitive in regard to which reinforcement scheme has the overall best behavior, but they shed some light on their strength and deformation response. These results are illustrated in Table 41:

Table 41 *Reinforcement effectiveness summary (100 mm). Source: Own.*

REINFORCEMENT EFFECTIVENESS C_{a1} = 100 mm					
ID	**Specimens**	**Avg. W_u (J)**	**Avg. V_u (kN)**	**Avg. W_u / V_u (J/kN)**	**Failure mode**
C0	A, B, C	56.7	35.64	1.59	***CB***
CH	A*, B*	881	49.26	17.9	***CB → SR***
	C*	562	68.27	8.23	***SR***
R1 – 5	A, B, C, D	948	76.40	12.4	***SR***
R2 – 2.5	A	996	73.77	13.5	***SR***
	B, C	834	64.26	13.0	***CP → DB***
R1 – 2.5	A, B, C	743	74.69	9.95	***CP → DB***
R1 – 2.5 – X	A*, B*, C*	740	67.98	10.9	***SR***

According to this information, hairpin-reinforced systems (*CH – 100*) that presented dual failure mode (specimens A and B) showed the best proportion between absorbed energy and achieved load (17.9). However, it is important to emphasize that these specimens achieved, on average, 74% of the expected failure load. Next place belongs to CFRP configuration *R2 – 2.5 – 100* (specimen A), with an energy – load proportion of 13.5. This specimen achieved steel rupture and failed at 98% of the expected load. Nevertheless, it should be noted that *R2 – 2.5 – 100* specimens exhibited variability in their failure mode, and that construction factors could have had an influence on their load – displacement response. Next places belong to configurations *R1 – 5 – 100* and *R1 – 2.5 – X – 100*, with energy – load proportions of 12.4 and 10.9, respectively. Both configurations showed reliability in their failure modes (steel rupture in all of them), as well as in their ultimate strength (101% and 102% of the theoretical load, respectively). Therefore, these CFRP reinforcement configurations are deemed as the most reliable, for this edge distance. Also, if the proportion of supplied to required area of reinforcement is considered, configuration *R1 – 2.5 – X – 100* would be the most effective one. Still, its capability relies on how well the orientation of the cracks is known, which leads to some degree of uncertainty.

7.4.2. Edge distance: 50 mm.

7.4.2.1. Hairpin-reinforced specimens.

- ***Strength and failure mode***

Strength parameters and failure mode results are displayed in Table 42:

Table 42 *Strength and failure mode CH – 50. Source: Own.*

STRENGTH & FAILURE MODE CH – 50							
Specimen	**V_u (kN)**	**Avg. V_u (kN)**	**V_u / $V_{Theo.}$**	**Avg. V_u / $V_{Theo.}$**	**V_u / V_{C0}**	**Avg. V_u / V_{C0}**	**Failure mode**
A*	42.96	45.38	0.64	0.68	3.23	3.42	***CB → SR***
B*	51.37		0.77		3.87		***CB → SR***
C*	41.82		0.63		3.15		***CB → SR***

All specimens developed steel rupture of the anchor but preceded by the formation of a concrete breakout body, as observed in two of the three *CH – 100* specimens. Given this mode of failure, no specimen achieved the theoretical load associated with anchor rupture, reaching, on average, 68% of this value. Regardless, these specimens improved the ultimate load attained by control specimens in 5.8 times, which represents a significant improvement. Lastly, a coefficient of variation of 9.4% was obtained, evidencing reliability in the results.

Figure 82 illustrates the force – displacement behavior of these specimens:

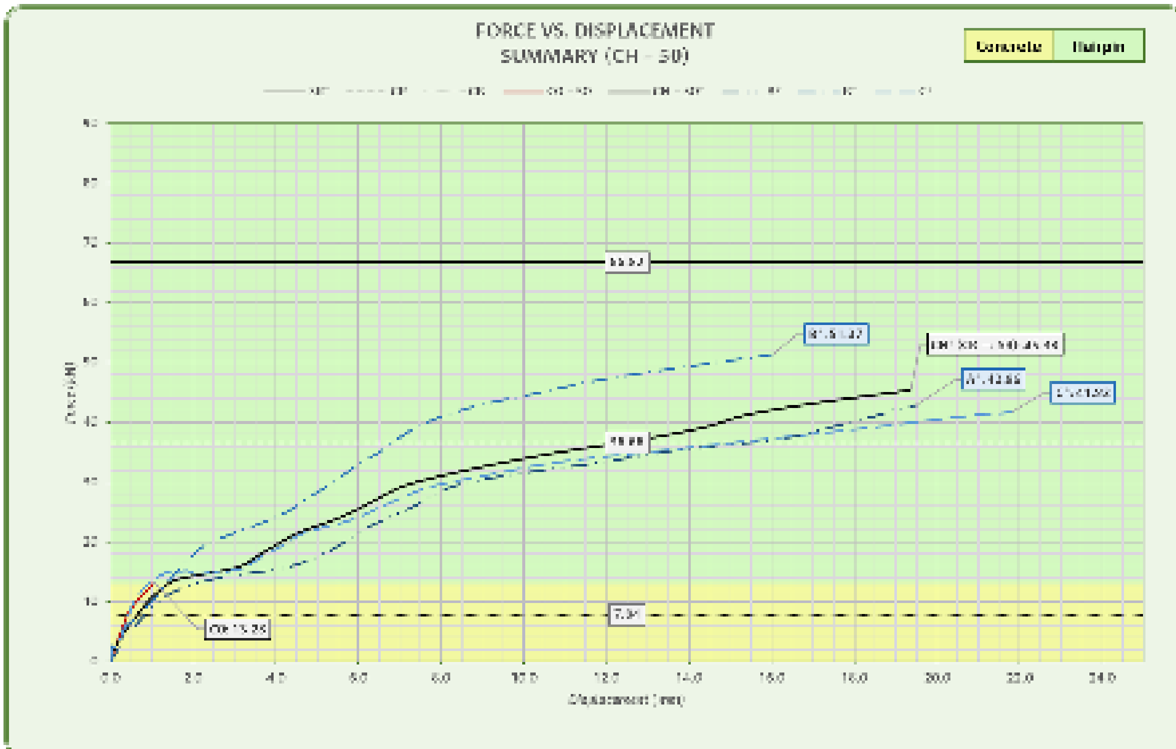

Figure 82 *Force vs. displacement CH – 50. Source: Own.*

The response of these specimens is marked by the fact that when they reached the experimental value of concrete breakout, the overall system loses rigidity, suggesting cracking and the subsequent formation of a breakout body. However, due to the displacements related to cracking, the anchors engage the hairpin, which is now part of the load-bearing system. The cast-in anchor reinforcement provides additional strength; yet, given that the breakout body has already formed, the anchor bends, as there is no concrete that provides confinement in front of the anchor. This interaction between bending and shear leads to steel failure, but at a lower load than if there was no significant influence of bending.

- ***Energy absorption***

Results associated with energy absorption are listed in Table 43:

Table 43 *Absorbed energy CH – 50. Source: Own.*

ABSORBED ENERGY CH – 50				
Specimen	**W_u (J)**	**Avg. W_u (J)**	**W_u / W_{C0}**	**Avg. W_u / W_{C0}**
A*	538	588	62.3	68.1
B*	570		66.0	
C*	656		76.0	

As a result of the nonlinear behavior achieved by the influence of bending, these specimens attained an absorbed energy capacity 68 times greater than that of unreinforced specimens located at the same distance to the edge. This behavior demonstrates that these anchors did not achieve the expected ultimate load, but developed large displacements that translate into a more ductile behavior.

- ***Failure mechanism***

The failure surfaces of specimens A* and B* are shown in Figures 83 and 84, respectively:

Figure 83 *Failure mechanism CH – 50 – A*. Source: Own.*

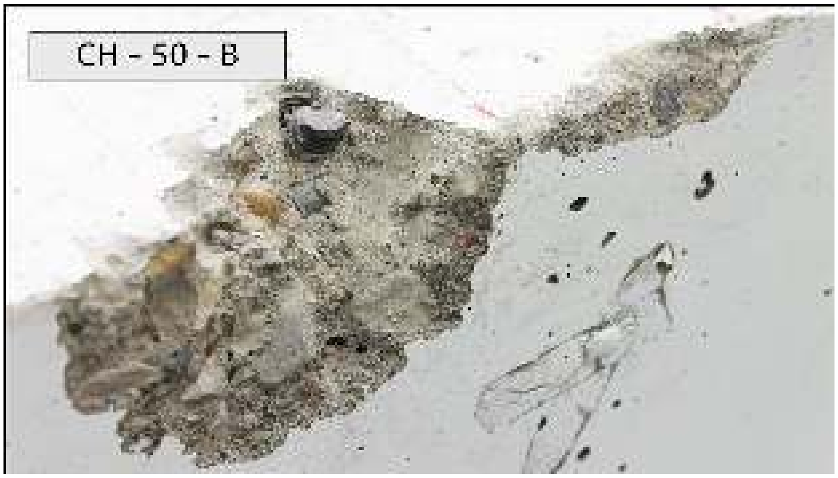

Figure 84 *Failure mechanism CH – 50 – B*. Source: Own.*

There is a noticeable size difference between the breakout bodies of specimens A* and B*. Specimen B*'s breakout body suggests that its hairpin had an installation of greater quality than that of specimen A*. This is because on specimen B* the hairpin would have activated early, concentrating cracks in a smaller zone than specimen A*. This also allowed specimen B* to reach a higher ultimate load. In conclusion, contrary to unreinforced anchors, where a larger concrete breakout body is synonym of a higher ultimate load, in hairpin-reinforced specimens, a smaller breakout body indicates earlier activation of the hairpin, which guarantees a higher achievable load.

On the other hand, a detail of specimen C* after the test is shown in Figure 85:

Figure 85 *Failure mode CH – 50 – C*. Source: Own.*

This picture illustrates the joint action of shear and bending. The rotation of the anchor, in conjunction with the degradation observed on the back of its cross-section, are indicators of the effect of bending over the specimen. In addition, it is important to highlight that rupture starts on the zone subjected to the combined action of high tensile stresses due to bending, and shear stresses due to the direct action of the external load.

7.4.2.2. CFRP-reinforced specimens.

7.4.2.2.1. R1 – 5 – 50.

One 5.0 in (127 mm) wide CFRP laminate on each anchor side. This corresponds to 79% of the design area.

- ***Strength and failure mode***

Strength-related data may be found in Table 44:

Table 44 *Strength and failure mode R1 – 5 – 50. Source: Own.*

STRENGTH & FAILURE MODE R1 – 5 – 50							
Specimen	V_u (kN)	Avg. V_u (kN)	V_u / $V_{Theo.}$	Avg. V_u / $V_{Theo.}$	V_u / V_{C0}	Avg. V_u / V_{C0}	Failure mode
A	51.42	42.82	0.68	0.57	3.87	3.22	***CS***
B	43.85		0.58		3.30		***CS***
C	33.16		0.44		2.50		***CS***

The ultimate load results of these specimens show significant variability, as there is high dispersion between them. The coefficient of variation of these results is 17.5%. On the other hand, it is important to note that all specimens failed due to concrete slicing, i.e., a portion of crushed concrete slid between the CFRP laminates, allowing huge displacements on the anchor, and leading eventually, to anchor pullout. This mode of failure is analyzed in further detail in the *Failure mechanism* section.

Overall, no specimen could achieve neither the failure mode nor the load desired, reaching, on average, 57% of the load associated with steel rupture. Nevertheless, the reinforcement did improve the capacity of the system, accomplishing more than three times the capacity of unreinforced systems.

Moreover, their load – displacement behavior is illustrated in Figure 86:

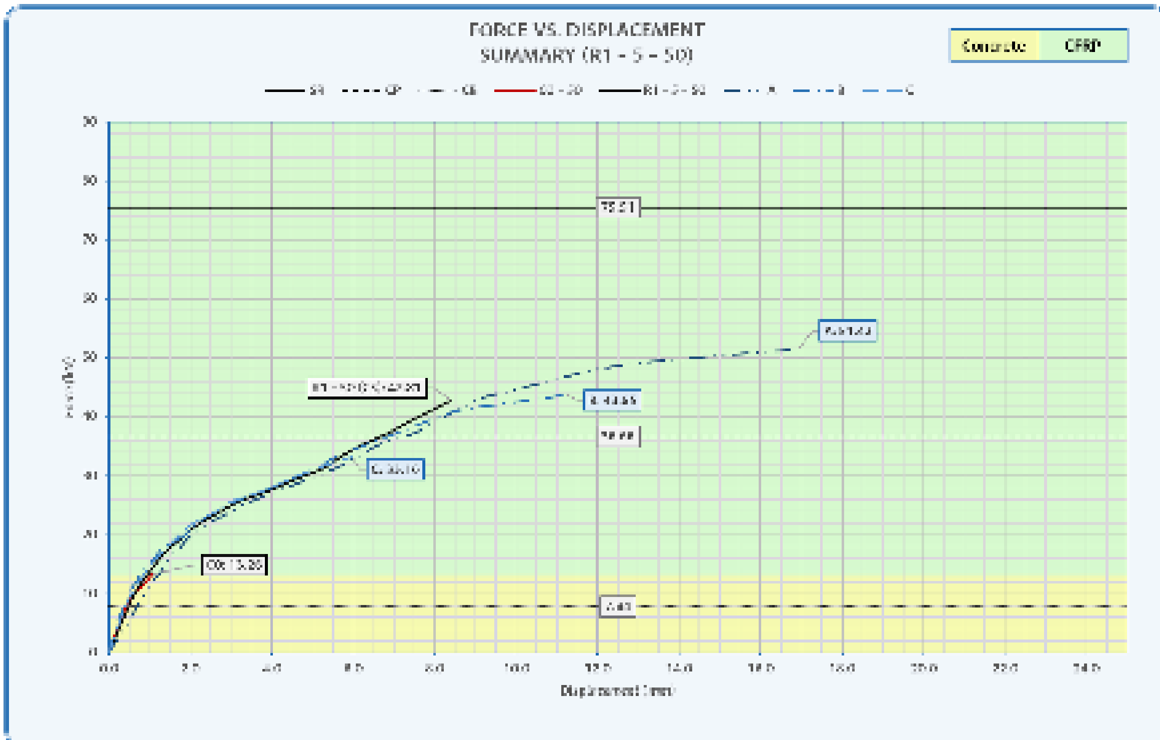

Figure 86 *Force vs. displacement R1 – 5 – 50. Source: Own.*

All specimens were similar in regard to the path of their response. However, once again, the dispersion between their ultimate loads and displacements is evident. Specimens A and B achieved loads higher to that associated with concrete pryout, whereas specimen C did not achieve this value.

- ***Energy absorption***

Concerning energy absorption, the results for all specimens are presented in Table 45:

Table 45 *Absorbed energy R1 – 5 – 50. Source: Own.*

ABSORBED ENERGY R1 – 5 – 50				
Specimen	**W_u (J)**	**Avg. W_u (J)**	**W_u / W_{C0}**	**Avg. W_u / W_{C0}**
A	625	371	72.4	43.0
B	350		40.6	
C	138		16.0	

Again, high dispersion is observed between the data, with a coefficient of variation of 53.7%. This shows an even higher dispersion in comparison with maximum load. Nevertheless, the absorption capacity of the reinforced systems signified an improvement in relation to unreinforced anchors.

- ***Failure mechanism***

Figure 87 shows the failure mode of specimen A:

Figure 87 *Failure mode R1 – 5 – 50 – A. Source: Own.*

As mentioned before, the crushed concrete in front of the anchor advanced in the same direction of the load, finding an exit between the CFRP laminates. This behavior is explained by the interaction between the fiber and concrete. Due to the differences in stiffness between both materials, some cracks did not go through CFRP, staying on concrete, as it is the material with the lowest tensile capacity. Therefore, the cracks headed to the edge of the slab, remaining on the border zone between the strips and unreinforced concrete. In addition, the concrete at the front of the anchor was completely crushed, due to the compressive stresses concentrated in that region. The combination of both effects generated a disintegrated breakout body that slipped between the fibers. Also, as the bond between the anchor and the concrete was lost, the anchor separated completely from the concrete member, indicating failure. This failure mode was observed in all specimens that corresponded to this reinforcement scheme.

Regarding cracks, all specimens showed not significant cracking on the top surface of the concrete. Some concrete breakout cracks formed, but as mentioned before, they were scarce, and concentrated mostly in the border region between the CFRP and the unreinforced concrete. However, on the lateral side, all specimens displayed the formation of a breakout body, due to the displacements to which the anchor was subjected. These observations are illustrated in Figure 88, for specimen B:

Figure 88 *Failure mode R1 – 5 – 50 – B. Source: Own.*

Finally, some fibers experienced such deformation, that some fibers reached their ultimate capacity, revealing local rupture of CFRP, as seen in Figure 89 for specimen A. Further information on why these fibers achieved strains this high, may be found on the following section “*Stress – strain behavior*”.

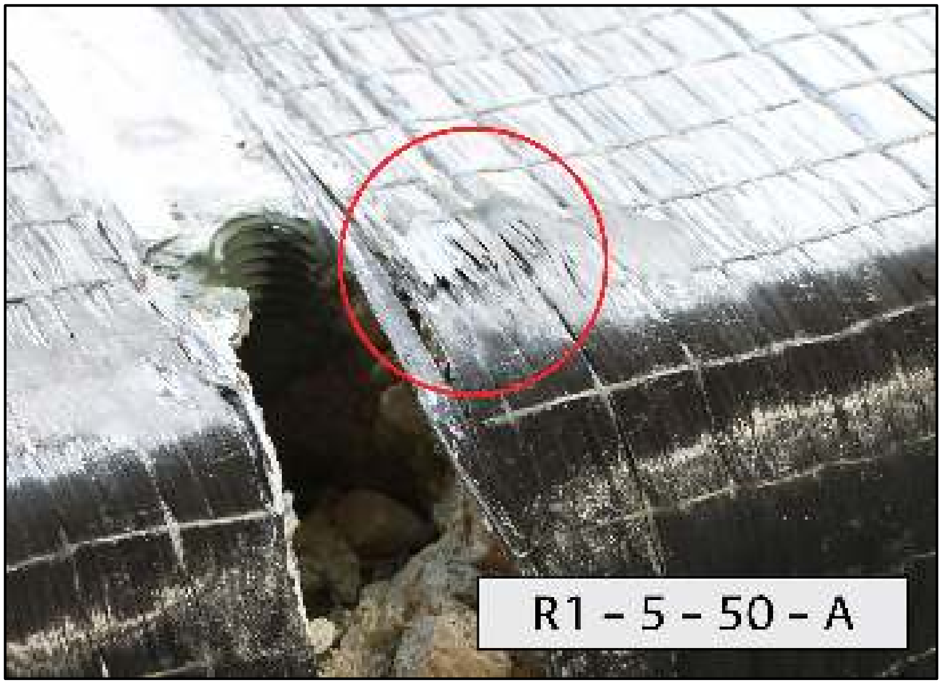

Figure 89 *CFRP rupture R1 – 5 – 50 – A. Source: Own.*

- ***Stress – strain behavior***

Strain gauges were installed on specimens B and C. Their location is shown in Figure 90:

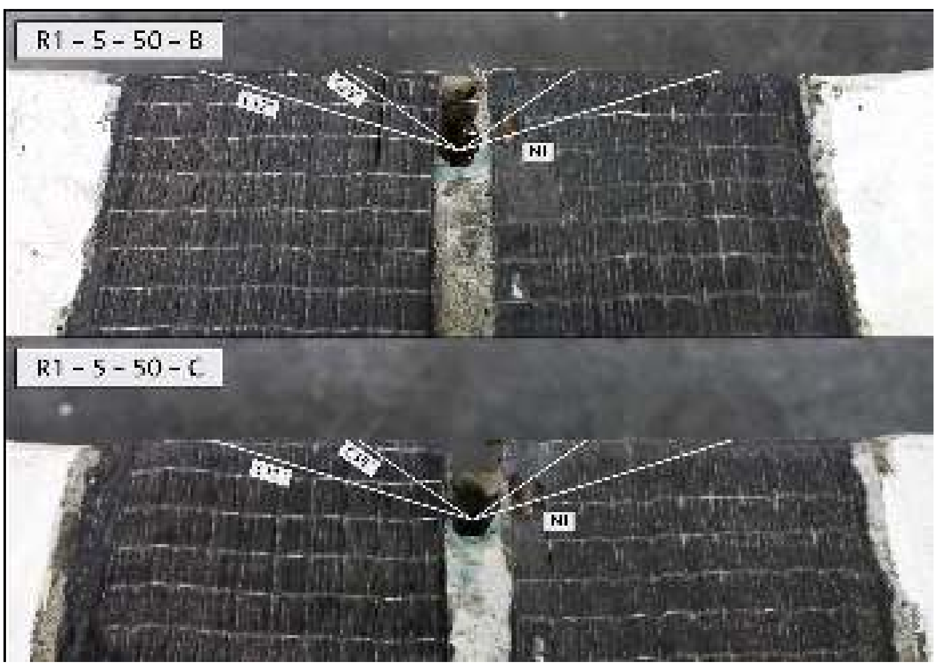

Figure 90 *Strain gauges location R1 – 5 – 50 (B, C). Source: Own.*

Table 46 shows the relation between the maximum unit strain registered during the test, and the ultimate strain specified by the CFRP manufacturer.

Table 46 *CFRP exigency ratio R1 – 5 – 50. Source: Own.*

CFRP EXIGENCY RATIO R1 – 5 – 50				
Specimen	**Strain gauge**	$\varepsilon_{f_{Máx.}}$	$\varepsilon^*_{f_u}$	$\varepsilon_{f_{Máx.}}/\varepsilon^*_{f_u}$
B	NI	0.0088	0.011	80.0%
C	NI	0.0051		46.4%

This table shows valuable information. First, it is evident that these maximum unit strain values are significantly higher than those registered in specimens located at 100 mm from the concrete edge. This is closely related to the failure mechanism observed in each case. As mentioned before, *R1 – 5 – 50* specimens did not show significant cracking on the concrete surface. This means that the CFRP located at the top of the member was not being pulled away as pronouncedly as in specimens with significant cracking (especially pryout cracks). As a result, the probability of failure by debonding decreased. In addition, the high stress concentration in the region between the anchor and the edge, exerted higher deformation on the CFRP fibers, which translated into unit strain values larger than any registered before in this study. In fact, specimen B recorded unit strains that were just 20% lower than the rupture-associated value, which means that for this configuration, some fibers could achieve strains way beyond failure by debonding. This also explains the preliminary rupture of some fibers, as illustrated in Figure 89 for specimen A.

On the other hand, the force – unit strain behavior registered by these gauges until the maximum load was achieved, is evidenced in Figure 91:

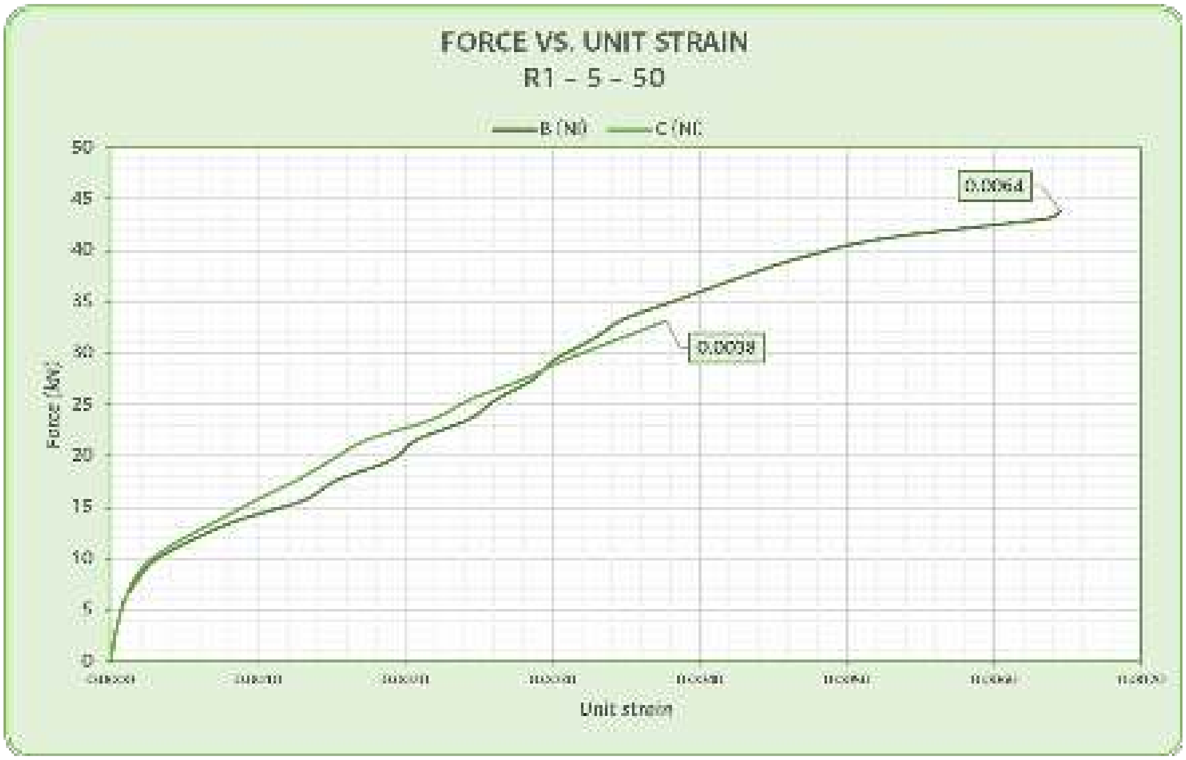

Figure 91 *Force vs. unit strain R1 – 5 – 50. Source: Own.*

Both curves show similar behavior, and with specimen B developing higher strains than specimen C, which concurs with their load – displacement response.

The results obtained in this configuration show that if the anchor is placed closer to the edge, the risk of debonding decreases, allowing for larger strains on the fiber. However, the lack of confinement in front of the anchor concentrates the failure in that region, due to the closeness between the anchor and the edge. This also results in the reinforced systems not being able to achieve their expected ultimate load. To address these weaknesses, configuration *R0 – 5 – 50* was developed.

7.4.2.2.2. R1 – 2.5 – 50.

This reinforcement configuration consisted of one 2.5 in (64 mm) wide CFRP laminate placed on each side of the anchor, which translates into 40% of the required reinforcement area.

- ***Strength and failure mode***

Table 47 presents the most relevant information regarding strength and mode of failure registered for this reinforcement configuration.

Table 47 *Strength and failure mode R1 – 2.5 – 50. Source: Own.*

STRENGTH & FAILURE MODE R1 – 2.5 – 50							
Specimen	**V_u (kN)**	**Avg. V_u (kN)**	**V_u / $V_{Theo.}$**	**Avg. V_u / $V_{Theo.}$**	**V_u / V_{C0}**	**Avg. V_u / V_{C0}**	**Failure mode**
A	35.46	35.92	0.47	0.48	2.67	2.70	***CS***
B	40.71		0.54		3.07		***CS***
C	31.59		0.42		2.38		***CS***

As in *R1 – 5*, all the specimens that belonged to *R1 – 2.5* displayed concrete slicing. Likewise, no specimen achieved an ultimate load close to the theoretical steel rupture one. However, these specimens showed less dispersion in the data, with a coefficient of variation of 10.4%. Nevertheless, the CFRP still improved the behavior with respect to control specimens, as reinforced specimens supported 2.7 times more load than unreinforced systems.

Figure 92 presents the load – displacement behavior of this reinforcement configuration:

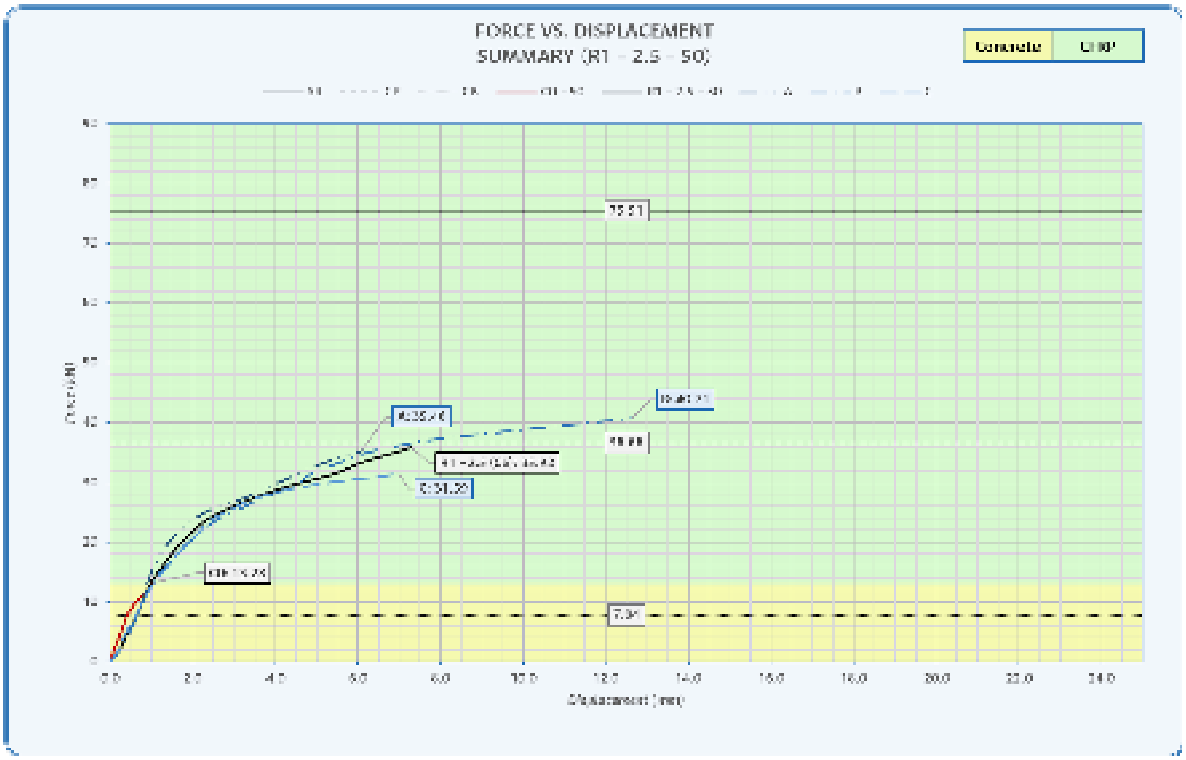

Figure 92 *Force vs. displacement R1 – 2.5 – 50. Source: Own.*

It is observed that all load paths are similar, differing in how much displacement was ultimately achieved. Also, all three specimens reached an ultimate load similar to that associated with concrete pryout. However, it is important to note that pryout was not the failure mode displayed by these specimens. In general, all samples represented an improvement when compared to control specimens. Yet, their ultimate load was 48% of the expected one.

- ***Energy absorption***

Concerning energy absorption, results for these specimens are summarized in Table 48:

Table 48 *Absorbed energy R1 – 2.5 – 50. Source: Own.*

ABSORBED ENERGY R1 – 2.5 – 50				
Specimen	**W_u (J)**	**Avg. W_u (J)**	**W_u / W_{C0}**	**Avg. W_u / W_{C0}**
A	149	234	17.3	27.1
B	389		45.1	
C	163		18.9	

This configuration achieved, on average, 27 times the absorption capacity registered in unreinforced specimens, with a coefficient of variation of 47.0%. However, specimen B demonstrated high dispersion in relation to specimens A and C. If the data of specimen B is not considered, the coefficient of variation decreases to 4.49%, and the absorbed energy proportion between reinforced and control specimens reduces to 18.1.

- ***Failure mechanism***

The failure mechanism of specimens from this configuration was very similar to that presented by *R1 – 5 – 50* anchoring systems. In all specimens concrete slicing was observed. The mechanism behind this behavior has already been explained. Figure 93 shows the mode of failure of specimen B:

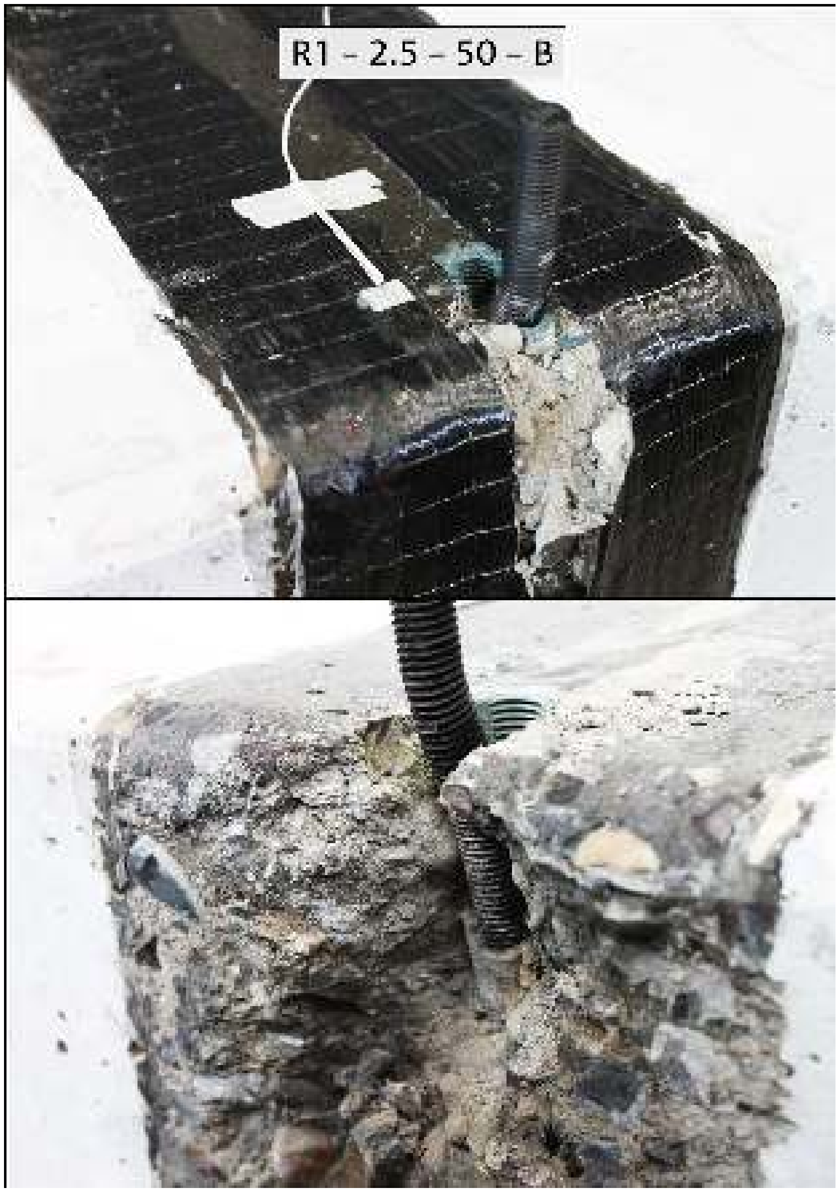

Figure 93 *Failure mode R1 – 2.5 – 50 – B. Source: Own.*

Concerning crack propagation, these specimens evidenced a slight increase in crack formation, in relation to *R1 – 5 – 50*. For instance, in specimen A (Figure 94), only the principal concrete breakout cracks developed at the top of the slab. Moreover, no concrete pryout cracks were observed on the surface of the specimen. However, on the lateral side of the member, the disintegration of the concrete was evident. Specimens B and C followed a similar pattern.

Figure 94 *Failure mode R1 – 2.5 – 50 – A. Source: Own.*

Finally, no indication of CFRP rupture was observed in any specimen.

- ***Stress – strain behavior***

Strain gauges were installed on specimens B and C. Their placement is illustrated in Figure 95, and the exigency ratio of the reinforcement of both specimens is presented in Table 49:

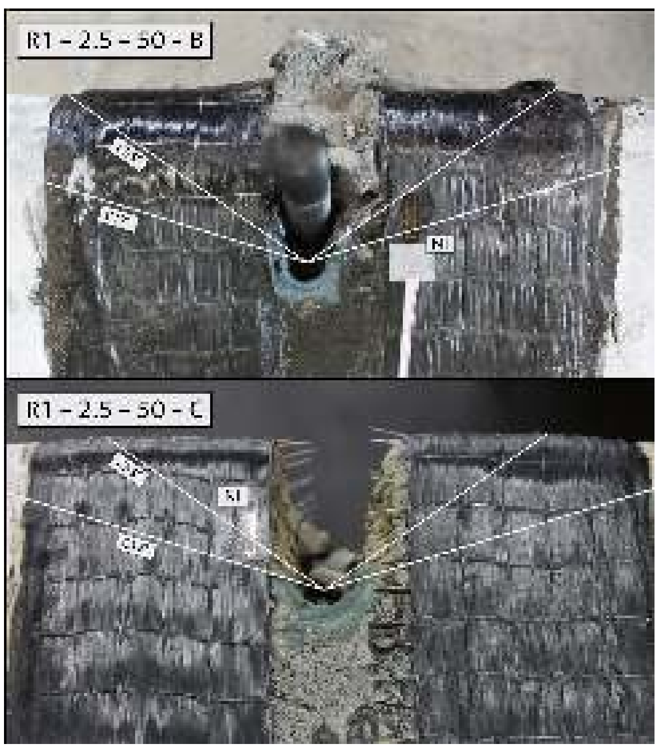

Figure 95 *Strain gauges location R1 – 2.5 – 50 – (B, C). Source: Own.*

Table 49 *CFRP exigency ratio R1 – 2.5 – 50. Source: Own.*

CFRP EXIGENCY RATIO R1 – 2.5 – 50				
Specimen	**Strain gauge**	$\varepsilon_{f_{Máx.}}$	ε^{*}_{fu}	$\varepsilon_{f_{Máx.}}/\varepsilon^{*}_{fu}$
B	NI	0.0031	0.011	28.2%
C	NI	0.0033		30.0%

Both specimens achieved a similar maximum load. However, these values are significantly lower than those registered in *R1 – 5 – 50*, even if both schemes displayed a similar behavior. This could be attributed to stiffness differences between both configurations. As *R1 – 2.5 – 50* specimens have narrower laminates, their stiffness is lower in comparison to *R1 – 5 – 50* samples. This could explain why more cracks are formed in these specimens. As a result, if using narrower strips is less effective in confining the breakout body, failure occurs earlier, thus, the CFRP cannot achieve higher unit strain values.

Figure 96 compares the force – unit strain behavior registered in specimens B and C until maximum load was attained:

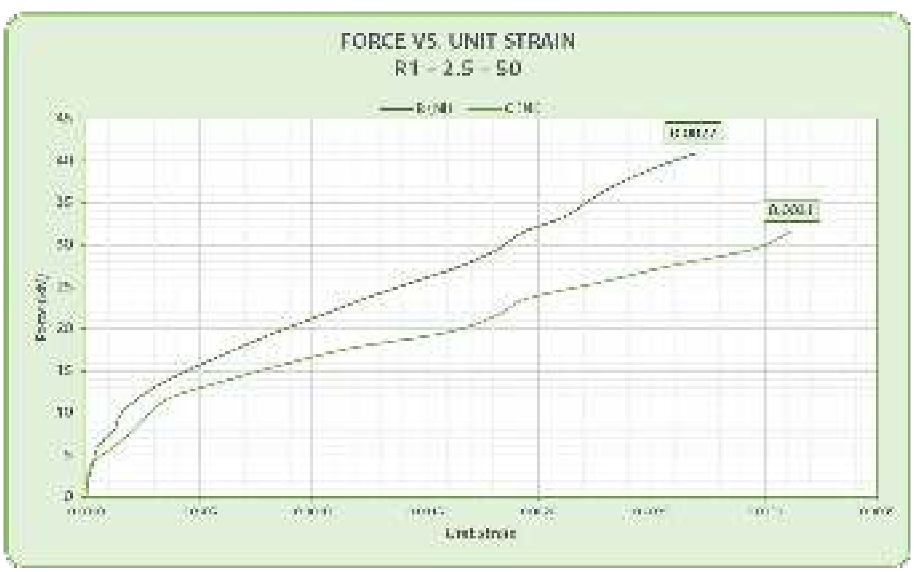

Figure 96 *Force vs. unit strain R1 – 2.5 – 50. Source: Own.*

The results demonstrate that specimen B performed more rigidly than specimen C. This could be attributed to a slightly better confinement, which delayed concrete slicing, and allowed for more load to be supported.

In general, the behavior of *R1 – 2.5 – 50* specimens shared some characteristics with configuration *R1 – 5 – 50*. This is, the space between the laminates permitted the development of a concrete breakout slice, which limited the maximum achievable capacity of the reinforced system.

7.4.2.2.3. R1 – 2.5 – X – 50.

These specimens consisted of one 2.5 in (64 mm) wide CFRP laminate placed on each side of the anchor, in X configuration. As the second steel was used for these anchors, the reinforcement area represented 45% of the required one. Also, these specimens are marked with a star (*) to differentiate them from those that employed the first steel. It is important to recall that, in this case, the load associated with steel failure is 66.82 kN.

- ***Strength and failure mode***

The performance of these reinforced systems, in terms of strength and failure mode, can be visualized in Table 50:

Table 50 *Strength and failure mode R1 – 2.5 – X – 50. Source: Own.*

STRENGTH & FAILURE MODE R1 – 2.5 – X – 50							
Specimen	**V_u (kN)**	**Avg. V_u (kN)**	**V_u / $V_{Theo.}$**	**Avg. V_u / $V_{Theo.}$**	**V_u / V_{C0}**	**Avg. V_u / V_{C0}**	**Failure mode**
A*	55.27	53.18	0.83	0.80	4.16	4.00	***DB***
B*	51.09		0.76		3.85		***DB***
C*	71.73	71.73	1.07	1.07	5.40	5.40	***SR***
D*	57.10	57.10	0.85	0.85	4.30	4.30	***CB → SR***

This scheme displayed high variability in its response. For instance, specimens A* and B* presented partial debonding of their laminates, while specimen D* demonstrated the formation of a concrete breakout body, followed by the rupture of the anchor. Finally, specimen C* showed a more rigid behavior than specimen D*, so its anchor failed without much incidence from bending. Specimens A*, B* and D* failed at similar loads and exhibited identical load – displacement behaviors (as seen in Figure 97); however, due to their different failure modes, only specimens A* and B* were grouped together.

Regarding their maximum attained loads, only specimen C* reached a load higher than expected, hence, the rupture of the anchor. Although specimen D* also experimented anchor rupture, due to the combination of factors that led to this failure mode, it only achieved 85% of the design load.

The load – displacement behavior of these reinforced anchors is presented in Figure 97:

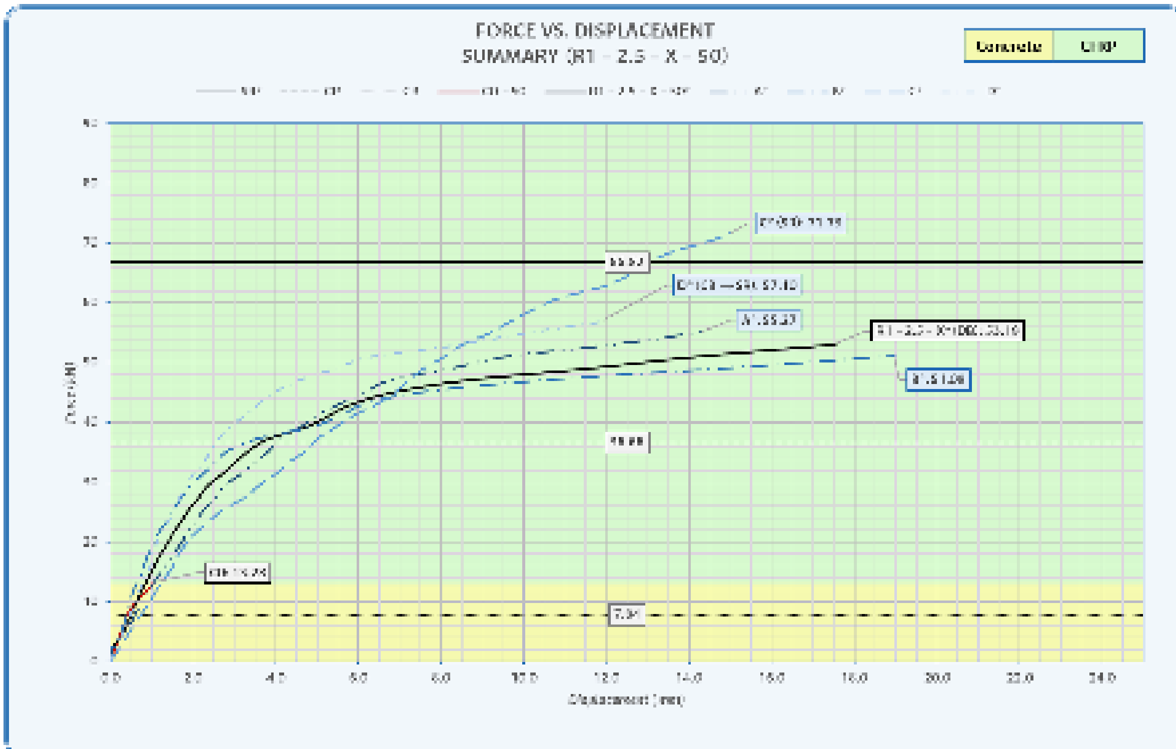

Figure 97 *Force vs. displacement R1 – 2.5 – X – 50. Source: Own.*

It is evident that specimens A* and B* developed large displacements due to insufficient stiffness of the reinforced system. This could have led to large strains on the CFRP, resulting in its debonding. In parallel, the laminates installed on specimen D* could have provided a more efficient confinement of the system, contributing to a higher rigidity, as observed in the path of its curve, in comparison to that of specimens A* and B*. Besides, a confined system that prevents the free displacement of the anchor is subjected to higher flexure, which could have acted in conjunction with shear to produce the rupture of the anchor. Lastly, conditions inherent to specimen C* allowed it to reach steel rupture. This is analyzed in further detail in the “*Failure mechanism”* section.

- ***Energy absorption***

Regarding energy absorption capacity, this information is illustrated in Table 51:

Table 51 *Absorbed energy R1 – 2.5 – X – 50. Source: Own.*

ABSORBED ENERGY R1 – 2.5 – X – 50				
Specimen	**W_u (J)**	**Avg. W_u (J)**	**W_u / W_{C0}**	**Avg. W_u / W_{C0}**
A*	592	698	68.6	80.9
B*	804		93.2	
C*	673	673	78.0	78.0
D*	526	526	61.0	61.0

Analogous to strength behavior, absorbed energy values differed due to the different mechanisms involved in each specimen. This high variability is undesired, as it reduces the reliability of this reinforcement scheme. However, it is possible that using a higher area of reinforcement, could lead to more homogeneous results. Regardless, the energy absorbed by these specimens ranged between 61.0 (specimen D*) to 93.2 (specimen B*) times the average energy absorbed by unreinforced specimens, which signifies a significant improvement.

- ***Failure mechanism***

The mechanism behind each failure mode is analyzed below. First, Figure 98 shows the state of specimen A* after the test:

Figure 98 *Failure mode R1 – 2.5 – X – 50 – A*. Source: Own.*

For this mode of failure, breakout cracks are mostly directed toward the edge of the concrete member, similar to the slicing mechanism observed in previous configurations. However, the X configuration increases the confinement of the breakout body, providing the system more resistance against displacement. Also, some concrete pryout cracks are observed behind the anchor. Neither of these reached the edge. It is also observed how the orientation of the laminates may have induced a slight reorientation of these cracks, as they seem to propagate on the opposite direction to the force when they reach the fiber. Moreover, specimen A* showed some localized rupture of the CFRP, as illustrated on the picture located at the top. Specimen B* showed a similar behavior, but its concrete breakout cracks were wider, which could explain the larger displacements attained.

On the other hand, Figure 99 shows specimen C*:

Figure 99 *Failure mode R1 – 2.5 – X – 50 – C*. Source: Own.*

The failure surface of the anchor demonstrates that the steel may have failed mainly though shear, with no significant contribution of bending, as its cross-section does not show notable deformation from the rest of the anchor. This, in addition to the lack of concrete breakout cracks at the top of the member, indicates effective confinement given by the CFRP laminates. However, it is observed that when anchor failure occurred, some concrete pryout cracks had already developed at the back of the anchor. Likewise, a concrete breakout body was beginning to form on the lateral face of the slab. Nevertheless, steel rupture prevailed over the other possible failure modes.

Lastly, specimen D* is analyzed (Figure 100):

Figure 100 *Failure mode R1 – 2.5 – X – 50 – D*. Source: Own.*

This specimen developed a concrete breakout body on the lateral side of the slab, which was contained by the CFRP laminates. Also, some concrete pryout cracks developed behind the anchor. However, their width was not significant. This could explain why the laminates did not debond and why the load – displacement behavior of specimen D* displayed the most rigid behavior just as it achieved the theoretical concrete pryout load. Nevertheless, the concrete at the front of the anchor crushed due to the high compressive stresses present in that region. This changed the support conditions of the anchor, which in conjunction with the confinement effect of the CFRP, led to more bending contribution. Finally, the interaction between shear and bending resulted in the rupture of the anchor at a lower load than the theoretical one that only considers shear action.

- ***Stress – strain behavior***

Strain gauges were installed on specimens A* and D*. Their results are shown below (Table 52):

Table 52 *CFRP exigency ratio R1 – 2.5 – X – 50. Source: Own.*

CFRP EXIGENCY RATIO R1 – 2.5 – X – 50				
Specimen	**Strain gauge**	$\varepsilon_{f_{Máx.}}$	$\varepsilon^*_{f_u}$	$\varepsilon_{f_{Máx.}}/\varepsilon^*_{f_u}$
A*	NI	0.0124	0.011	112.7%
D*	NI	0.0066		60.0%

This information shows strains on specimen A* higher than the CFRP rupture strain reported by the manufacturer. This means that on this specimen, the fiber was used beyond its design capacity. This is completely normal, as design reported values involve statistic approaches that provide more reliability. Values this high explain why a strip of laminate debonded, and why there was some evidence of CFRP rupture near the strain gauge, as shown in Figure 98. Also, it should be noted that the strain gauge installed on specimen A* stopped working 9 seconds before the ultimate load was achieved. Thus, the fiber may have experimented even larger unit strains than those reported in this document.

On the other hand, specimen D* registered unit strains 57% above the theoretical debonding value $(\varepsilon_{fd} = 0.0042)$. It could be affirmed that these strain values could not have been attainable, if the formation of a concrete pryout body was more developed.

The force – unit strain behavior of both specimens until the maximum recorded load is illustrated in Figure 101:

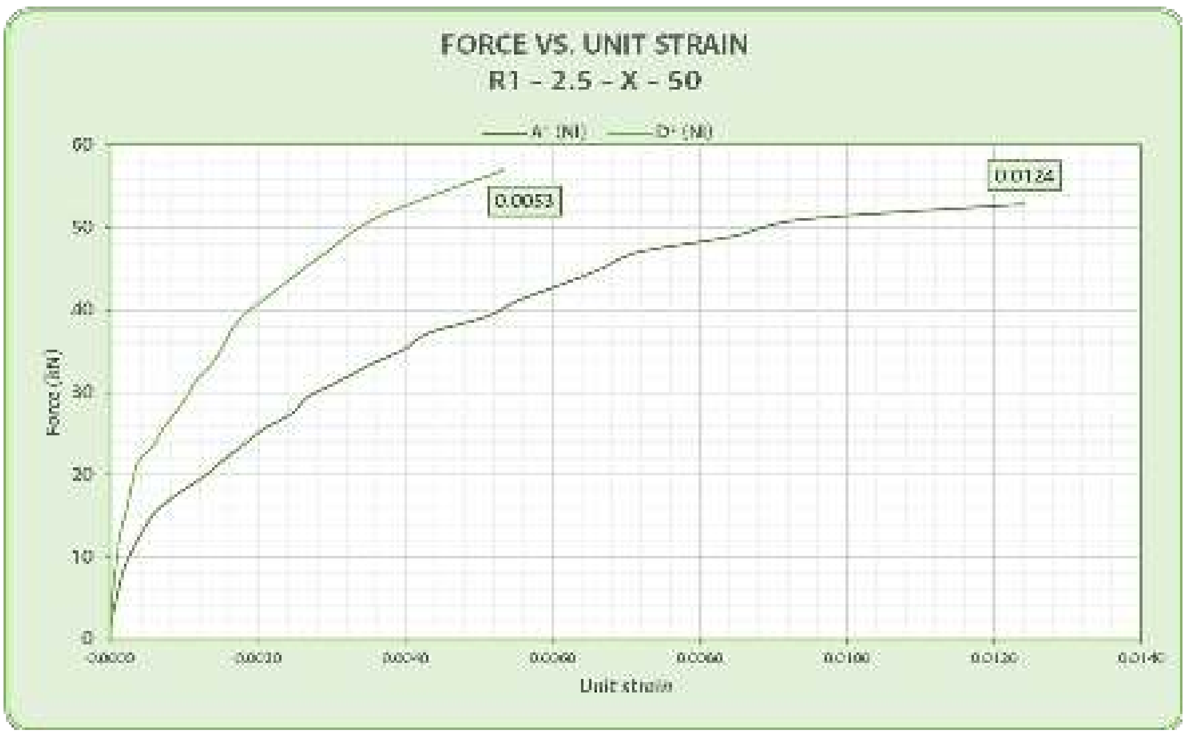

Figure 101 *Force vs. unit strain R1 – 2.5 – X – 50. Source: Own.*

Specimen D* shows a more rigid behavior, which complies with the load – displacement behavior presented in Figure 97. Differences between both responses were analyzed in the "*Failure mechanism*" section. Overall, this graph indicates that, given certain conditions, CFRP can be required to its maximum capacity, but this not necessarily means that the desired failure mode or capacity will be achieved.

7.4.2.2.4. R0 – 5 – 50.

This reinforcement configuration was created to address the concrete slicing phenomenon observed in *R1 – 5 – 50* and *R1 – 2.5 – 50* reinforcement configurations. It comprised one 5.0 in (127 mm) wide CFRP laminate. Its installation consisted of moving some fibers, to make an opening for the anchor to pass through. This configuration also employed the second steel; this is indicated with a star (*) on their respective specimen ID. This configuration employed 45% of the reinforcement area required by design.

- ***Strength and failure mode***

First, strength-related information is presented in Table 53:

Table 53 *Strength and failure mode R0 – 5 – 50. Source: Own.*

STRENGTH & FAILURE MODE R0 – 5 – 50							
Specimen	**V_u (kN)**	**Avg. V_u (kN)**	**V_u / $V_{Theo.}$**	**Avg. V_u / $V_{Theo.}$**	**V_u / V_{C0}**	**Avg. V_u / V_{C0}**	**Failure mode**
A*	59.39	61.13	0.89	0.91	4.47	4.60	***DB***
B*	54.16		0.81		4.08		***DB***
C*	69.83		1.05		5.26		***DB***

First, it should be pointed out that all specimens failed due to debonding. However, the laminate of specimen C* debonded at a load higher than that associated with steel rupture. As most elements are designed to sustain certain minimum load, this would indicate an adequate behavior. Nevertheless, it suggests some uncertainty concerning failure mode.

Regarding data dispersion, the coefficient of variation for ultimate load is 10.7%, which could be interpreted as acceptable. Yet, the span between capacity values corresponds to 25.6% of the mean, which evidences significant dispersion in the data. Overall, this configuration reached, on average, a maximum load that corresponds to 91% of the theoretical expected value associated with anchor rupture.

Moreover, the load – displacement behavior of these specimens is evidenced in Figure 102:

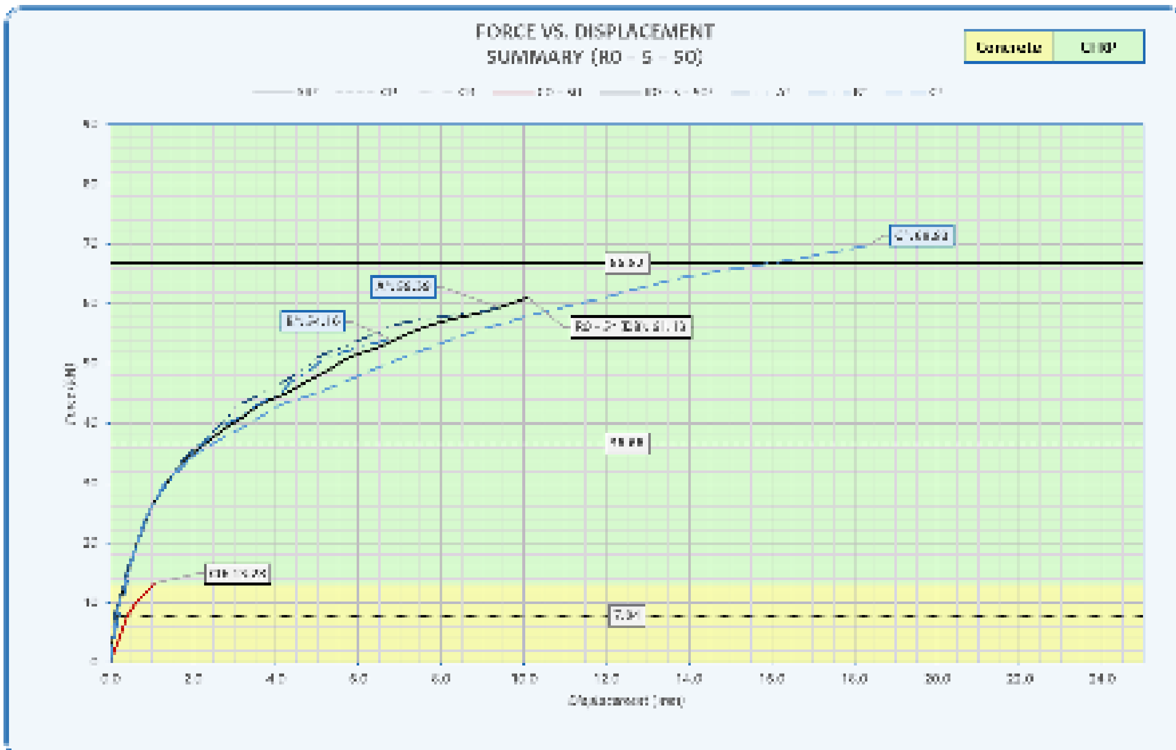

Figure 102 *Force vs. displacement R0 – 5 – 50. Source: Own.*

All specimens follow similar trajectories. It is also observed that at lower loads, the specimens show more stiffness than control samples. This could be evidence of concrete and CFRP acting in conjunction. As the load increases, cracks begin to form, reducing the overall rigidity of the system, as seen in other reinforcement configurations. Given that the three curves are similar in their path, it is important to analyze each failure mechanism separately. This analysis may be found in its correspondent section.

- ***Energy absorption***

In regard to energy absorption, Table 54 summarizes the most important information:

Table 54 *Absorbed energy R0 – 5 – 50. Source: Own.*

ABSORBED ENERGY R0 – 5 – 50				
Specimen	**W_u (J)**	**Avg. W_u (J)**	**W_u / W_{C0}**	**Avg. W_u / W_{C0}**
A*	427	553	49.5	64.1
B*	268		31.1	
C*	964		111.7	

Once again, significant dispersion is observed between the results. On average, these systems absorbed 84 times more energy than an unreinforced connection, which implies higher ductility as well. As in all CFRP-reinforced specimens, the sound emitted by the laminates during the test, act as an indicator of proximity to failure. Therefore, although failure by debonding is sudden, the load-bearing mechanism of CFRP functions as a warning sign.

- ***Failure mechanism***

Figure 103 shows the back bottom side of the anchor, after completely retiring the laminate from specimen A*. It is observed that most of the concrete at the front of the anchor was crushed, allowing for free displacement of the anchor in that direction. Also, the anchor was kept in its place due to the confining force of the cured fibers located around it. It could be concluded that the force of the laminate debonding also separated the anchor from the concrete substrate. Therefore, the anchor got pulled out with the laminate.

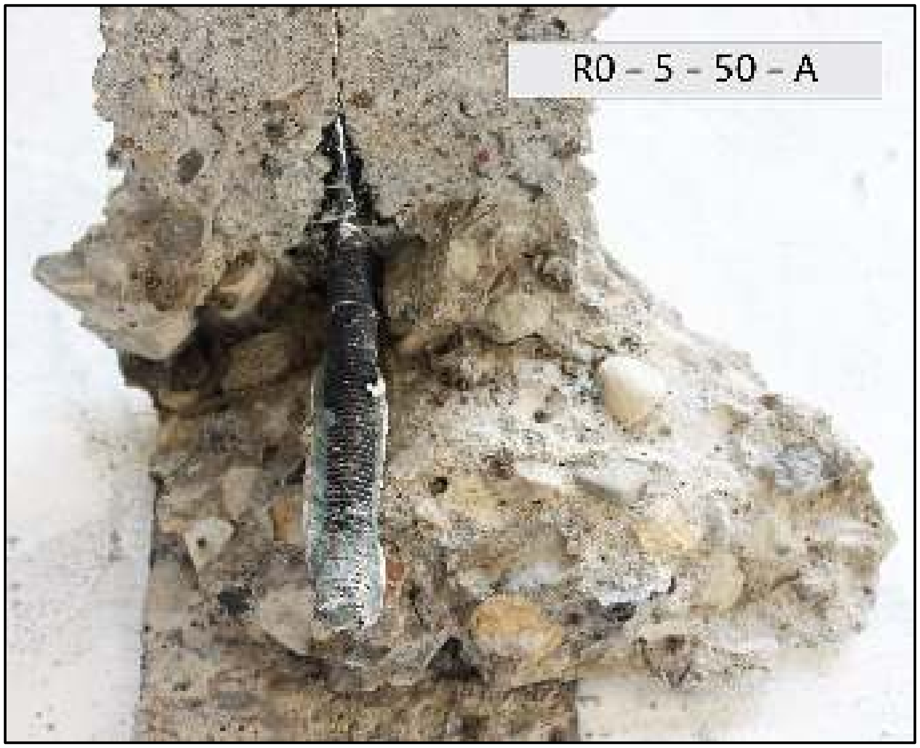

Figure 103 *Failure mode R0 – 5 – 50 – A*. Source: Own.*

On the other hand, Figure 104 shows the failure of specimen B*:

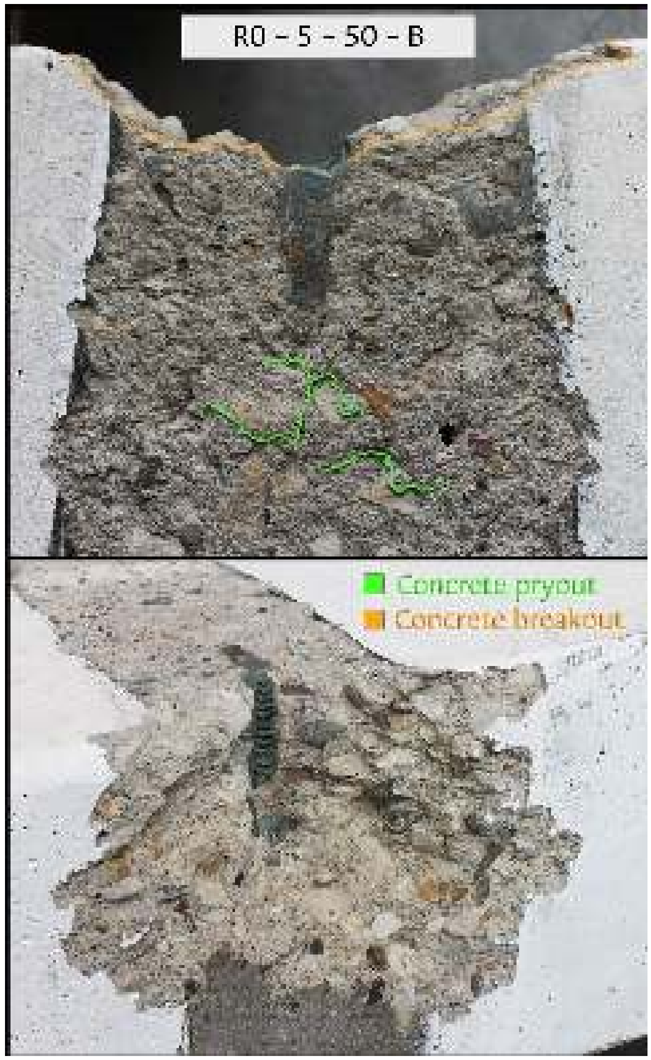

Figure 104 *Failure mode R0 – 5 – 50 – B*. Source: Own.*

This specimen showed concrete breakout cracks that extended beyond the fiber, achieving the formation of a concrete breakout body. The reduced size of this piece of concrete implies that its formation occurred at a low load, given the reduced mechanical interlock between both portions. This also explains why concrete pryout cracks were not as developed when the system reached failure. Therefore, the mode of failure of specimen B* could be attributed to the large displacements and rotations that the detached concrete breakout body induced on the CFRP laminate.

Finally, the failure mode of specimen C* is presented in Figure 105:

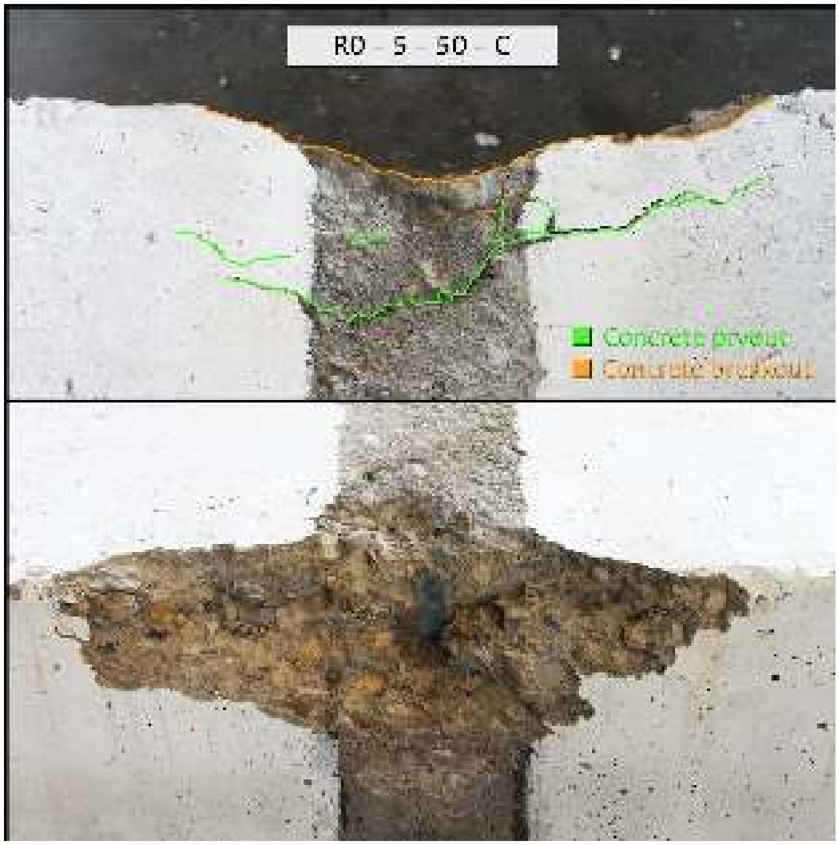

Figure 105 *Failure mode R0 – 5 – 50 – C*. Source: Own.*

Contrary to specimen B*, specimen C* showed a larger concrete breakout body. The less pronounced angle of the cracks indicates that its full formation happened at higher loads; hence the more developed concrete pryout cracks. Therefore, the debonding of this laminate could be attributed to the joint action of the concrete breakout and concrete pryout bodies. Finally, the load at which debonding occurred shows that anchor rupture could have been close from happening as well.

- ***Stress – strain behavior***

No strain gauges were installed on these specimens. However, due to the failure mode displayed by these specimens, it is possible to affirm that their fibers attained strains similar or higher than those associated with debonding.

7.4.2.2.5. Overall analysis (50 mm)

- ***Strength and failure mode***

Table 55 summarizes all information associated with strength and modes of failure for specimens located at 50 mm from the edge.

Table 55 *Strength and failure mode summary (50 mm). Source: Own.*

STRENGTH AND FAILURE MODE SUMMARY C_{a1} = 50 mm						
ID	**Specimens**	**Avg. V_u (kN)**	**Avg. V_u / $V_{Theo.}$**	**Avg. V_u / V_{C0}**	**$A_{Reinf.}$ / $A_{Des.}$**	**Failure mode**
C0	A, B, C	13.28	1.69	–	–	***CB***
CH	A*, B*, C*	45.38	0.68	3.42	1.09	***CB → SR***
R1 – 5	A, B, C	42.82	0.57	3.22	0.79	***CS***
R1 – 2.5	A, B, C	35.92	0.48	2.70	0.40	***CS***
R1 – 2.5 – X	A*, B*	53.18	0.80	4.00	0.45	***DB***
	C*	71.73	1.07	5.40		***SR***
	D*	57.10	0.85	4.30		***CB → SR***
R0 – 5	A*, B*, C*	61.13	0.91	4.60	0.45	***DB***

In parallel, overall load – displacement behavior is illustrated in Figure 106:

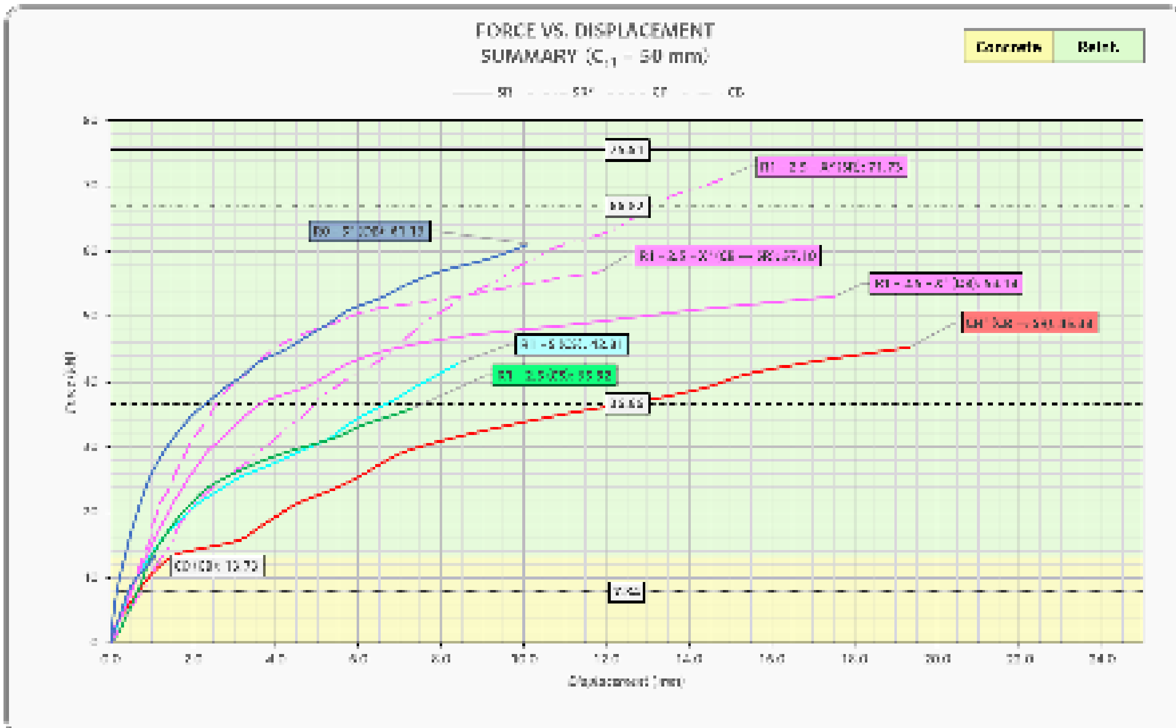

Figure 106 *Force vs. displacement summary (50 mm). Source: Own.*

This edge distance revealed a wide range of possible outcomes in terms of ultimate load and failure mode. However, all reinforced specimens evidenced significant improvements in relation to unreinforced samples. Each of the configurations is analyzed below.

Regarding *R1 – 5 – 50* specimens, their failure mode was characterized by the sliding of a concrete breakout slice through the space left between the CFRP laminates. The loss of confinement in front of the anchor led to an anticipated failure, reaching 57% of the expected load. This mode of failure is not dependent on the anchor material properties. Therefore, in relation to the value of steel rupture of the second anchor batch, the overall load achieved by this reinforcement system would be 64% of the theoretical one.

Likewise, *R1 – 2.5 – 50* specimens showed a similar behavior, reaching ultimate loads of 48% and 54% of the theoretical loads associated with steel rupture of the first and second batches of anchors, respectively. The main difference between the response of this reinforcement scheme and the previous one, is that *R1 – 5 – 50* specimens reached an ultimate load 19% higher than *R1 – 2.5 – 50* specimens. This is attributed to the higher stiffness of the former configuration, which delays more effectively crack formation and propagation. However, this shared behavior suggests that reinforcement area does not have a significant influence on the mode of failure, at least for the reinforcement proportions used in this research.

On the other hand, X-reinforced specimens showed a better performance overall. This is attributed to the orientation of the laminates, which were more effective in taking the internal stresses related to concrete breakout and concrete pryout. Also, this scheme mitigated the slicing effect, due to a stronger confinement of the concrete located in front of the anchor, which allowed for higher ultimate loads. However, variability in the failure modes obtained suggest unreliability of the system. Regardless, with only 45% of the required area, this configuration showed an outstanding behavior. It is possible that increasing the reinforcement area would lead to better results, and even to a consistent steel rupture failure mode.

The last of the CFRP configurations, *R0 – 5 – 50*, also showed a significant improvement in relation to the first two reinforcement schemes. Moreover, its failure mode was constant, which makes it more predictable. Even if debonding was displayed by all specimens, the ultimate load was 91% of the theoretical one. This is a key aspect, because in design, achieving the required load would be deemed as more important than obtaining a certain mode of failure. Yet, the main action to mitigate the debonding effect could be the use of CFRP anchors. Besides, it could be possible that increasing the area of reinforcement could also lead to better results, as this configuration employed only 45% of the required area.

Lastly, hairpin-reinforced samples are analyzed. None of these specimens achieved a “pure” steel rupture failure mode, which did happen in one of the *CH – 100* specimens. Comparing these two reinforcement schemes, it was evident that *CH – 50* specimens had a higher probability of developing a concrete breakout body, due to their proximity to the edge, which means cracks have a shorter path to reach the edge, and a higher stress concentration in the region in front of the anchor. As a result, *CH – 50* managed to attain ultimate loads of 68% of the theoretical steel rupture one, which is slightly lower than the proportion achieved by the *CH – 100* specimens in relation to their expected failure load (74%).

- ***Energy absorption***

A summary of the energy absorption capacity of all 50 mm specimens is found in Table 56:

Table 56 *Energy absorption summary (50 mm). Source: Own.*

ENERGY ABSORPTION SUMMARY C_{a1} = 50 mm					
ID	**Specimens**	**Avg. W_u (J)**	**Avg. W_u / W_{C0}**	**$A_{Reinf.} / A_{Des.}$**	**Failure mode**
C0	A, B, C	8.63	–	–	***CB***
CH	A*, B*, C*	588	68.1	1.09	***CB → SR***
R1 – 5	A, B, C	371	43.0	0.79	***CS***
R1 – 2.5	A, B, C	234	27.1	0.40	***CS***
R1 – 2.5 – X	A*, B*	698	80.9	0.45	***DB***
	C*	673	78.0		***SR***
	D*	526	61.0		***CB → SR***
R0 – 5	A*, B*, C*	553	64.1	0.45	***DB***

Similar to load improvements, all specimens showed gains in energy absorption properties in relation to control ones. These enhancements ranged between 27 to almost 81 times the energy absorbed by an unreinforced anchor. These improvements are also reflected in the ductility of the systems and are dependent on the mode of failure demonstrated by each test specimen.

In this regard, the best behavior was displayed by specimens A*, B* and C* of the X-reinforcement scheme, followed by hairpin-reinforced specimens, which demonstrated a trade between capacity and deformation achieved.

- ***Reinforcement effectiveness***

To concentrate strength and energy characteristics in a single parameter, the reinforcement effectiveness is calculated, which results are summarized in Table 57:

Table 57 *Reinforcement effectiveness summary (50 mm). Source: Own.*

REINFORCEMENT EFFECTIVENESS C_{a1} = 50 mm					
ID	**Specimens**	**Avg. W_u (J)**	**Avg. V_u (kN)**	**Avg. W_u / V_u (J/kN)**	**Failure mode**
C0	A, B, C	8.63	13.28	0.65	***CB***
CH	A*, B*, C*	588	45.38	13.0	***CB → SR***
R1 – 5	A, B, C	371	42.82	8.66	***CS***
R1 – 2.5	A, B, C	234	35.92	6.51	***CS***
R1 – 2.5 – X	A*, B*	698	53.18	13.1	***DB***
	C*	673	71.73	9.38	***SR***
	D*	526	57.10	9.21	***CB → SR***
R0 – 5	A*, B*, C*	553	61.13	9.05	***DB***

The best relation between energy absorbed for unit of force achieved was displayed by specimens A* and B* of CFRP configuration *R1 – 2.5 – X – 50*. This shows the significant improvement obtained with diagonal bands, which give a better confinement to the front region of the anchor, while effectively taking the tensile stresses associated with crack formation. However, these specimens achieved 80% of the ultimate load. As mentioned in the "*Strength and failure mode*" section, increasing the area of reinforcement would probably lead to better results and to a consistent mode of failure. Yet, some uncertainty is still linked to this reinforcement scheme, as it depends on a reliable characterization of crack orientation.

Hairpin-reinforced specimens (*CH – 50*) showed the overall second-best behavior. The main disadvantage of this configuration was also the ultimate load achieved, as it corresponded, on average, to 68% of the expected one. In this case, the area of reinforcement would not provide any significant improvement; a better behavior relies on the quality of the hairpin installation. Nevertheless, the effects of the stress concentration that takes place when placing the anchoring system very close to the edge, should not be overlooked.

Then comes configuration *R0 – 5 – 50*, which absorbed 9.05 joules for each kilonewton supported. The advantages of this system consisted of confinement characteristics, the reduced dispersion in the results, and the fact that it was the configuration that overall performed best in the ultimate load aspect, reaching 91% of the theoretical steel rupture load. Increasing the area of reinforcement to a value close or higher to the required area by design would most probably lead to better results. Therefore, as a result of the consistency of the obtained results, this scheme is deemed as the one with the best behavior.

Lastly, configurations *R1 – 5 – 50* and *R1 – 2.5 – 50* did not achieve the expected results, demonstrating the lowest increases in strength due to a failure mode that emerged given the geometric conditions of the reinforcement. It is important to note that even if *R1 – 5 – 100* showed an excellent behavior, this did not translate to its 50 mm to the edge counterpart. Thus, the importance of varying edge distance for an adequate performance assessment.

8. CONCLUSIONS

- The use of CFRP as a post-installed anchor reinforcement is highly effective in terms of increasing strength, ductility, and changing the mode of failure of shear-loaded anchoring systems located close the edge.
- The test results obtained in this experimental program revealed that to reduce the behavior variability linked to the distance from the anchor to the edge, and to increase the confinement of the breakout body, the most effective reinforcement scheme would consist of only one laminate. While the laminate is being installed, a hole should be punctured, so the anchor can pass through.
- On the other hand, diagonal CFRP laminates improve the behavior with respect to configurations with laminates perpendicular to the edge, due to their axis being perpendicular to the crack path, as well as for them guaranteeing a better confinement on the anchor's front. However, their efficiency is highly dependent on the angle of the crack. If this path can be reliably predicted, X-reinforced systems are optimal for reinforcing shear-loaded anchors proximate to free-edges.
- The response of CFRP-reinforced anchoring systems does depend on the quality of the installation. However, there is more uncertainty associated to cast-in anchor reinforcement (hairpins), as its response is highly sensitive to its installation.
- Through the ACI 318 concrete breakout equations, it is possible to calculate the capacity of near-edge shear-loaded anchors, providing a margin of security in the calculations, which is supported by the 5 percent fractile approach for anchor qualification found in ACI 355.4.
- The combined effect of shear and bending moment decreased substantially the capacity of some tested specimens, demonstrating the importance of anchor confinement to reduce rotational deformations associated with bending.

9. RECOMMENDATIONS

- Before proposing a design equation, it is recommended to test the configurations that proved the best behavior in this investigation but varying the area of CFRP reinforcement. Therefore, a more detailed and optimized design may be achieved.
- This study focused on shear perpendicular to the edge. Various applications that involve anchors in need of retrofitting consist of shear parallel to the edge. Future studies could focus on the effectiveness of the proposed schemes given forces acting in different directions.
- Similarly, only one edge was considered. Additional research could consider members with two or more edges, or with insufficient depth. Furthermore, the connection of a steel bracing system to a reinforced concrete frame could be tested, to validate the response of CFRP-strengthened connections to lateral loads.
- To comply with the previous recommendation, the study of CFRP reinforcement for groups of anchors is also relevant.
- Given the observed interaction between bending and shear, this phenomenon should be studied in further detail, to accurately predict the response of anchors subjected to these actions.
- Consequence of the two different batches of anchors received in this research, it is of great importance to always test the mechanical properties of the materials used in academic or practical applications. Thus, guaranteeing more reliability in construction works.
- Various CFRP laminates reached unit strains larger than the effective strain associated with the design load. Future research should study in more detail the relation between external load and unit strain achieved on the laminate, to accurately depict the mechanical behavior of the strengthened system as a whole.

10. REFERENCES

ACI Committee 318. (2019). Building Code Requirements for Structural Concrete and Commentary. In *318-19 Building Code Requirements for Structural Concrete and Commentary*. American Concrete Institute. https://doi.org/10.14359/51716937

ACI Committee 440. (2017). *Guide for the design and construction of externally bonded FRP systems for strengthening concrete structures*. American Concrete Institute.

American Institute of Steel Construction. (2016). *Specification for Structural Steel Buildings*.

American Society of Civil Engineers, & Structural Engineering Institute. (2017). *Seismic evaluation and retrofit of existing buildings: ASCE/SEI, 41-17*. American Society of Civil Engineers.

Bokor, B., Sharma, A., & Hofmann, J. (2020). Experimental investigations on the concrete edge failure of shear loaded anchor groups of rectangular and non-rectangular configurations. *Engineering Structures*, *222*. https://doi.org/10.1016/j.engstruct.2020.111153

BPIE. (2011). *Europe's buildings under the microscope. A country-by-country review of the energy performance of buildings*.

European Committee for Standardization. (2018). *EN 1992-4: Eurocode 2: Design of concrete structures – Part 4: Design of fastenings for use in concrete*.

Fuchs, W., Eligehausen, R., & Breen, J. E. (1995). Concrete Capacity Design (CCD) Approach for Fastening to Concrete. *ACI Structural Journal*, *92*(I), 73–94.

Gkournelos, P. D., Triantafillou, T. C., & Bournas, D. A. (2021). Seismic upgrading of existing reinforced concrete buildings: A state-of-the-art review. *Engineering Structures*, *240*, 112273. https://doi.org/https://doi.org/10.1016/j.engstruct.2021.112273

Haukohl, R. C., Lipinski, B., & Wagner, M. L. (2019). Design considerations for rail post anchorage into concrete. *Construction Specifications Institute*.

Mahrenholtz, C., Lin, P. C., Wu, A. C., Tsai, K. C., Hwang, S. J., Lin, R. Y., & Bhayusukma, M. Y. (2015). Retrofit of reinforced concrete frames with buckling-restrained braces. *Earthquake Engineering and Structural Dynamics*, *44*(1), 59–78. https://doi.org/10.1002/eqe.2458

Mallée, R., Eligehausen, R., & Silva, J. F. (2012). *Anchorage in Concrete Construction* (1st ed.).

Rendón, J. (2016). *Reforzamiento y actualización sísmica de estructuras*.

Vita, N., Sharma, A., & Hofmann, J. (2022). Bonded anchors with post-installed supplementary reinforcement under tension loading – Experimental investigations. *Engineering Structures*, *252*. https://doi.org/10.1016/j.engstruct.2021.113754